DTU Library

Novel approaches to estimating time-dependent dose variations in lung radiotherapy: Time-resolved Monte Carlo simulations, scintillator dosimetry, and simulations of anatomical changes

Sibolt, Patrik

[Link back to DTU Orbit](#)

Novel approaches to estimating time-dependent dose variations in lung radiotherapy:

Time-resolved Monte Carlo simulations, scintillator dosimetry, and simulations of anatomical changes

PATRIK SIBOLT

PhD DISSERTATION

June, 2018

Supervisors:

Claus E. Andersen

Claus F. Behrens

Herlev og Gentofte Hospital

DTU Nutech
Center for Nuclear Technologies

$f(x+\Delta x) = \sum_{i=0}^{\infty} \frac{(\Delta x)^i}{i!} f^{(i)}(x)$ {2.7182818284}

Preface

The work in this thesis was conducted within the PhD project entitled "Improving Motion Managed Radiotherapy for Lung Cancer Patients using Monte Carlo Simulations and Scintillator Dosimetry". This PhD project was carried out as collaboration between the Radiation Physics Division at the Center for Nuclear Technologies (Nutech), at the Technical University of Denmark (DTU), where I was employed, and the Department of Oncology at Herlev and Gentofte Hospital. Furthermore, it was partly carried out with external collaborators located at the Department of Radiation Physics, Skåne University Hospital in Lund, Sweden, and the Carleton Laboratory for Radiotherapy Physics, Carleton University in Ottawa, Canada, where also two shorter research stays were conducted. The project was supervised by the senior scientist Claus E. Andersen at DTU Nutech and the lead senior scientist Claus F. Behrens at the Radiotherapy Research Unit at Herlev and Gentofte Hospital.

Acknowledgements

Abstract

Lung cancer is one of the most common cancer diagnoses worldwide, unfortunately with patients suffering from poor prognosis. There is therefore a pressing need for improving treatment outcome and this is being widely addressed in the implementation of more complex treatment techniques, where radiotherapy of lung cancer patients is becoming more and more patient specific with a treatment delivery that is guided by the monitoring of the respiratory motion. However, ensuring high quality of complex radiotherapy in a heterogeneous anatomy such as the thorax is a challenging task. Additionally, the treated geometry is time-dependent and subject to both inter- and intra-fractional variations affecting both tumor position and material density distribution.

The work presented in this thesis has been motivated by the need to improve methods for estimating and verifying the dose delivered during motion managed radiotherapy of lung cancer patients. A major factor contributing to dose deviations in lung radiotherapy is inter-fractional variations. Anatomical changes such as pleural effusion, atelectasis and tumor shrinkage occur over the course of treatment and manifests in the form of density alterations also within the irradiated volume. By estimating the dosimetric effect of systematically simulated anatomical changes a foundation for assessing the need for adaptation of the treatment plan was established. The method was applied to a set of treatment situations of different complexity. In general the results demonstrated the need for patient- and treatment-specific investigation of the dosimetric effect caused by anatomical changes.

While inter-fractional changes often occur randomly over the course of treatment, the respiratory-induced intra-fractional motion is more predictable but in the same time also more challenging as any change in motion will influence the delivered dose immediately during irradiation. Addressing the questions of when, where and possibly why dose deviations occur requires methods for both accurate measurements and calculations where the dynamic motion of both the treatment beam configuration and the heterogeneous patient anatomy is taken into account. This study has therefore also focused on the development of tools for time-resolved scintillator measurements and accurate Monte Carlo dose calculations in a thoracic-like geometry.

An in-house developed dynamic thorax phantom was demonstrated to enable time-resolved plastic scintillator dosimetry during reproducible respiratory-like motion. Furthermore this dosimetry setup, mimicking radiotherapy in a patient-like geometry, was used as a basis for initial validation of a novel approach to time-resolved Monte Carlo simulations also developed during the current project. With the implementation of the Monte Carlo simulations into an automated workflow the tools were furthermore made accessible by minimizing the user interaction.

Based on the work carried out in the thesis it was concluded that there is a need for estimating dose variations in time-dependent heterogeneous geometries. Tools addressing this issue, both by measurements and dose calculations, were developed and demonstrated to be reliable. These tools were observed to have great potential to be used in a quality assurance program for dosimetric verification of complex treatment delivery techniques in radiotherapy of lung cancer patients.

Resumé (in Danish)

Lungekræft er en af de mest almindelige kræftdiagnoser verden over og samtidig har den en dårlig prognose for helbredelse. Der er derfor et presserende behov for bedre behandlinger, eksempelvis baseret på strålebehandling, som er mere individualiseret den enkelte patient og dennes respiratoriske bevægelse. Kvalitetssikring af kompleks strålebehandling i en heterogen anatomi som thoraxen er imidlertid en udfordrende opgave, og tumorposition og densitetsfordeling påvirkes af at den behandlede geometri er tidsafhængig og underkastet både inter- og intra-fraktionelle variationer.

Arbejdet præsenteret i denne afhandling er motiveret af behovet for at forbedre metoder til estimering og verifikation af den dosis, der bliver leveret under bevægelsesstyret strålebehandling af lungekræftpatienter. En væsentlig faktor, der bidrager til dosisafvigelser i stråleterapi af lungekræft, er inter-fraktionelle variationer. Anatomiske forandringer såsom pleuravæske, atelektase og mindskning af tumorens størrelse forekommer i løbet af behandlingen og manifesterer sig i form af densitetsændringer, også inden for det bestrålede volumen. Ved at estimere den dosimetriske effekt af systematisk simulerede anatomiske ændringer blev der etableret et grundlag for vurdering af behovet for tilpasning af behandlingsplanen. Metoden blev anvendt på behandlingsplaner af varierende kompleksitet og resultaterne demonstrerede et generelt behov for patient- og behandlingsspecifik undersøgelse af den dosimetriske effekt forårsaget af anatomiske ændringer.

Mens inter-fraktionerede ændringer ofte opstår tilfældigt over behandlingsforløbet, så er de vejrtræknings-inducerede intra-fraktionelle bevægelserne mere forudsigelige, men også mere udfordrende med hensyn til at ændringer i vejrtrækning vil påvirke afgivet dosis umiddelbart under bestråling. For at kunne svare på hvornår, hvor og muligvis hvorfor dosisafvigelser opstår, kræves metoder til både dosimetri og dosisberegninger med høj præcision, hvor der også tages hensyn til den dynamiske bevægelse af både behandlingsfeltet og den heterogene patientanatomi. Dette studie har derfor også fokuseret på udvikling af værktøjer til tidsopløst scintillatormålinger og præcise Monte Carlo dosisberegninger i en thoraxlignende geometri.

Et internt udviklet dynamisk thoraxfantom blev demonstreret for at muliggøre tidsopløst scintillatordosimetri under reproducerbar respiratorisk bevægelse. Endvidere er det udviklede dosimetrisystem, der efterligner strålebehandling i en patient-lignende geometri, blevet anvendt som grundlag for indledende validering af en ny metode for tidsopløste Monte Carlo-simuleringer, der er udviklet under det aktuelle projekt. Med implementeringen af Monte Carlo-simuleringerne i en automatiseret arbejdsgang blev værktøjerne også gjort tilgængelige for en bredere kreds af brugere idet behovet for brugerens interaktion er minimeret.

Baseret på arbejdet i afhandlingen blev det konkluderet, at der er behov for at estimere dosisvariationer i tidsafhængige heterogene geometrier. Værktøjer, der løser dette problem, både ved målinger og dosisberegninger, blev udviklet og påvist at være pålidelige. Disse værktøjer har stort potentiale til at blive anvendt i et kvalitetssikringsprogram til dosimetrisk verifikation af komplekse behandlingsteknikker i strålebehandling af patienter med lungekræft.

Publications and presentations

The thesis is based on the following four manuscripts (hereafter referred to by their roman numerals). The manuscripts are described in an order relevant for the thesis, not in the order of publication. Paper I-III have all been published in peer-reviewed international journals, while paper IV is still to be submitted. Furthermore, all papers have been presented as oral presentations and posters at international conferences. This section lists the scientific contributions created throughout this PhD project. The papers are presented in the thesis with a text identical to the original manuscripts.

I. Sibolt, P., Ottosson, W., Sjöström, D., Larsen, C., & Behrens, C. F. (2015). Adaptation requirements due to anatomical changes in free-breathing and deep-inspiration breath-hold for standard and dose-escalated radiotherapy of lung cancer patients. *Acta Oncologica*, *54*(9), 1453-1460.

II. Sibolt, P., Andersen, C. E., Ottosson, W., & Behrens, C. F. (2017). Time-resolved plastic scintillator dosimetry in a dynamic thorax phantom. *Radiation Measurements*, *106*, 373-377.

III. Sibolt, P., Cronholm, R. O., Heath, E., Andersen, C. E., & Behrens, C. F. (2017). Automated four-dimensional Monte Carlo workflow using log files and real-time motion monitoring. *Journal of Physics: Conference Series*, 847(1), 012030.

IV. Sibolt, P., Andersen, C.E., Behrens, C.F., Cronholm, R.O., Heath, E. (2018). First validation of a user code for time-resolved Monte Carlo simulations of dose delivered to a dynamic thorax phantom using scintillator dosimetry. Manuscript.

Co-authorship not covered in this thesis:

i. Ottosson, W., Sibolt, P., Larsen, C., Andersen, J. A. L., Borissova, S., Mellemgaard, A., & Behrens, C. F. (2015). Monte Carlo calculations support organ sparing in Deep-Inspiration Breath-Hold intensity-modulated radiotherapy for locally advanced lung cancer. *Radiotherapy and Oncology*, *117*(1), 55-63.

ii. Ottosson, W., Rahma, F., Sjöström, D., Behrens, C. F., & Sibolt, P. (2016). The advantage of deep-inspiration breath-hold and cone-beam CT based soft-tissue registration for locally advanced lung cancer radiotherapy. *Radiotherapy and Oncology*, *119*(3), 432-437.

iii. Møller, D. S., Nielsen, T. B., Brink, C., Hoffmann, L., Lutz, C. M., Lund, M. D., ..., Sibolt, P., … & Nyhus, C. H. (2017). Heterogeneous FDG-guided dose-escalation for locally advanced NSCLC (the NARLAL2 trial): Design and early dosimetric results of a randomized, multi-centre phase-III study. *Radiotherapy and Oncology*, *124*(2), 311-317.

Oral presentations at national and international conferences:

A. Sibolt, P., & Andersen, C.E. (2015). On the use of Monte Carlo in radiation dosimetry. Presented at the National workshop on accelerator dosimetry.

B. Sibolt, P., Behrens, C.F., & Andersen, C.E. (2016). Time-resolved scintillator dosimetry and 4D Monte Carlo simulations of lung cancer radiotherapy. Presented at the 4th Øresund Workshop on Radiotherapy.

C. Sibolt, P., Cronholm, R. O., Andersen, C. E., Behrens, C. F., & Heath, E. (2016). Trajectory log file based 4Ddefdosxyznrc simulations and time-resolved scintillator dosimetry in a dynamic thorax phantom. Presented at the International Conference on the use of Computers in Radiotherapy.

D. Sibolt, P., Ottosson, W., & Andersen, C.E. (2016). Time-resolved plastic scintillator dosimetry in a dynamic thorax phantom. Presented at the 18th Solid State Dosimetry conference.

E. Sibolt, P., Cronholm, R. O., Heath, E., Andersen, C. E., & Behrens, C. F. (2016). Automated four-dimensional Monte Carlo workflow using log files and real-time motion monitoring. Presented at 9th IC3DDose.

F. Sibolt, P. (2017). Monte Carlo based four-dimensional dose calculation methods in lung cancer radiotherapy. Presented at the 5th Øresund workshop on radiotherapy.

G. Sibolt, P. (2017). Four-dimensional Monte Carlo in Radiotherapy – Photons and Protons. Presented as invited speaker at the international 4D treatment planning workshop.

H. Sibolt, P., Andersen, C.E., Behrens, C.F., Cronholm, R.O., & Heath, E. (2018). Verification of time-resolved Monte Carlo simulations of dose delivered to a dynamic thorax phantom using scintillator dosimetry. Presented at the 6th Øresund workshop on Radiotherapy.

Poster presentations at national and international conferences:

a) Sibolt, P., Ottosson, W., Sjöström, D., Larsen, C., & Behrens, C. F. (2015). Adaptation requirements due to anatomical changes in free-breathing and deep-inspiration breath-hold for standard and dose-escalated radiotherapy of lung cancer patients. Presented at BiGART2015.

b) Sibolt, P., Ottosson, W., Behrens, C.F., & Sjöström, D. (2016). PO-0886: Does lung capacity influence the geometrical reproducibility in DIBH radiotherapy of NSCLC patients? *Radiotherapy and Oncology, 119, S425-S426.* Presented at ESTRO35.

c) Ottosson, W., Sibolt, P., Behrens, C. F., & Andersen, C. E. (2017). EP-1461: Scintillator dosimetry reveals lung tumor size dependency of 6 MV AAA dose calculations. *Radiotherapy and Oncology, 123*, S780.Presented at ESTRO36.

d) Sibolt, P., Ottosson, W., Andersen, C.E., & Behrens, C.F. (2017). Monte Carlo evaluation of dose-escalated lung radiotherapy in free-breathing and deep-inspiration breath-hold. Presented at BiGART2017.

e) Sibolt, P., Andersen, C. E., Behrens, C. F., Cronholm, R. O., & Heath, E. (2017). Abstract ID: 78 Verification of time-resolved Monte Carlo simulations of dose delivered to a dynamic thorax phantom using scintillator dosimetry. *Physica Medica: European Journal of Medical Physics, 42*, 15-16. Presented at the International Conference on Monte Carlo Techniques for Medical Applications.

Acronyms

Abbreviation	Description
3D	Three-dimensional
4D	Four-dimensional
4DtMC	Time-resolved Monte Carlo
AAA	Anisotropic-Analytical-Algorithm
ART	Adaptive Radiotherapy
CBCT	Cone Beam CT
CM	Component module
CPE	Charged Particle Equilibrium
CT	Computed Tomography
CRT	Conformal external beam radiotherapy
CTV	Clinical Target Volume
DE	Dose-escalated
DIBH	Deep-Inspiration Breath-Hold
DIM	Dose Interpolation Method
DIR	Deformable Image Registration
DVF	Deformation vector field
ECUT	Electron cutoff energy
EPID	Electronic Portal Imaging Device
FB	Free-breathing
GTV	Gross Tumor Volume
Gy	SI derived unit for absorbed dose (Gray)
HU	Hounsfield Units
IGRT	Image-guided radiotherapy
IMRT	Intensity-modulated radiotherapy
ITV	Internal Target Volume
K_{col}	Collision KERMA
KERMA	Kinetic Energy Released in Matter
keV	kilo electron volt
kV	Kilovoltage
lat	Lateral
LINAC	Medical linear accelerator
lng	Longitudinal
MC	Monte Carlo
MidV	Mid-ventilation respiratory phase
MIP	Maximum Intensity Projection
MLC	Multi Leaf collimator
MRI	Magnetic Resonance Imaging
MU	Monitor Units
MV	Megavoltage
NSCLC	Mon-Small Cell Lung Cancer
nsplit	Number of sub-photons during photon splitting
OAR	Organ at Risk
PCUT	Photon cutoff energy
PDF	Probability density function
PE	Pleural Effusion

PET	Positron Emission Tomography
PMMA	Poly(methyl methacrylate)
PSD	Plastic Scintillator Detector
PTV	Planning Target Volume
QA	Quality assurance
RA	RapidArc
SBRT	Stereotactic Body Radiotherapy
SD	Standard Deviation
SF	Single conventional open field
ST	Standard fractionated
TPS	Treatment Planning System
TS	Tumor Shrinkage
VMAT	Volumetric modulated arc therapy
vrt	Vertical
VRT	Variance reduction technique
XCSE	Photon cross-section enhancement

Content

1 Introduction

1.1 Background

Lung cancer patients suffer from a high mortality rate and poor local control rate when undergoing radiotherapy as a part of their treatment. As lung cancer is one of the most common cancer diseases worldwide, this implies an urgent need for improvements [1,2]. Dose escalation has been demonstrated to increase local control and could lead to an increased cure rate, why studies are conducted using modern radiotherapy techniques in order to enable escalation of the radiation dose to the tumor [3–7].

Radiotherapy of lung cancer patients does, however, suffer from uncertainties related to baseline shifts, delineation, organ motion and respiration, and extensive safety margins are usually added to the tumor volume [8,9]. The resulting large irradiated volumes limit escalation of the dose to the tumor and uncertainties therefore need to be handled more efficiently. More sophisticated image guidance methods, using direct registration on the soft-tissue of the lung tumor [10,11], as well as respiratory guided treatment delivery methods [12–14] can assist in minimizing the safety margins around the target and thus the volume of adjacent normal tissue being irradiated.

Additionally, the heterogeneous geometry in the thorax and the density alterations occurring due to anatomical changes further contribute to the uncertainties in lung radiotherapy. With decreasing margins, more complex delivery techniques and possibly escalated dose levels, adaptation of the treatment plan due to anatomical changes will also become more essential as they have been demonstrated to have the largest effect on the delivered dose to the tumor [15].

The reason for emphasizing the challenges in radiotherapy of lung cancer patients is to demonstrate how multiple sources of uncertainties are present. The main common factor for the presented challenges is the difficulty to handle them as they change over time. The time-scale over which they occur is, however, different for the variety of factors listed and time-resolving the appearance of the challenges is essential. While e.g. anatomical changes can appear and disappear again over the range of days or weeks, respiratory movement will move the target and also cause density alteration in the order of seconds. In combination with these time-dependent changes there is of course also the factor of the dynamic beam delivery that needs to be taken into account if the aim is to assess the effect of changes during irradiation. Thankfully there are tools available to handle some of the challenges mentioned here. However, there is a need to improve on the applicability, accuracy and efficiency of the methods used in order to ensure that the correct dose is delivered to the target and that the expected dose to organs at risk (OARs) is correctly estimated.

1.2 Main purpose

The overall aim of this thesis has been to address the major time-dependent challenges in radiotherapy of lung cancer patients. By improving on methods in existing commercial solutions as well as developing in-house methods for time-resolved dosimetry and time-resolved accurate dose calculations, the thesis consists of work related to the accurate determination of dosimetric variations caused by time-dependent changes in the thoracic region of lung cancer patients. Specifically the thesis work is related to the following aims.

I. Find levels of anatomical changes to assist in the online decision between continued treatment and adaptation. The aim was to establish action levels, above which adaptation of the treatment plan is necessary and below which continued treatment is considered safe, for both standard fractionated treatment as well as dose-escalated treatment in both free-breathing and deep-inspiration breath-hold.

II. Develop and validate a dosimetry solution for time-resolved measurements in a geometry mimicking the thorax of a lung cancer patient. The aim was to create a thorax phantom with controllable motion enabling reliable scintillator dosimetry inside a spherical tumor located within a low-density material.

III.   Create an environment to make four-dimensional (4D) Monte Carlo (MC) simulations more accessible by minimizing the user interaction. The aim was to develop an automated workflow for creation and execution of 4D MC input files together with an automated generation of a TPS compliant dose distribution file.

IV.   Develop and validate a user code for time-resolved MC simulations enabling calculation based determination of steep dose gradients with good temporal agreement to measurements. The aim was to experimentally validate a novel approach to time-resolved MC simulations by use of the previously in-house developed scintillator dosimetry system in a dynamic thorax phantom.

1.3   Thesis structure

The chapters in the present thesis are constructed in an order dealing with the challenges moving from anatomical changes occurring at a time-scale of days/week to the anatomical and geometrical changes due to respiratory motion taking place within seconds during treatment.

Chapter 2 discusses radiotherapy of time-dependent geometries in lung cancer patients and describes the difference between inter-fractional and intra-fractional changes, why they are important to quantify and how to handle them by introducing various treatment techniques and quantitative methods. This chapter also relates to Paper I, where a method for quantifying the dosimetric effect of anatomical changes is studied with the aim to investigate the need for adaptation of treatment due to anatomical changes.

Chapter 3 is a step towards managing the dosimetric changes over a much shorter range in time. Here the development of a dynamic thorax phantom enabling time-resolved dosimetry is described. The design of and software solution for the in-house developed phantom is presented together with a method for synchronizing the dosimetry, motion of the phantom as well as the linear accelerator logfiles. The chapter furthermore addresses the dosimetric challenges in the thoracic region, what type of detectors that are suitable for the situation and how the plastic organic scintillator is used for time-resolved measurements in the dynamic thorax phantom. This chapter is therefore related to Paper II, where the development and verification of the system for time-resolved scintillator in the dynamic thorax phantom is presented.

Chapter 4 takes the next step and discusses the challenges of commercial solution for dose calculation in heterogeneous media and why the use of Monte Carlo simulations is essential for carrying out precise time-resolved dose calculations. In the chapter a number of available methods enabling four-dimensional dose calculations are mentioned, while focus is on the MC user code that has been applied and further developed in this thesis. The chapter is therefore related to Paper III, where the implementation of the 4D MC user code into an automated workflow is described. Here a further description of Paper IV is also presented in order to describe the work behind developing and validating the time-resolved Monte Carlo user code, and what the plan is to improve on that user code in the future.

Chapter 5 is finally a summary of the work carried out and presented in this thesis, including the main conclusions and a broader look at future perspectives.

Chapter 6-9 are the manuscripts written during the PhD project and in this thesis referred to as Paper I-IV.

Hereafter follows the bibliography, with all references included in the thesis as well as the manuscripts.

2 Radiotherapy of time-dependent geometries

2.1 Radiotherapy of lung cancer patients

Radiotherapy has the purpose of delivering the prescribed dose to the treated tumor while minimizing the dose to the surrounding normal tissue as much as possible. Although this is true for all cancer diagnoses treated with radiation, this aim is more difficult to achieve for targets in some regions in the patients than others. Radiotherapy of lung cancer is one of the most complex cases as it is subject to several challenges limiting the possibilities to maximize the ratio between dose to target and dose to OARs. Increasing the radiation dose to the lung tumor is a method to increase the cure rate [3]. However, increasing the target dose without eliminating treatment-related uncertainties will also increase the dose to OARs and might thereby lead to severe side effects [16]. If the irradiated volume is minimized, as is the case for stereotactic body radiotherapy, delivering a higher dose over few fractions has for inoperable stage I non-small cell lung cancer (NSCLC) patients proven to improve quality of life and reduce toxicity [17]. Also later stage NSCLC patients would benefit from increased target dose and despite the RTOG-0617 trial presenting discouraging results [4,5] there are still indications of the potential in escalating dose to otherwise conventionally fractionated treatments [6]. While the RTOG-0617 trial escalated the dose homogeneously to the entire target volume, including margins, an ongoing Danish multi-center phase-III trial (NARLAL2) is investigating the effects of a Positron Emission Tomography (PET) guided inhomogeneous dose-escalation [7]. This approach mimics, to a certain degree, the inhomogeneous dose distribution and the steep dose gradients observable in stereotactic treatments and is thereby enabling the dose to normal tissue to remain at the same level as for conventional fractionated treatments. The NARLAL2 study is in this manner able to investigate target doses of up to a total of 95 Gy / 33 fractions in mean dose to the tumor while preserving the same normal tissue constraints and requiring no increase in lung mean dose (Figure 1). This high dose level is to be compared to conventional fractionation where 60-66 Gy are delivered over the 30-33 treatment fractions and currently the recommended prescription in order to minimize the risk of acute toxicity (current fractionation scheme recommended by the Danish Oncological Lung Cancer Group, DOLG).
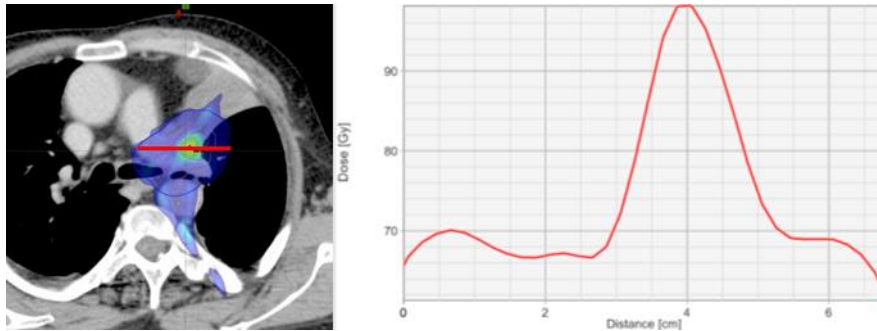
Figure 1. Example of a dose-escalated for a NSCLC patient (not part of NARLAL2 and therefore not optimized according to the NARLAL2 protocol). PET-active volume is used to guide the escalation of up to maximum doses above 100 Gy, while restricting the mean dose to the GTV to a maximum of 95 Gy and maintaining similar doses to OARs as standard fractionated treatment.

Most important when conducting dose escalated radiotherapy in a complex geometry such as the thoracic region is most likely the way the challenges and uncertainties are handled in order to ensure high quality and consistency of the treatment. The use of image-guided radiotherapy (IGRT) is essential and has great potential in minimizing the traditionally extensive margins added to the tumor volume due to uncertainties related to e.g. baseline shifts, tumor motion, delineation, and respiration [8,9]. The approach to IGRT will however also impact the margin needed and an institutional decision on imaging frequency and matching method is necessary [11]. In addition to managing motion uncertainties by applying safety margins, treatment techniques such as gating and tracking can also be used, and a collection of these methods are discussed

further in section 2.2. They are all indications of how improvements in radiotherapy of lung cancer patients can be technique driven. The same indication was proven in the RTOG-0617 trial where the use of intensity-modulated radiotherapy (IMRT) instead of three-dimensional (3D) conformal external beam radiation therapy (CRT) resulted in lower rates of toxicity [18]. The major difference between IMRT and 3DCRT, giving rise to the reduction in toxicity rates, is the improved conformity of the target dose and the resulting reduction in dose to the adjacent normal tissue and the effect has been manifested in several studies [19–23]. Dose conformity has further increased after the introduction of volumetric modulated arc therapy (VMAT) but there are still several consideration to account for during treatment planning and delivery [24]. One of the most discussed considerations is the so called interplay effect between the motion of the medical linear accelerator (LINAC) dynamic beam configuration and the target motion. This effect has in several studies been observed to be insignificant in terms of target dose, e.g. if treatment is delivered using multiple arcs [25] or that the dosimetric effect is blurred out over the course of a multiple-fraction treatment [26]. While the interplay effect might be blurred out over many fractions and negligible for most cases around the mean cranio-caudal motion amplitude of 1 cm, amplitudes up to $3 - 4$ cm have been observed [13], and evidence suggest that the effect increases with target motion magnitude as well as treatment plan complexity [27].

Despite thorough consideration of all of the above mentioned intra-fractional variation, occurring within seconds during irradiation, there are still aspects to consider that are not easy to account for during treatment preparation or by the choice of treatment technique. Over the course of several fractions there will be anatomical changes affecting the treatment geometry by density changes in an already complex heterogeneous setting. It has been demonstrated that density deviations due to anatomical changes have the greatest impact on the dose actually delivered to the target [15]. Furthermore, the random nature of the appearance (and disappearance) of anatomical changes adds to the complexity and require a different approach than the methods applied towards the variations occurring at a much shorter time period [28]. In Paper I the aspects of several types of anatomical changes, their dosimetric effect and the need for methods to adapt the treatment is addressed and in section 2.3 this is discussed further.

2.2 Managing intra-fractional changes

In order to enable management of intra-fractional variations it is required to have time-resolved information regarding the motion taking place during irradiation. This information is generally obtained during pre-treatment four-dimensional (4D) computed tomography (CT) and images acquired during 4DCT is correlated with the respiration as that is the main factor contributing to the motion [29,30]. By correlating motion with imaging in 4DCT it is possible to acquire better and more useful images than using 3DCT. However, as the internal motion during 4DCT is usually tracked using an external surrogate marker there is a risk of bad correlation resulting in image artifacts [31].

Many solutions for tracking the respiratory motion is available; including external marker-based systems and surface-guided solutions but also internal markers and measures of breath flow or temperature are used [13]. What is important is that these techniques might also be used at the LINAC in order to facilitate respiratory-guided treatment delivery. In the sections below some of the commonly used methods for motion managed radiotherapy are briefly described. Not covered here is the use of motion models used to describe the relationship between markers and the internal motion, which might be applied in order to estimate and better correct for the effects of respiratory motion [32].

What all of the discussed approaches have in common is, however, the fact that there is still a need for margins taking care of any residual uncertainty. Due to for example image artifacts there is an uncertainty in the CT-based (and often PET-supported) delineation of the gross tumor volume (GTV). Additionally there is an uncertainty in the extension of clinical microscopic disease, why a clinical target volume (CTV) is defined by adding a margin to the GTV. Finally the planning target volume (PTV) is defined [33], based on any residual uncertainties and errors, in order to ensure that the prescribed dose is delivered to the CTV with an acceptable probability. In radiotherapy of lung cancer the CTV to PTV margins is most commonly based on

the method introduced by van Herk [8]. The concept relies on taking all systematic and random error components, related to any part of the treatment preparation or treatment delivery, into account and calculating the CTV to PTV margin using population based statistics. In this context it is important to emphasis that margins should be defined based on the statistics of the specific clinic, using statistics from applying the IGRT and treatment delivery techniques available at that specific site. As has been observed in many studies before, the choice of positioning strategy and treatment technique will influence the size of the margins needed [11].

2.2.1 Motion encompassing methods

Motion management has in its beginning been dominated by the use of methods where the motion of the target has been encompassed into the delineation of the GTV. This is to date still a very common approach and over the years different strategies have been developed on how to make use of the motion information acquired during free-breathing 4DCT. The structure created based on the tumor and a motion-encompassing safety margin is called the internal target volume (ITV) [33]. Delineation can be conducted by adding structures delineated at every phase of the respiratory cycle or by the use of the so called maximum intensity projection (MIP) [34]. By this approach the target dose coverage is ensured at any point during beam on, given that the tumor moves as imaged on the 4DCT. However, this approach will simultaneously also inherently result in a high dose to the surrounding lung tissue and any other adjacent normal tissue.

A similar method to the ITV approach is the use of a probabilistic calculation of the safety margin by considering the tumor motion as randomly distributed positioning errors [8]. The probabilistic safety margin is added to the GTV delineated on the breathing phase closest to its time-weighted average position, the so called mid-ventilation (MidV) phase. In this way, the MidV concept results in a smaller treatment volume than the ITV approach, while still achieving dose coverage with an acceptable probability.

2.2.2 Gating

Both the ITV and MidV concepts are managing the motion in a passive manner, with the latter giving rise to smaller irradiated volumes. In order to further reduce the irradiated volume there are approaches to motion management where irradiation is carried out in a single phase or a few phases of the breathing cycle by using real-time information on the tumor position. By this so called respiratory gating approach the beam is on only at a predefined tumor position window, or gating window [13]. The gating window is either set to match with the expiration or inspiration phases of the free-breathing cycle in order to maximize the duration of the window. However, an immediate drawback of this approach will still be an increase in treatment time due to a low duty cycle as the beam on time is limited to only a fraction of the breathing cycle.

In free-breathing respiratory gating it can be beneficial to treat during the inspiration phase as it usually has a longer duration than the expiration phase. Additionally it has a small advantage in an increased lung volume which will help in sparing the lung tissue. This benefit is further enhanced if the gating window is moved closer to the inspiration maximum which is utilized in the deep-inspiration breath-hold (DIBH) technique (Figure 2). DIBH furthermore benefits from an increased inspiration level as it also can increase the distance between the target and critical organs such as the heart. Studies suggest that the DIBH approach helps in sparing normal tissue when used in lung cancer radiotherapy [14]. Despite the elimination of uncertainties related to the respiratory motion, the breath-hold approach might introduce uncertainties due to e.g. variations in breath-hold level from breath-hold to breath-hold or fraction to fraction. It will therefore be important to incorporate this into the safety margins added to the target [11]. However, it should be noted that the uncertainties depend on the motion monitoring system used (marker, surface, internal or external) and whether or not visual and/or audio feedback is utilized.
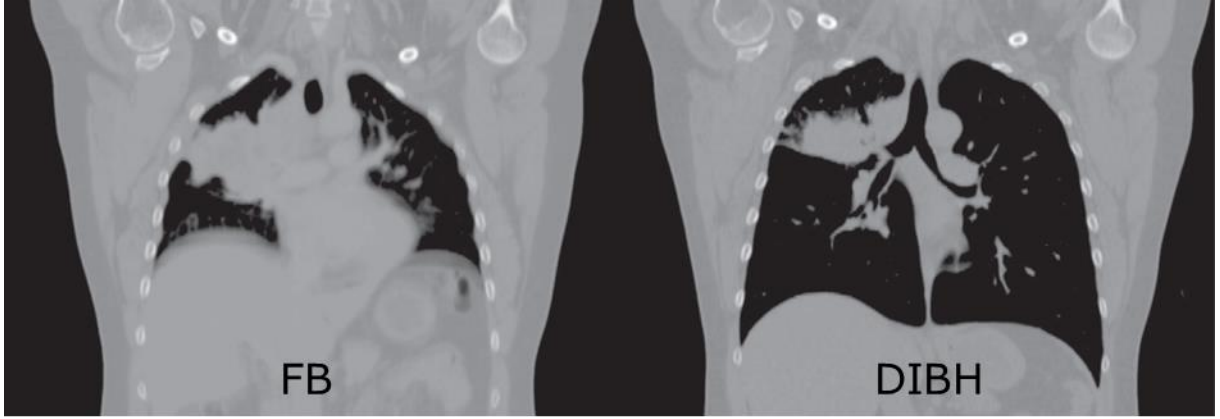
Figure 2. Coronal slices of a NSCLC patient CT scanned in both free-breathing (FB) and deep-inspiration breath-hold (DIBH). The increase in total lung volume for this patient was by Ottosson *et al.* observed to be 167% in DIBH (figure adopted with permission)[14].

2.2.3 Tracking

Tumor tracking is another methods using real-time information about the target position. However, in contrast to the respiratory gating techniques, tracking has the aim of delivering the treatment during the entire breathing cycle without significant increase in treatment time. By continuously compensating for the tumor motion in real time a 100 % duty cycle can be achieved without increasing the treatment volume. The tracking method can be realized by either following the target motion using continuous compensation of the dynamic beam configuration [35–40], or by using a robotic treatment couch in order to move the patient in the opposite path of the real-time monitored internal motion [41–43].

The actual method for locating the tumor in real-time is needless to say essential in any implementation of tumor tracking. Methods including kV-based imaging [44], combined kV/MV imaging [45] and electromagnetically guided tracking [46] have proven feasible. However, many of the motion tracking systems currently rely on the use of implanted markers and are thereby invasive and only a surrogate to the true 3D internal motion. With recent developments of magnetic resonance imaging (MRI) LINACs there is a possibility to conduct non-invasive real-time tumor tracking in 3D without the use of ionizing radiation [47]. MRI-guided tumor tracking has been proven feasible and will mostly likely emerge further in the near future as new systems are validated and the quality and consistency is ensured [48–50].

One important aspect to consider is the uncertainties related to many of the above mentioned tracking methods. The major contributor to the geometrical errors has been reported to be the latency between the target motion and its realignment with the beam [51], measurable using e.g. continuous portal imaging or portal imaging in combination with linac MLC logfiles and tracking logfiles [52,53]. Using measurements of the latency it is not only possible to locate the contributors to it but also to use the information in order to reconstruct the actually delivered target dose. In the current state of tumor tracking, the latency is present for all methods and therefore continually updated motion models might be a solution for better prediction of how to correct the beam or treatment couch in order to compensate for the internal motion.

2.3 Managing inter-fractional changes

Efforts on minimizing the added safety margins, accounting for not only motion but also systematic and random errors related to baseline shifts and delineation, have been carried out by improvements in the use of 4DCT and complex treatment techniques, as covered in the sections above. Additionally, daily positioning by soft-tissue match on the tumor has proven to reduce the margins caused by errors associated with using surrogate structures such as bony anatomy for setup [11,54]. However, studies suggest that inter-fractional variations due to anatomical changes have larger impact on the delivered dose to the target compared to

errors due to setup uncertainties and breathing motion [15]. It has furthermore, previously been concluded that managing inter-fractional anatomical changes in standard fractionated radiotherapy in free-breathing require individualized adaptive strategies [15,28,55].

Statistics extracted from lung cancer patients treated in the radiotherapy department at Herlev & Gentofte Hospital showed that around 25% of the patients had anatomical changes. Changes were related to pleural effusion, atelectasis, tumor shrinkage or pneumonia/pneumonitis, with the appearance or disappearance of atelectasis dominating the statistics. Literature with similar statistics support the observed prevalence of anatomical changes [28], and furthermore mentions the risk of tumor or organ shift due to the changes. Additionally an adaptive strategy was considered necessary for 12% of all the patients included. What is perhaps most noteworthy is that lung tissue changes due to pleural effusion or atelectasis was found to randomly appear and disappear during the course of treatment. Basically, if conducting CBCT imaging only on a weekly basis an atelectasis change could take place and disappear again in between the two imaging fractions without being discovered. Therefore daily CBCT imaging with soft tissue visualization is yet again recommended for the treatment of lung cancer patients.

Moving towards treatment techniques such as DIBH, where the breathing motion has been mitigated, the effects of anatomical changes dominate even more over the intra-fractional uncertainties and having an adaptive strategy therefore becomes even more essential. Adaptation requirements due to anatomical changes in DIBH was therefore investigated and compared to corresponding requirements for free-breathing, both for standard fractionated and dose-escalated treatments. Details on this study have been presented in Paper I and the quantitative methods as well as the dosimetric implications are further discussed in section 2.3.1 below.

2.3.1 Dosimetric effects of anatomical changes

The anatomical changes discussed in the context of lung cancer radiotherapy are changes resulting in an alteration of tissue density and / or geometrical displacements (Figure 3). Appearance of atelectasis is the collapse or closure of the lung or at least parts of it, resulting in a volume of higher density. Disappearance of atelectasis will have the opposite effect as the re-opening of the lung allows air flow and again reduces the density. Similarly, the fluid in the lung caused by pleural effusion will give rise to an increase in density in that part of the lung. With the patient lying supine on the treatment couch this fluid-filled area is usually located posteriorly as gravity plays its role. Inflammation of lung tissue caused by pneumonia/pneumonitis will also increase the lung tissue density as it appears. What might be challenging with pneumonitis are the diffuse changes in density taking place rather than the distinguished changes in density as caused by atelectasis and pleural effusion. Finally, tumor shrinkage is also a change in density which is important to take into account despite it being a direct response to the treatment of the target and is not considered an anatomical change in the same context.
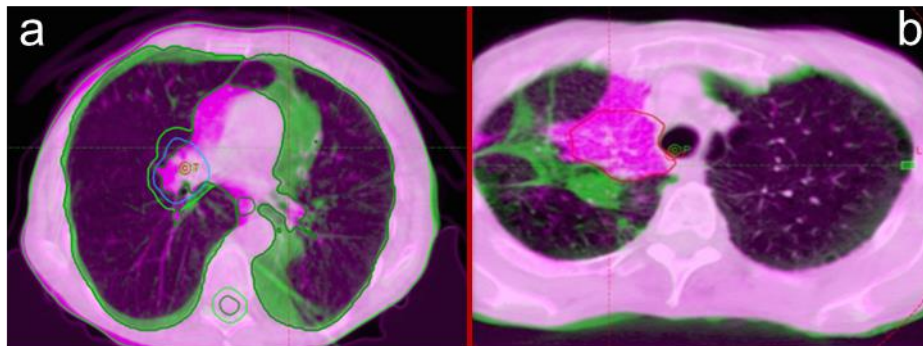
Figure 3. Clinical examples of anatomical changes in the form of density alterations with potentially severe dosimetric impacts if not accounted for. The examples include a) the appearance of an atelectasis in the dorsal region adjacent to the columna with a resulting shift of the entire mediastinum, and b) the appearance of pneumonitis and the disappearance of an atelectasis just anterior to the tumor location, causing a dramatic shift in the tumor position.

Thankfully, CBCT soft tissue visualization is readily available giving the possibility to react on any detected geometrical or anatomical changes. Adaptive radiotherapy (ART) is the concept of mimicking the dose distribution, or at least certain dose volume histogram based parameters or constraints, of the original treatment plan as much as possible by making adjustments to the plan as a reaction to the detected density changes. In order to enable re-planning it is first of all necessary to re-scan the patient according to the same procedure as for the original treatment plan; i.e. either by e.g. free-breathing 4DCT or breath-hold CT. Thereafter new delineation and re-planning can be conducted.

The process of re-planning is, however, cumbersome and puts a heavy workload on the entire chain of pre-treatment preparations. Due to limited amount of time it is furthermore not always possible to adapt from one treatment day to the next, possibly creating an extra gap between fractions. Methods are therefore applied in order to first quantify the dosimetric effects of the detected changes before initiating the full process of re-planning. Quantification of dosimetric effects caused by anatomical changes can be carried out directly based on the patient-specific CBCT acquired, but can also be carried out in advance for changes that can be considered standard. Performing re-calculations on CBCT directly would probably be the fastest way of estimating the dosimetric effect of anatomical changes. However, the length of the CBCT scan does not always include the entire extension of the target area and the image quality is, furthermore, inadequate making it impossible to achieve an acceptable level of dose uncertainty. Instead the changes observed in the acquired CBCT can be delineated and propagated over to the planning CT, where density override and recalculation is then carried out. The drawback of this solution is the added uncertainties related to delineation, image registration and Hounsfield Unit (HU) specification. However, the uncertainties are relatively small and the approach serves as a feasible method to determine whether or not to re-plan.

In Paper I density alterations directly in the planning CT were carried out in order to mimic tumor shrinkage and pleural effusion. The changes of the CT information were performed in a heterogeneous phantom (CIRS IMRT thorax phantom; CIRS, Inc., Norfolk, Virginia, USA) as well as on sixteen patients scanned in both free-breathing and DIBH. On all CT scans the anatomical changes were simulated by step-wise adding simulated fluid in the dorsal region and by step-wise decreasing tumor size in the regions adjacent to lung tissue. The systematic increase in simulated pleural effusion and tumor shrinkage was a method to enable distinction of certain levels below which the dosimetric effects were low enough not to require any treatment adaptation. The novelty of the study lies in the application of the method on standard as well as dose-escalated treatment plan in both free-breathing and DIBH. In this aspect the main conclusion of the study was the potential benefit of using DIBH instead of free-breathing regarding the robustness of mean GTV dose to tumor shrinkage.

Note that geometrical changes (e.g. shifts), pneumonitis and atelectasis were left out from the systematic determination of the adaptation requirements in this study. The reason for that was the consideration of these changes being patient-specific, with diffuse density changes, and highly dependent on the location and size of the tumor as well as the change itself. Individualized estimation of the dosimetric effects of any of these changes is therefore recommended immediately at the stage of detection. As previous studies have indicated [15], the change of large volumes with atelectasis have the greatest impact, and that is also indicated by the fact that the tumor shrinkage, i.e. the density changes close to the irradiated volume, had greater effect than pleural effusion on both target coverage and dose to the spinal cord.

The impact of Paper I in the clinical practice in the radiotherapy department at Herlev & Gentofte Hospital has been the introduction of what might be referred to as a form of traffic light system (Figure 4). The study supported in the determination of the action levels used to determine whether or not to move on with an adaptive process. In the clinical practice geometrical and anatomical changes are now analyzed in terms of magnitude in relation to two different action levels. Below the first no action is needed, while consultation is required between the two levels and immediate action is mandatory if above the higher action level. By introduction of such a system the workload has reduced significantly as only those cases where adaptation is truly needed will go through the re-planning procedure. The study furthermore supported the establishment of

DIBH as a valid solution for radiotherapy of NSCLC patient. DIBH has since been clinically implemented at Herlev & Gentofte Hospital as a routine approach for tumors with motion amplitude > 10 mm.

	d = deviation	Treat	X	Call physicist
T	Deviation of tumor	d ≤ 3mm	3 mm < d ≤ 10 mm	d > 10 mm
N	Deviation of lymph nodes	d ≤ 5 mm	5 mm < d ≤ 10 mm	d > 10 mm
K	Deviation of the spinal cord	d ≤ 5 mm	5 mm < d ≤ 10 mm	d > 10 mm
	VRT	d ≤ 5 mm	5 mm < d ≤ 10 mm	d > 10 mm
	LAT	d ≤ 10 mm	10 mm < d ≤ 15 mm	d > 15 mm
	LNG			
S	Tumor shrinkage	d ≤ 5 mm	d > 5 mm	Tumor not visible
MB	Deviation: Mediastinum (M)	d ≤ 10 mm	d > 10 mm	Match on T, N or C not ok
	Body (B)	d ≤ 15 mm	d > 15 mm	
APE	Atelectasis (A)	None A	Match ok	Match not ok
	Pneumonia (P)	None P	Match ok	Match not ok
	Pleural effusion (E)	E ≤ 10 mm	E > 10 mm	Match not ok
T2	Deviation of secondary tumor	d ≤ 5 mm	5 mm < d ≤ 10 mm	d > 10 mm
			3 X → Send to extra physicist check	

Figure 4. Table with thresholds for the different positional deviations or anatomical changes that can occur during treatment of NSCLC patients. The table is a screenshot of the tolerance levels implemented, with the support of the findings in Paper I, in the Radiotherapy Department, Department of Oncology, at Herlev & Gentofte Hospital.

3 Time-resolved dosimetry in a moving lung

3.1 Dosimetric challenges in the thoracic region

With an adaptive strategy in place the inter-fractional changes are handled and a method to react on dosimetric changes is in place. Remaining then is a method to ensure that the delivered dose is the expected and that it is not altered due to the intra-fractional variations, mainly caused by breathing motion. However, dosimetry in the thoracic region is a challenging task putting high demands on dose calculation algorithms as well as experimental methods. In order to cope with the dosimetric challenges it is first of all important to understand how ionizing radiation is delivering its dose to the medium in radiotherapy. Medical LINACs are based on the acceleration of electrons and the production of bremsstrahlung photons by collision in a target placed in the LINAC head. The photons produced are then collimated in order to shape the treatment beam according to the target volume inside the treated object. Throughout this study a 6 MV beam on a TrueBeam (Varian Medical Systems) has been used for all treatment planning and delivery. In this context, 6 MV denotes a photon spectrum produced by the use of electrons accelerated to an energy of 6 MeV. The photon beam produced from that acceleration is a spectrum of photon energies ranging from 0 MeV up to a maximum of 6 MeV, with a mean energy around 1.5 MeV. This implies that the ionizing radiation of a 6 MV photon beam predominantly interacts by Compton scattering[56]. The Compton Effect is the scattering of the primary photon with parts of its initial kinetic energy being transferred to an electron in an outer layer of an atom. Thereby the result is a scattered photon with less energy than the primary photon and a recoil electron carrying the transferred kinetic energy subtracted by its initial binding energy. The energy transferred to the secondary electrons is referred to as the kinetic energy released per unit mass, KERMA (K). However, when considering the interaction of the incident photons with matter it is clear that the energy is not deposited to the medium by the photons directly. Instead it is the secondary electrons that, by elastic and inelastic scattering, interact with the medium and deposit the energy as ionization or excitation. The interactions of the secondary electrons result in either local deposition of energy due to collisions or transfer of energy to photons by radiative bremsstrahlung. The KERMA can therefore be split up into two parts and be describe according to $K = K_{col} + K_{rad}$, where the subscripts *col* and *rad* represents the collision and radiative KERMA, respectively. As the photons produced through bremsstrahlung will transport their energy away from the area of interest, the collision KERMA can be considered a good approximation of the locally absorbed dose in the medium. The absorbed dose to a medium, D_{med}, or rather the mean energy, $d\bar{\varepsilon}$, imparted by ionizing radiation to a mass, dm, can thus be expressed in relation to the photon fluence in the medium, $(\Phi_E)_{med}$, as

$$D_{med} = \frac{d\bar{\varepsilon}}{dm} = /CPE/ = K_{col} = \int_0^{E_{max}} E(\Phi_E)_{med}\left(\frac{\mu_{en}}{\rho}\right)_{med} dE, \qquad \text{Eq. 1}$$

where $(\mu_{en}/\rho)_{med}$ is the mass energy absorption coefficient of the medium, describing the fraction of incident photon energy resulting in local dose deposition and the absorbed dose is given in the unit Gy (J/kg). However, a prerequisite to describing the absorbed dose as collision KERMA is the presence of so called charged particle equilibrium (CPE) and this is the root cause to the major challenges for dosimetry in heterogeneous geometries, such as the thorax. Basically, CPE requires that the number of charged particles of a given type and energy transported out of the volume to equal the number of particles with same properties entering. This is typically not true when leaving a low density medium and entering a higher density material, due to the rather long range of the secondary electrons. Therefor a lack of CPE is present at shallow depths and not present until a depth approximately corresponding to the range of the secondary electrons is reached. Additionally, lack of CPE exists if e.g. the treatment field size is smaller than the range of the secondary electrons. As heterogeneities translate into a volume including media of different densities, it is clear that the secondary electron ranges will differ depending on the media they are currently in. In the case of lung cancer radiotherapy, the targeted tumor is usually surrounded by low density lung tissue, where the electron ranges are much longer than in soft tissue, resulting in the lack of CPE at least in the edges of the tumor (depending on the dimensions of the tumor).

3.1.1 Dose calculation solutions

Many commercial treatment planning systems (TPSs) use dose calculation algorithms that suffer from challenges to handle the lack of CPE in the proximity of heterogeneities such as air cavities, lung and bone [14,57–59]. All treatment planning described in this thesis was carried out using the Anisotropic-Analytical-Algorithm (AAA) provided in the Varian Eclipse TPS (Varian Medical Systems). The algorithm is described as a three source pencil-beam convolution-superposition model and has previously been described in detail and been thoroughly tested, also in terms of its ability to handle heterogeneities [60–63]. The three sources are attributed to the primary photons (defined as a point in the focal spot of the target), the scattered photons (scattered in the components of the LINAC head), and the contaminating electrons (due to photon interactions in the LINAC head). The defined beam is split into what is referred to as beamlets, and the final dose distribution (based on information on material electron density and geometrical cross-sections) is calculated by superpositioning the dose from all three sources for each beamlet. As AAA handles the energy deposition by separating the sources into a depth component and a lateral component, the inhomogeneity correction will also be divided into two parts where they are independently scaled using the inverse relative electron density. With an initial dose kernel calculated in water, this scaling approach implies that all the voxels in the geometry are considered as water but with varying density. Similar to most commercial algorithms, AAA is therefore based on approximations, which are mainly applied in order to reduce calculation times. For AAA the major approximations influenced by the presence of heterogeneities result in the scatter of secondary particles not being correctly accounted for and also in the smoothing of lateral dose distributions in tissue boundaries [60,64].

The accuracy of AAA in calculating dose to a tumor surrounded by lung tissue was especially of interest during the investigation of the dosimetric effects of anatomical changes (section 2.3). A comparison of AAA calculated dose with measurements was therefore carried out. A previous study has reported that the AAA (v.10) calculated dose for delivery on an iX LINAC (Varian Medical Systems) underestimates the dose in the center of the tumor with an increasing deviation for decreasing tumor sizes as compared to scintillator measurements [65]. In the present study, one conventional single open field plan and one RapidArc plan (both 6 MV) were created for the more modern TrueBeam LINAC on a standard 3DCT of an in-house developed thorax phantom designed to enable scintillator dosimetry (further described in section 3.2). Treatment planning and dose calculation was carried out in the Eclipse TPS using AAA (v.13.6). Additionally, the treatment plans were in this study recalculated, preserving the number of monitor units (MU), using the more modern Acuros algorithm (Varian Medical Systems) [66].

Comparison between the two dose calculation methods and measurements were carried out based on the dose in the center of spherical tumors of varying dimensions (1-9 cm in diameter) inside a 9 cm wide cylindrical lung insert (Figure 5). While results demonstrate how Acuros calculations are within 1% from the measured dose for most tumor sizes (except for the 1 cm tumor), the results clearly demonstrate the limitations of AAA with an increasing deviation as the tumor size decrease. This supports and extends the findings in the previous study [65] demonstrating that the limitations of AAA dose calculations in the thoracic region are independent of treatment machine and delivery technique. Noticeable is however that for the completely homogeneous setup (9 cm) the AAA algorithm performs better than the Acuros algorithm, supporting previously reported results from similar comparisons in a homogeneous setup [67].

The results are also an indication of how different approaches to tissue inhomogeneity corrections manifest as better or worse accuracy in dose calculations in crucial geometries such as the thorax of a lung cancer patient. In order to fully account for the lack of CPE it is necessary to explicitly account for heterogeneities instead of applying corrections based on approximations. This is carried out in Monte Carlo (MC) based solutions where photon interaction probabilities are employed together with an explicit model of the electron scatter in any geometry. The benefits of MC and further description of the codes developed and used in this thesis are presented in Chapter 4.
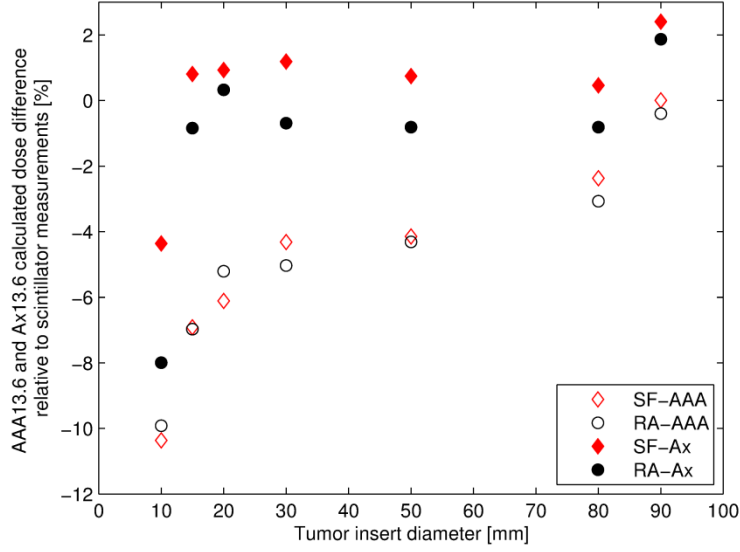
Figure 5. Dose differences between calculations and scintillator measurements for a single open field (SF) and a RadpidArc (RA) plan calculated with the AAA and Acuros algorithms. Results presented for treatments delivered to the thorax phantom for a set of tumor sizes ranging from 1 to 8 cm in diameter (9 cm equals homogenous PMMA geometry).

3.1.2 Scintillator dosimetry

Measuring the absorbed dose to a tumor surrounded by low-density lung tissue is challenging similarly to dose calculations in that same geometry. The material and size of the detector used will impact the reliability of measurements in such scenarios and it is therefore important to search for an optimal detector under these conditions. In addition to searching for a detector suitable for dosimetry in heterogeneous geometries the present thesis also focuses on being able to perform time-resolved measurements as the current state of art in lung cancer radiotherapy include dynamic treatment techniques using real-time motion information (see section 2.2).

Traditionally, dose verification in radiotherapy is based on comparisons of the expected and actually delivered accumulated dose. Measurements have often been performed using a single, or an array of, ionization chamber(s) or diode(s). For complex treatment techniques such as e.g. tracking there is, however, a need to resolve the dose as a function of time. With the use of time-resolved dosimetry it can be possible to distinguish the underlying cause of a potentially failed delivery, even if it is not so from an analysis based on only the accumulated dose. Treatment delivery can fail due to many factors, such as e.g. inconsistent MLC motion, gantry motion, and interplay effects. By locating the point in time where the dose deviations occur the root cause will be easier to uncover. Time-resolved dose verification methods have previously been presented based on the use of electronic portal imaging devices (EPID) [68–70], fiber-coupled aluminum oxide crystals [71], as well as the Scandidos Delta4 diode array [72]. However, in the present thesis the aim was to perform time-resolved measurements in a thoracic-like geometry, mimicking not only the heterogeneous anatomy but also including the internal respiratory-induced motion.

Fiber-coupled plastic scintillator detector (PSD) have the ability to record dose per pulse with an impressively low uncertainty and have been proven to be suitable for dosimetry in that kind of complex geometry and for small, complex and dynamic megavoltage (MV) photon beams [73–77]. Therefore, all measurements in this thesis were conducted using a BCF-60 PSD (Saint-Gobain Ceramics & Plastics Inc.), with a diameter of 1 mm and a length of 2 mm. The PSD was used in combination with the in-house developed ME40 scintillator

13

dosimetry system and the setup has previously been described and further studied for its potential use in time-resolved verification of dynamic radiotherapy [75,77]. In summary, studies conclude that the PSD system, with a 0.1 ms readout and mm spatial resolution, is well suited for detailed time-resolve measurements in small dynamic radiotherapy dose increments.

Chromatic removal (stem) calibration of the PSD was conducted according to the procedure (method C) described by Guillot *et al.* in a solid water calibration phantom [78]. The stem calibration together with an absolute dose calibration was applied to the ME40-based measurements according to a procedure previously described [79].

3.2   Dynamic thorax phantom

With the choice of BFC-60 PSD as the primary detector for all measurements conducted in this thesis, there was a need to find a thoracic-like phantom where the positioning of the PSD inside a moving tumor was enabled. Commercial solutions at the start of this thesis did not facilitate such requirements and a dynamic thorax phantom was thus developed in-house. In Paper II the development of the dynamic thorax phantom as well as its combination with the ME40 PSD system is described in detail. The aim of that study was to develop and validate a novel dosimetry system, combining and synchronizing an in-house developed dynamic thorax phantom with an in-house developed PSD dosimetry system. In sections 3.2.1-3.2.3 the design of the phantom, the motion controlling software and its synchronization with LINAC trajectory logfiles is summarized.

3.2.1   Phantom design

The design of the phantom body has previously been described in detail [80] and aimed at mimicking the thorax of a lung cancer patient. It was designed and built with the purpose of having a well-defined geometry. One of the most important aspects was the decision on material composition, why the body consists of PMMA, the simulated lungs consist of low-density balsa wood and the tumors are made out of PMMA. These choices were made based on the densities and there equivalence to soft-tissue and lung tissue. Furthermore in order to mimic the cortical bone of the spine, delrin was chosen as material for the cylindrical insert to be placed in the posterior region of the phantom. All dimensions of the phantom aimed at mimicking a standard lung cancer patient. The outer dimensions of the body were therefore decided to have a width of 34 cm, height of 23 cm and length of 40 cm (Figure 6). Furthermore the body was the capacity to hold three larger hollow cylinders (50 cm in length, 10 cm in diameter) with the purpose of making the choice of geometrical composition flexible. The cylinders can therefore be filled with different inserts in order to simulate either hetero- or homogeneous geometries. The standard setup would be to fill the central cylinder entirely with PMMA while the two lateral cylinders would also include balsa wood inserts positioned centrally in the longitudinal direction. Also the dimensions of the lung inserts were built in order to mimic the dimensions of a standard lung (15 cm in length and 9 cm in diameter). To further add to the flexible geometry, the PMMA spheres simulating lung tumors were built in multiple diameters ($1 - 8$ cm) implying that also the balsa wood inserts were built with different cavity sizes in order to embed the PMMA spheres in the simulated lungs. The design of the inserts enables PSD measurements in the center of the tumor.

3.2.2   Controlling the motion

In order to replicate the respiratory motion of a lung cancer patient, the thorax phantom was connected to a motorized linear stage (A-LST0250B-C, Zaber Technologies Inc.) using a PMMA rod mounted on the stage and attached to the end wall of one of the lateral cylinders (Figure 6). The linear stage has a built in controller with a motion range of 254 mm. The motion is driven by a 2-stepper motor with a unidirectional uncertainty of 63 μm. Controlling the motor can be achieved by using the vendor provided Zaber Console software, with a limited amount of pre-defined commands available. However, it can also be controlled by developing a LabVIEW (National Instruments) script with or without the use of a library of instrument

drivers provided by the manufacturer. One important aspect behind the choice of the stage was the maximum force accessible as it needed to be able to move the cylinder insert at a range of various velocities. This specific stage has a capacity for the lowest velocity (0.0047 mm/s) to apply a force 350 N in the direction of motion, which was considered sufficient.

In order to simulate a complex realistic dynamic breathing motion of the tumor and lung insert, a LabVIEW script for controlling the motion of the linear stage was in-house developed. This was partly based on the vendor-provided instrument drivers. The development was a process of trial and error, where first of all communication between the motion controlling software and the stage was a major issue. The stage was during irradiations positioned far from the computer in the control room where the script was located. This implied the need for adapters along the way which in the end were discovered to disturb the signal. With the correct combination of cords and adapters the communication issue was resolved. Communication between the script and the linear stage was in the final version conducted through a 115200 baud RS232 serial port. While the communication issue was resolved it was not trivial to introduce continuous motion of the stage. However, by scripting a method to update the velocity rather than requesting a move to a new position, a continuous motion was possible. The final script therefore operates by first moving the cylinder insert to a home position, most often corresponding with the center of the phantom in this thesis for an optimal position of the lung insert and tumor before initiating the accelerator beam and scintillator measurements. However, this is fully optional and can be defined in the user interface of the script. The motion of the cylindrical insert is initiated by making a choice of requesting a simple built-in motion or by providing an input file describing the desired motion. The input should include the expected position as a function of time and can be manually generated or based on a patient-specific breathing pattern. During motion the motion controlling software records the position as a function of time and continuously updates the velocity of the stage in order to continue along the desired motion pattern.

3.2.3 Synchronization with linear accelerator

The positional information from the phantom motion software was required to be synchronized with the measurements in order to fully enable time-resolved dose verification of dynamic radiotherapy using the ME40 scintillator dosimetry system [75]. Synchronization was achieved using an external 10 V ramp signal (period: 6 s), simultaneously recorded by both systems. One essential aspect of synchronizing the motion of the phantom with the ME40 system is the simultaneous synchronization with the LINAC log files, as the ME40 system is triggering on the treatment beam sync pulse. This enables the use of the dynamic thorax phantom dosimetry system as tool for validation of time-resolved dose calculation solutions, e.g. based on Monte Carlo simulations, also contributing to a valuable tool for quality assurance of respiratory-guided radiotherapy.
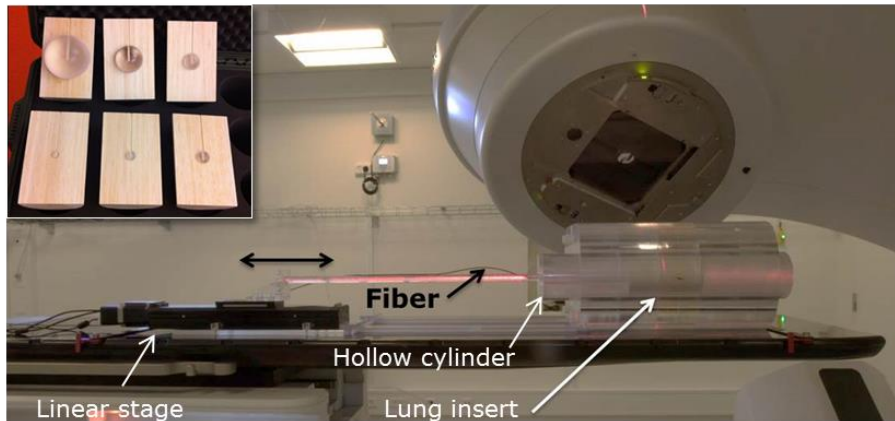

Figure 6. The dynamic thorax phantom set up on the treatment couch and connected to the linear stage for full control of the motion of lateral cylinder insert. In the upper left corner is an illustration of the balsa wood insert and various tumor sizes available.

4 Monte Carlo simulations

In section 3.1.1 the known challenges and limitations of the commercial dose calculation algorithm (AAA) used for treatment planning in this thesis were discussed. The demonstrated limitations in accurately calculating dose in heterogeneous geometries were mainly attributed to approximations in the methods applied to correct for geometrical density variations. A brief comparison to measurements and a different commercial solution (Acuros) demonstrated that a more complex method to correct for inhomogeneities can achieve higher accuracy in the dose calculated in a thoracic-like phantom. However, in order to completely calculate dose accurately in heterogeneous geometries with lack of CPE the material and density variations must be accounted for.

Monte Carlo has the highest accuracy for radiotherapy dose calculation and is considered as the gold standard [81–84]. In MC every primary photon is transported through the LINAC head and the patient or phantom geometry. Each interaction is randomly sampled and cross-section data is used to describe the results of the event. That implies that probability distributions are applied in order to determine every detail of the interaction taking place; including the change in particle direction, the energy deposited, and the production of secondary particles. The same method is then applied to all secondary particles. For the photons the tracking of each interaction is feasible due to the sparse distribution of events taking place. For the electrons, however, a condensed history approach is applied as the number of interactions is much higher and accounting for all the interactions would be time-consuming. Furthermore, the electron interactions predominately result in small energy depositions and directional changes why a cluster of electron interactions can be considered to occur in a single step. With the MC approach described here it is therefore clear that material and density variations in the dose calculation geometry is explicitly accounted for as each event is followed based on cross-section data specific for the voxel of interaction. The statistical nature of the MC method does, however imply that there will be an associated statistical uncertainty that needs to be minimized by simulations of a large number of particles. Why this is essential in time-resolved MC simulations and how it can be handled is described further in section 4.3.

4.1 The EGSnrc user code

In the present thesis all MC simulations have been carried out within the EGSnrc package [85]. The EGS part of the abbreviation for this user code is short for electron gamma shower, and describes the fact that it is able to handle transport of electrons (and positrons) and photons, while nrc indicates that it has been developed by the National Research Council in Canada. The particle transport of neutrons and protons are therefore not possible to simulate. Within the EGSnrc package there are a number of specific purpose codes designed to transport particles through specific geometries such as the LINAC head, cylindrical or cubic voxelized patient/phantom geometries, and cavities. The specific purpose codes utilized here for simulation of particle transport through the LINAC head and the patient/phantom dose calculation geometry were BEAMnrc and DOSXYZnrc, respectively.

4.1.1 BEAMnrc

BEAMnrc is an extension of EGSnrc enabling simulations of a LINAC head with the use of a set of component modules (CMs) [86]. The CMs model the components of the head (e.g. monitor chamber, flattening filter, etc.) as defined by a set of geometrical parameters written in plain text. In the input files for the BEAMnrc simulation a set of further specifications are defined, describing e.g. the primary source, particle transport parameters and scoring plane. The required input parameters will, however, vary between different so called source routines. Throughout this thesis a source routine, SOURCE 21, was applied as it enables the use of a phase space file as a description of the primary source. This is necessary in the case of simulating the Varian TrueBeam accelerator as the vendor instead of providing the user with the geometrical specifications of all its components provides a phase space file scored below all the static components of the LINAC head.

With the use of this source routine it is instead required to input the path to the specific phase space file, together with a specification of the charge of the particles and which CM they are incident on (in this case above the collimator jaws). The end result after running the BEAMnrc simulation will be another phase space file, which then can be used as the input source for particle transport through further components in the LINAC head or in the dose calculation geometry.

4.1.2 DOSXYZnrc

In order to simulate the dose deposition in the patient or phantom geometry the DOSXYZnrc user code requires a voxelized representation of it. In the present thesis all simulations were carried out in geometries with material and density specified in predefined MC phantom files (.egs4phant). As for BEAMnrc there are multiple source routines to be used in DOSXYZnrc. The SOURCE 20 routine is to be use in the case where the particle source is a BEAMnrc-produced phase space file and when the aim is to simulate a dynamic treatment delivery with continuous variation of the incident angle [87]. In addition to specifying the path to the phase space source as well as the phantom file, source 20 based DOSXYZnrc input files should hold information in the form of a number of sets of parameters. These include information on the incidence angles, isocenter location and distance from scoring plane to isocenter. Additionally, in the method applied in this thesis, the MLC simulation is conducted within the DOSXYZnrc simulation using an external SYNC based BEAMnrc simulation. For every set of parameters there is an associated index, functioning as a scaled version of the MU index, ranging from 0 to 1. The parameter set for each incident particle is chosen by random selection of an index, between 0 and 1, and the following particle transport is then handled by EGSnrc. In this manner the temporal information is shared between the BEAMnrc and DOSXYZnrc simulations. The resulting calculated dose in each voxel is output as absorbed dose per incident particle together with an associated statistical uncertainty [88]. The output is listed in a .3ddose file with same dimensions as the calculation geometry.

4.2 Four-dimensional Monte Carlo

Sharing temporal information between the simulations of the particle transport through the linac head with the simulation in the patient geometry implies the possibility for separately defined dose calculation geometries for each primary particle. This opens up for interesting methods for 4D dose calculations of dynamic beam delivery to a moving, or even deforming, anatomy.

Several methods have been developed to calculate dose in time-dependent geometries and one of the first methods was the convolution approach. Describing the respiratory breathing pattern as a probability density function (PDF) enabled the possibility for convolution of the dose or the incident beam fluence by the PDF [89–92]. These methods are able to account for the dose blurring due to the internal motion, and the fluence convolution approach furthermore accurately account for the spatial dependence of the dose distribution. However, the limitation of the convolution methods is the fact that it only handles rigidly moving anatomies, while deformations can not be accounted for. More accurate approaches have since been developed, taking also deformations, density variations and differential organ motion into account. The concept of synchronizing dynamic beam delivery and patient motion in 4D dose calculation and the evolution of the different methods available has previously been well described in the literature [93]. These methods include dose-mapping methods, energy-mapping methods, and the voxel warping method, further described in section 4.2.1.

4.2.1 Four-dimensional dose calculation methods

Dose-Mapping methods

The most straightforward method of 4D dose calculation is possibly the dose-mapping approach. Using this method generally imply that dose is calculated on different respiratory phases and accumulated by applying a time-weighted factor based on the fraction of the total breathing cycle that the chosen breathing phases occur.

Since the first introduction of dose accumulation methods in radiotherapy [94], there have been several studies using the approach [95–97]. What is noteworthy with this approach is that it is applicable to any dose calculation algorithm, even if many of these studies utilized the superior accuracy in Monte Carlo for use in heterogeneous anatomies. All dose-mapping methods do, however, require information about the transformations between the reference geometry and the target geometries in order to facilitate dose accumulation based on the energy deposition in the variable geometries. This information is often acquired from rigid or deformable image registration [98]. For the purpose of a deforming anatomy in radiotherapy dose calculation the determination of a deformation map using deformable image registration is preferred.

There are a variety of options regarding the transfer of dose between the different CT data sets. One common method is based on mapping the center of voxel between the reference CT data set and the target CT data sets of the respiratory phases. The deformation map is applied in order to find the location of the target voxel corresponding to the reference voxel of interest. The dose in the target voxel including the deformed center of mass is then remapped back to the reference voxel. However, there may be several voxels overlapping with the deformed reference voxel and the use of remapping the dose in the center of mass ignores this fact. Instead, interpolation methods have been introduced where contributions from neighboring voxels in the secondary data sets are interpolated to the voxel containing the transformed COM of the reference voxel [99]. The deformation vectors are applied to each voxel in the reference dose grid (x,y) in order to find the corresponding location on the target dose grid (x',y') (Figure 7 a). The dose in the neighboring voxel are then linearly interpolated on the target dose grid and copied back to the reference dose grid (Figure 7 b).
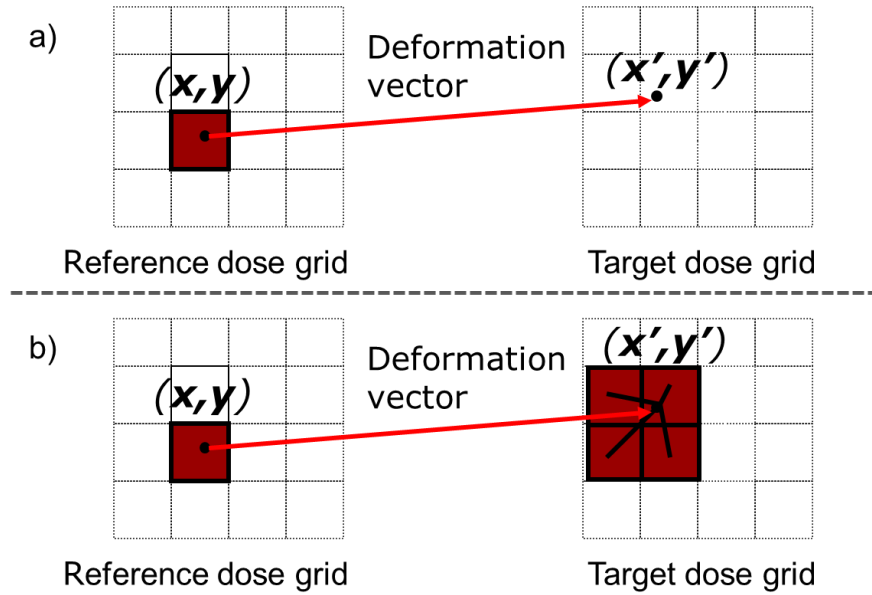
Figure 7. Schematic illustration of the dose interpolation method, where a) deformation vectors are applied to find the target voxel corresponding to the reference voxel, and b) the dose in the neighboring voxels is interpolated on the target grid and then copied back to the reference voxel.

It is crucial to mention that the dose accumulation approaches discussed in this section are purely geometrical solutions. They thereby suffer from assumptions and limitations where the main issue is that they ignore density changes resulting in the loss of energy and mass conservation. It may furthermore lead to inaccuracies at tissue boundaries and they are also not able to include interplay effects. Studies have reported that inaccuracies in calculated dose occur in regions with large dose or density gradients [100,101].

The error in the dose calculated by the interpolation approach can however be quantified [101]. Consider interpolating the dose in two neighboring voxels, v_1 and v_2, in the target dose grid and copying that dose back

to the reference voxel, w_1 (Figure 8). The remapped dose, d^{DIM}, in the reference voxel using dose interpolation methods (DIM) can then be expressed as Eq. 2. However, if mass, M, was to be conserved, the correctly mapped dose, d^T, would be calculated based on the energy, E, deposited according to Eq. 3.

$$d^{DIM}(w_1) = \frac{d'(v_1) + d'(v_2)}{2} \qquad \text{Eq. 2}$$

$$d^T(w_1) = \frac{E(v_1) + E(v_2)}{M(v_1) + M(v_2)} \qquad \text{Eq. 3}$$

By simply calculating the error, ε, in the mapped dose (Eq. 4-5) as the difference between the two cases, it can be concluded how the error in the accumulated dose depend on the density and dose gradients in the deformed calculation geometry.

$$\varepsilon[d^{DIM}(w_1)] = d^{DIM}(w_1) - d^T(w_1) \qquad \text{Eq. 4}$$

$$\varepsilon[d^{DIM}(w_1)] = \frac{[d'(v_1) + d'(v_2)]\left(1 - \frac{M(v_2)}{M(v_1)}\right)}{2\left(1 + \frac{M(v_2)}{M(v_1)}\right)} \qquad \text{Eq. 5}$$
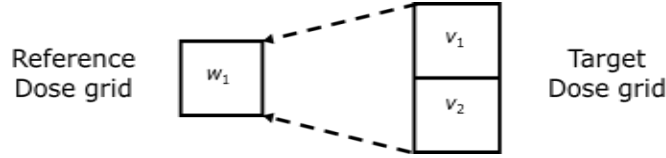
Figure 8.Example of dose interpolation from two target voxels, v_1 and v_2, back to the reference voxel, w_1.

Energy/mass transfer methods

As a response to the lack of energy conservation in the dose interpolation methods, two approaches were proposed which ensure conservation of energy during dose mapping. The first method relies on mapping the energy between geometries and is called the energy transfer method [101]. This method simulates the particle transport in secondary image sets corresponding to the respiratory phase at that point in time. Using deformation vector fields (DVFs), the energy deposition is then mapped to the reference geometry. That implies that this approach heavily relies on the accuracy of the deformation map. Due to discontinuities in the deformable image registration there is a risk of mapping energy to a reference voxel without mass being consistent between the target and reference voxel. This is especially important in the case of dose delivery in heterogeneous geometries such as the thorax where voxels might have large differences in density. This issue was, however, later addressed by mapping the mass together with the energy in an energy/ mass transfer method [102], and has since been applied in a range of studies [103–105].

If considering a transformed target volume, $T\{V_{ref}\}$, with the mass of the reference voxel, v_{ref}, conserved, the mapped dose in the reference voxel when energy and mass is conserved can be expressed as Eq. 6 [102] (Figure 9).

$$D_{ref} = \frac{E(T\{V_{ref}\})}{M_{ref}} \qquad \text{Eq. 6}$$

One of the main advantages of the energy/mass transfer approach is that there is no need for irregular boundary detection during particle transport. One limitation might however be the requirement of interpolating the deformation vector field and densities in order to simulate a continuous motion, even if its impact can be reduced by reducing the motion between the used phases to less than the voxel dimension[105].
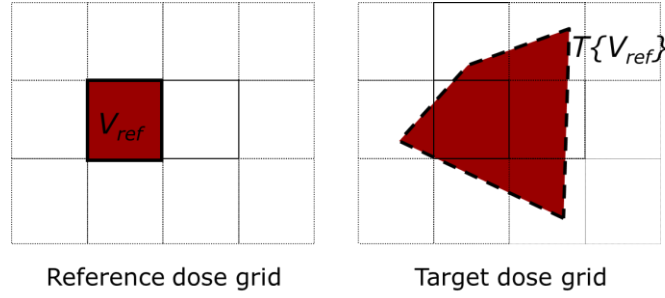
Figure 9. Schematic example of the localization of the deformed voxel volume on the target grid used in the energy / mass transfer approach to 4D dose calculation. Based on deformation vector fields the energy deposited in the deformed target volume is transferred back to the reference voxel.

Direct voxel tracking methods

The second approach developed in order to ensure conservation of energy and mass is the voxel warping approach [100]. In this method the voxels in the secondary image sets are warped according to the deformation taking place. Mass is preserved as density alteration are taken into account when the dose to the deformed voxel is mapped back to the reference voxel. During the particle transport it is due to the nature of this approach necessary for irregular boundaries to be detected at each particle transport step. This approach was first introduced as an alteration of the DOSXYZnrc user code called defDOSXYZnrc, which models the deformation by applying displacement vectors in order to shift the reference voxel nodes [100,106]. As for any 4D dose calculation method in radiotherapy where anatomical deformations occur, the deformation map should preferably be based on deformable image registration (Figure 10). Throughout this thesis, however, only rigid phantom motion is considered and therefore, in order to ensure accurate motion modelling the displacement vectors were manually defined based on the known motion of the dynamic thorax phantom. The method to handle 4D dose calculations by voxel warping was built in to a separate 4D MC user code called 4DdefDOSXYZnrc [107]. As input to the code a reference to the location of a file containing the general displacement vector is required. Additionally, the 4DdefDOSXYZnrc code includes a displacement vector scaling factor as a function of the normalized cumulative MU index, which describes the actual motion during irradiation.
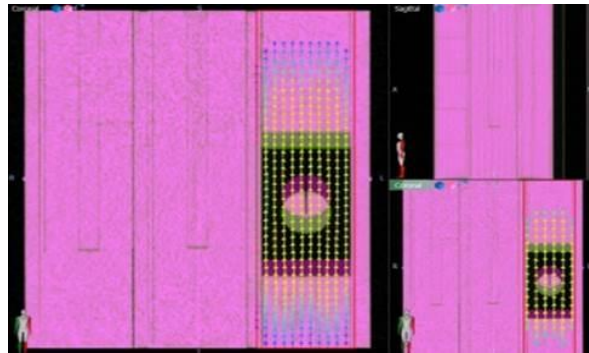
Figure 10. Example of deformation vector field obtained using commercial deformable image registration software (Velocity, Varian Medical Systems) applied to the MC compliant voxelized phantom of use in this study. Notice the variation in deformation strength over the longitudinal direction of the rigidly moving cylinder. Manually defined vector field of equal strength were instead applied during simulations in this study.

In order to describe the procedure of 4D simulations with 4DdefDOSXYZnrc, an example using the Varian TrueBeam phase space source is given here but can be applied to any medical LINAC. The vendor provided phase space is scored just above the secondary collimator jaws and used as an input to the simulation of particle transport through the same jaws (Figure 11). During simulation, a randomly sampled MU index is used; i) to look up collimator opening from jaw and leaf sequencing files, ii) to look up gantry, collimator and couch rotations together with isocenter location from the input files, and iii) to determine the respiratory phase, find the deformation scaling factor, deform the geometry accordingly and transport the particle (Figure 12). During voxel deformation new densities are calculated for each voxel to ensure conservation of mass. Particle transport and energy deposition is thereafter carried out in the deformed voxels. The resulting dose is thereby automatically accumulated in the reference dose grid.
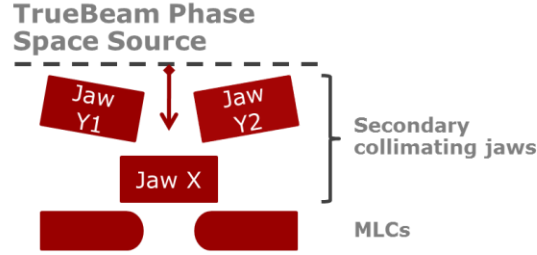
Figure 11. Schematic figure illustrating the use of a phase space scored just above the first non-static components as particle source.
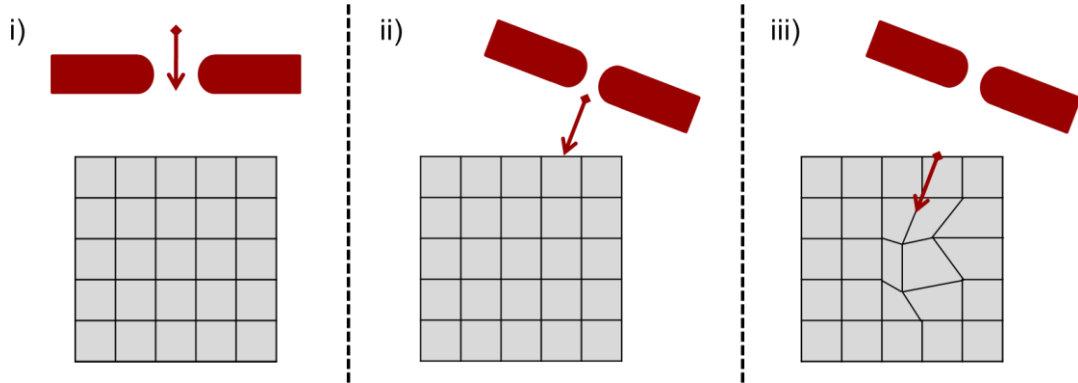
Figure 12. Four-dimensional dose calculation by the voxel warping approach initiates by using a randomly sampled MU index to look up i) collimator openings from jaw and leaf sequencing files, ii) gantry, collimator and couch angles, together with isocenter location from input file, and iii) to determine respiratory phase, deform geometry and transport particle.

The voxel warping method applied in 4DdefDOSXYZnrc was recently validated experimentally on an Elekta Agility LINAC (Elekta AB, Stockholm, Sweden), using gafchromic EBT3 film measurements and RADPOS 4D dosimetry in a dynamic Quasar phantom (Modus Medical, London, ON, Canada) with a lung insert [108] (Figure 13). The 4DdefDOSXYZnrc code has in this thesis been further validated during the implementation of the code into an automated 4D MC workflow (section 4.2.2 and Paper III) and has also been further developed into a code for time-resolved MC simulations (section 4.3 and Paper IV).
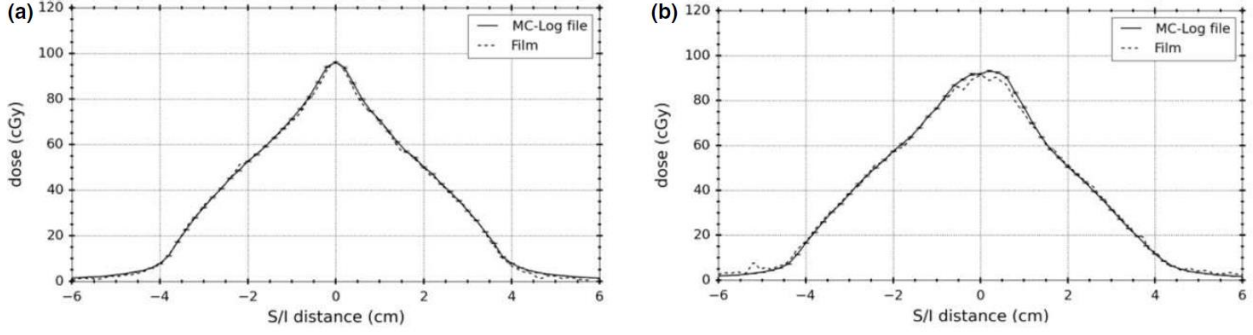
Figure 13. Dose profile comparisons between film measurements and log-file based 4DdefDOSXYZnrc simulations for 4×4 cm² (left) and VMAT (right) plan deliveries on a moving phantom along the superior/inferior direction (top row) (adopted from Gholampourkashi *et al.* [108] with permission).

4.2.2 Automated Monte Carlo workflow

Since the introduction of reliable MC based 4D dose calculation solutions more than a decade ago there has been a long list of studies proving the usefulness and potential in being utilized more routinely in the clinic. Searching in the literature for 4D MC will result in a list of more than 50 publications touching upon the subject. The studies are looking at everything from development of new codes and finding applications to reports on methods for faster calculations. However, there is a lack of studies reporting any routine use of 4D MC in a clinical setting and there is more so a lack of commercial solutions. The lack of readily available solutions for fast implementation of 4D MC could possibly be solved by the development of an automated workflow with minimal user interaction.

In Paper III of this thesis the implementation of 4DdefDOSXYZnrc code into an automated workflow is described. The workflow was designed based on a set of python codes for generation of input files, triggering of beam or patient/phantom simulations, as well as conversion of resulting 3ddose distribution to TPS compliant dose files. In this setup the workflow can be triggered by the appearance of a set of files required to create the MC input files. The files needed in its current implementation include plan, dose, and structure DICOM files exported from the TPS together with treatment-specific LINAC logfiles and synchronized motion recordings. Details on the various steps that are followed in the workflow are presented in Table 2 in Paper III. By application in a dynamic beam delivery to an in-house developed thorax phantom, the validity of the setup was demonstrated and its potential use in routine patient-specific quality assurance emphasized.

Throughout this thesis the absolute dose calibration of the MC simulations was based on the method further described in Appendix A. Note that MC calculated doses are reported as dose to medium rather than being converted to dose to water. The perception in the beginning of this project was that comparison to commercial dose calculation algorithms should be based on converted MC doses as the commercial solutions are reporting dose to water. The method usually applied was based on the use of average stopping power ratios calculated for the primary energy spectrum in the transport media [109]. However, recent publications discussing this issue report that Monte Carlo calculated dose preferably should be reported as dose to medium, for better consistency with previous radiotherapy experience and also due to an increased final uncertainty in the calculated dose if converted to dose to water [110–112].

4.3 Time-resolved Monte Carlo

Four-dimensional dose calculation methods described in section 4.2.1 are mostly reporting the accumulated 3D dose as the end results. Despite the fact that 4D calculations are accounting for both LINAC and patient/phantom motion temporal information about the dose deposition is usually lost. This leads to difficulties when resolving the underlying cause for a deviation from the expected dose distribution. In order to resolve this issue and to determine the time-dependent accuracy of the delivery there is a need to include

the temporal information in the final dose output from the 4D method applied. This can potentially be achieved with many of the described methods, but especially so for MC based solutions where e.g. management of the temporal resolution is readily accessible and easily adjusted.

As a part of the work in this thesis an adjustment and initial validation of the 4DdefDOSXYZnrc dose accumulating user code (see section 4.2.1 regarding the voxel warping method) for enabling temporally resolved output was carried out. This part of the project was initiated during a research stay at and carried out in collaboration with the Carleton Laboratory for Radiotherapy Physics at Carleton University in Ottawa, Canada, under the supervision of Emily Heath. The main details about the development and validation of the final version of the time-resolved MC (4DtMC) code are covered in Paper IV. In this section some further details about the process of development and validation are presented. The new 4DtMC code was implemented into an adjusted version of the automated 4D MC workflow, described in section 4.2.2, where the automated inclusion of the extra inputs needed and the triggering of the relevant output was added.

4.3.1 User code development

With the use of a method for generating input files based on treatment-specific LINAC logfiles and phantom motion patterns (see sections 3.2.3 and 4.2 as well as Paper II and Paper III) there is a potential for a fine temporal resolution. In the case of irradiations carried out on a Varian TrueBeam LINAC, the limiting factor is the temporal resolution of the LINAC trajectory logfiles where the resolution setting is restricted to 20 ms at its finest. However, a 20 ms resolution between the logfile control points used to generate the list of beam parameter sets in the 4D MC input files will e.g. result in more than 4000 beam settings to be simulated if the treatment time exceeds 80 s (see example of RapidArc treatment exceeding 80 s beam on time in Paper IV). With the use of the phantom setup described in this thesis (section 3.2 and Paper II) the motion pattern is sampled with a temporal resolution of approximately 29 ms, set to correspond well with the logfiles. Using a commercial solution instead will of course affect the sampling frequency as the choice of respiratory monitoring method and a potential interpolation of the motion pattern might influence the uncertainty of the final dose calculation. The temporal resolution of 20 ms applied here, with a slight interpolation in the breathing pattern, was the highest achievable with the log files temporal resolution being the limiting factor. This resolution can e.g. be set into relation with a resolution of approximately 400 ms which would be the case for many dose mapping solutions where the breathing cycle (commonly 15 breaths per minute) is split into ten phases.

The main challenge with reporting dose as a function of time instead of only reporting the accumulated dose is the increase in the number of histories needed in order to maintain a similar statistical uncertainty. While the 4D dose accumulation approach in 4DdefDOSXYZnrc does not require additional histories in comparison to standard 3D simulations using DOSXYZnrc, the introduction of dose output as a function of time would imply an increase in the number of histories in relation with the number of control points simulated. Basically, if reporting the dose for all voxels in the 3D phantom this could mean an increase of the number of histories by three orders of magnitude. Such an approach is CPU demanding and for most departments the number of CPUs available will limit the efficiency of the patient-specific quality assurance program.

Variance reduction techniques

In order to improve on the efficiency of the 4DtMC simulations in order to achieve an acceptable statistical uncertainty the thought of introducing variance reduction techniques (VRTs) was raised. In all 3D and 4D simulations conducted previously during the project no VRTs were applied except for the use of cutoff energies and occasional use of photon splitting. The use of cutoff energy is the use of an energy level below which particle transports are stopped with the effect that any particle with energy below the cutoff level will deposit its remaining energy locally. Different particle types can be given individual cutoff energies and can also be varied for different geometrical regions. The use of an electron cutoff energy (ECUT) can be highly efficient as a large number of interactions with small energy losses are taking place, while a photon cutoff

energy (PCUT) is usually set to a low value since it will not influence the calculation time to same extent. Throughout this project an ECUT of 0.7 MeV and a PCUT of 10 keV was employed.

For further efficiency improvements the photon splitting technique was considered and tested in the 4DtMC simulations. Already at the stage of introduction the photon splitting method was found to improve the efficiency of a factor of 5 when used in dose calculations for external photon beams [113]. The technique is based on the splitting of photons into a number of sub-photons (nsplit), of weights split accordingly, with a uniform distribution of interaction sites along the initial direction. Still, introduction of the photon splitting method into the 4DtMC simulations with an nsplit = 25 did not improve on the efficiency enough for the resulting calculation times to be feasible for the time-frame of the current project. Running the simulations on a 100 CPU cluster to a resulting dose with an acceptable uncertainty of around 2-3 % in the hose dose regions would require an estimated calculation time greater than eight days for a single treatment plans of the types investigated here.

It should be noted that the concept of 4DtMC as described in this thesis is motivated by the need for resolving when during irradiation a detected dose deviation occurs. The time-resolved simulations would therefore usually be preceded by a 4D MC simulation where the deviation in the accumulated dose has been observed. Thereby, the location of the deviations of interest for further investigation is known and the dose output can be focused on a few voxels in the phantom. This approach was employed throughout the testing of the 4DtMC simulations as the dose output was only scored in a voxel corresponding to the location of the PSD during irradiation of the in-house developed thorax phantom (see section 3.2). A VRT that is able to utilize the limitation of the dose calculation volume to a smaller group of voxels, or even a single voxel is the photon cross-section enhancement (XCSE). The XCSE technique has previously been thoroughly described and tested by Wulff *et al.* and has been implemented in the EGSnrc user codes CAVRZnrc, DOSRZnrc, and egs_chamber [114]. The average distance between photon interactions (mean free path length) is relatively long compared to the dose calculation geometry for the MeV photons used in radiotherapy. Increasing the cross section by a given factor will increase the density of photon interactions. In XCSE this is carried out by, at each interaction site, adding a fictitious interaction to each real interaction without altering the direction or energy of the incident photon. In the user codes mentioned, this was implemented as a way of increasing the cross section in a volume ("shell") surrounding a certain voxel/volume of interest which is usually the detector volume. Test carried out by Wulff *et al.* discovered that the choice of shell dimension and XCSE factor could be optimized [114]. They found that the increase in efficiency reached a maximum for a shell thickness of 1 cm and that for a water-filled sphere (1 cm in diameter), at 10 cm depth surrounded by water, the use of e.g. a XCSE factor of 8 resulted in a relative dose efficiency of 60. These settings were in this study transferred over to the implementation of XCSE in the time-resolved version of the 4DdefDOSXYZnrc code. However, due to the cubic voxelized dose calculation geometry the XCSE was tweaked and a spherical shell thickness of 1 cm was here interpreted as surrounding the voxel of interest by including voxels within 1 cm in all directions, resulting in a cube surrounding the voxel. This implementation lead to a dramatic increase in efficiency with a difference by a factor or 16 compared to the corresponding simulations carried out using photon splitting. With optimizing the use of CPU resources the resulting calculation time could be reduced to less than 48 hours (for some cases less than 24 hours) for simulations resulting in acceptable statistical uncertainty. This was considered sufficient and all following tests with the time-resolved MC code were therefore carried out using a XCSE factor of 8 in a cube extending 1 cm from the voxel of interest in all directions.

4.3.2 Experimental validation

During development of the 4DtMC code several test found a high level of statistical uncertainty despite the introduction of the various VRTs discussed in section 4.3.1. In a further attempt to increase the efficiency, in keeping an acceptable level of statistical uncertainty while reducing the calculation time, the data was re-binned to a time-resolution of 100 ms instead of the initial 20 ms. The results presented will all have a temporal resolution re-binned to 100 ms.
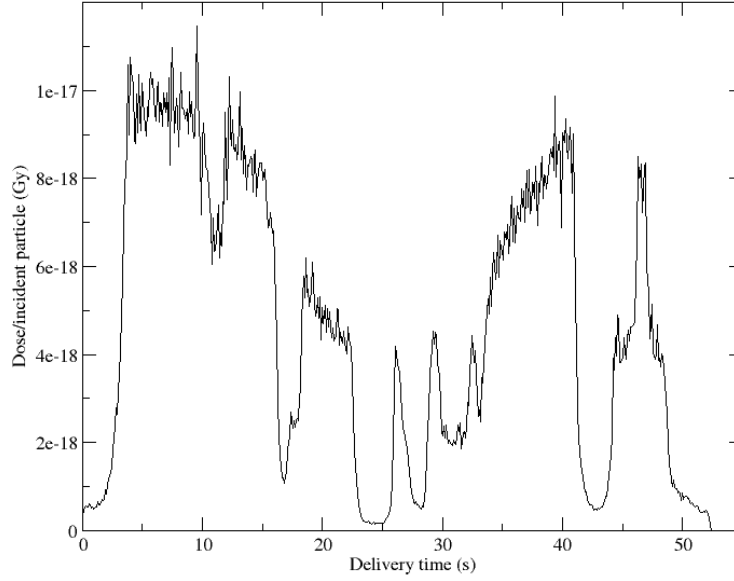
Figure 14. Initial results of time-resolved MC simulated dose per incident particle for a RapidArc plan delivered to a static thorax phantom.
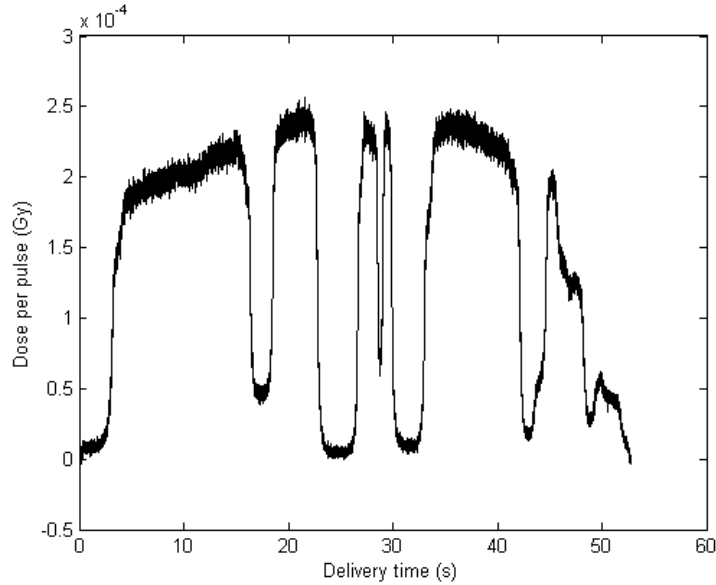
Figure 15. Plastic scintillator detector measured dose per pulse as a function of delivery time for a RapidArc plan delivered to a static phantom.

Initial tests

While the initial runs were focused on testing the functionality of the new code the initial tests of 4DtMC of a 6 MV half-arc RapidArc treatment also put emphasis on the statistical uncertainties that reached up to 30% even in the high dose regions (Figure 14). This was later resolved using more histories and by optimizing the XCSE as described in section 4.3.1.

In addition to the initial tests being used for efficiency optimization, also the workflow of input file generation based on the logfiles and motion profiles was analyzed. The 4DtMC results illustrated in Figure 14 could already after visual inspection be concluded to differ significantly from the expected dose profile as measured

using the PSD in the thorax phantom in static mode (Figure 15). One factor contributing to the discrepancies in these initial tests was the fact that the geometry used differed between the 4DCT used for delineation and treatment planning in the TPS and the phantom setup used during irradiation. While the contra-lateral lung insert was filled with PMMA during image acquisition and treatment planning, the irradiation was carried out with the corresponding insert being filled with balsa wood. This was due to measurements being carried out after a re-scanning but still based on treatment planning on the initial CT. The reason for re-scanning was, in addition to including the lung inserts in both lateral cylinder, to include a fiber dummy which in the initial scan was not included, resulting in a thin air cylinder through the lung insert and half of the PMMA tumor. The following simulations were therefore conducted based on the delineation, treatment planning and irradiations carried out in the final CT imaged geometry. Furthermore, the inclusion and exclusion of the treatment couch in the MC phantom was investigated, but results demonstrated so significant difference depending on the use of the treatment couch during simulations.

Time-resolved MC versus scintillator measurements for a range of treatment plans

Note that the final CT acquisition was performed as a 3DCT with the phantom static in the position corresponding to the MidV position during the regular sinusoidal motion later applied during irradiations. In using a 3DCT any uncertainties due to imaging artifacts related to motion were eliminated and any recorded one-dimensional motion during irradiations could later be incorporated to the 4D MC simulations. Treatment plans were created according to the method described in Paper IV. In brief, one single open field (SF) plan and one half-arc RapidArc plan were created with the isocenter in the center of the spherical tumor. Additionally, the two plans were shifted 2.5 cm in the caudal (longitudinal) direction and the final four plans were irradiated with the phantom in both dynamic (one-dimensional motion of the cylinder containing the lung and tumor inserts, with a 25 Hz breath rate and a 20 mm peak-to-peak amplitude) and static (no motion) mode, rendering in a total of 8 different scenarios.

Corresponding 4DtMC simulations were carried out using 1 billion histories together with a XCSE factor of 8, resulting in a statistical uncertainty of $2 - 3$ % in the high dose region when re-binned to a temporal resolution of 100 ms. Comparison between scintillator measurements and 4DtMC simulations are described and presented in Paper IV. One of the first conclusions was the observed improvement in the temporal synchronization between the measurements and simulations when analyzing the SF plan with the isocenter shifted and the phantom in motion. However, a dose difference was also observed, especially in the low dose region of that same comparison. The next step was to analyze the comparison for the RapidArc plans. As for the conventional plan, the dose profiles were in general considered to have similar fluctuations in dose over time with an indication of a good temporal synchronization between measurements and simulations. However, already for the least complex case with the half-arc plan isocenter centered in the tumor and a static phantom, the compared dose distributions as a function of time revealed large differences in some intervals during the time since beam on (Figure 30 in Paper IV).

Unfortunately, the MC doses were found to be higher than the measured doses in some regions, while lower in other regions in the same time as the MC calculated dose gradients appear earlier than corresponding measured dose gradient in some regions and later in others. This makes troubleshooting a challenging task since a large amount of factors are influencing the complex comparison investigated. The statistical uncertainty together with the measurement uncertainty implies that most deviations are not statistically significant. However, in some regions there are significant differences. While some of them are in the low dose areas, where the much higher statistical uncertainty can explain the deviations to a certain extent, there are also a number of significant differences in high dose regions.

A rather long list of possible explanations was generated, ranging from the questioning of the MLC model, the difference in size between the active scintillator detector volume and the dose calculation voxel size, the uncertainties in density assignment based on tissue based HU calibration, to uncertainties in how the XCSE works when the isocenter is shifted so that the center of the tumor is actually located in the edge of the fields. Some factors could more or less be ruled out due to previous observations of good correlation between

27

4DdefDOSXYZnrc calculated accumulated doses and scintillator measurements. Also, e.g. the factor of the uncertainties in the stem calibration when different lengths of the fiber are in the field was deemed unlikely to have affected the results, based on experience measuring output factors in a similar setup without observing such anomalies. Therefore, most of the reasoning circled back to the factor of the potential misalignment of the scintillator detector and its corresponding 4DtMC calculation voxel.

Verification of scintillator position in MC phantom

Focusing on the steep gradients giving rise to rapid increase and consecutive decrease in dose there is an indication of a misalignment between the scintillator detector during measurements and the 4DtMC simulations either in time or position. The choice of the primary voxel of interest, most likely to contain the active volume of the fiber-coupled plastic scintillator, was based on visual inspection of the MC phantom. Thereby, there is a small uncertainty in the correlation between the true position during irradiation and the position during MC simulations. Before measurements the scintillator is positioned in the PMMA tumor by sliding it in to the cylindrical cavity drilled with high precision to a length to focus the detector volume in the center of the tumor. Due to the potential uncertainty in the positional correlation between measurements and simulations an investigation was carried out based on the analysis of voxels adjacent to the primary voxel.

First of all accumulated dose extracted from the 4DdefDOSXYZnrc simulations was re-analyzed for the voxels surrounding the primary voxel. This was conducted for all 8 measured scenarios, where first of all the plans delivered to the static phantom were also re-simulated using the 3D MC user code DOSXYZnrc. The voxels analyzed ranged 4 voxels in each direction from the primary voxel. The primary voxel had the longitudinal, vertical and lateral positions (100, 48, 115), and the voxels with minimum dose difference between simulations and measurements, were located at a distance of (0, 0, 0), (0, -1, 0), and (0, +2, -1) from the primary voxel for the static DOSXYZnrc, static 4DdefDOSXYZnrc, and dynamic 4DdefDOSXYZnrc, respectively. The optimal voxel for each set of simulated plans were calculated based on the root mean square error. Similarly the overall optimal voxel was extracted by including all simulations and calculating the minimum root mean square error. The overall optimal voxel was calculated to correspond exactly with the primary voxel. The dose differences between simulations and measurements for the eight treatment scenarios are presented in Table 1.

With the overall optimal voxel, based on the accumulated 4D MC doses, corresponding with the primary voxel the next step was to look at the time-resolved MC simulations. 4DtMC simulation were therefore conducted for the centered RapidArc plan on the static phantom, with the voxel of interest (to which also the focus of the XCSE was shifted) placed in the six voxels adjacent to the primary voxel of interest in each direction. The aim was to distinguish if the dose gradients were more accurately placed when moving in one of the directions. Despite variations being observed depending on the choice of voxel, no one single voxel demonstrated significantly better agreement with measurements over the entire beam on time (Figure 16).

Table 1. The dose differences between simulations and measurements for the eight treatment scenarios are presented for both for the primary voxel and the optimal voxel for the set of simulated plans, denoted with their distance to agreement with the primary voxel located at (100, 48, 115). The dose differences are presented as percentage difference [%] with the scintillator as reference and all have a standard uncertainty of ±1.7 percentage units (k=1), based on a statistical uncertainty of 0.5% in the MC simulations and a scintillator measurements uncertainty of 1.6% [115]. Highlighted values are the scenarios differing with more than two standard uncertainties.

Simulation set	3D MC static	4D MC static		4D MC dynamic	
Distance from (100, 48, 115)	(0, 0, 0)	(0, -1, 0)	(0, 0, 0)	(0, +2, -1)	(0, 0, 0)
Single field, centered	3.2	2.9	3.4	1.9	3.2
Single field, shifted	-2.7	-3.1	-3.1	**-5.8**	**-5.3**
RapidArc, centered	-0.5	2.6	1.7	**13.2**	**23.1**
RapidArc, shifted	1.4	0.1	1.2	-1.4	-2.5
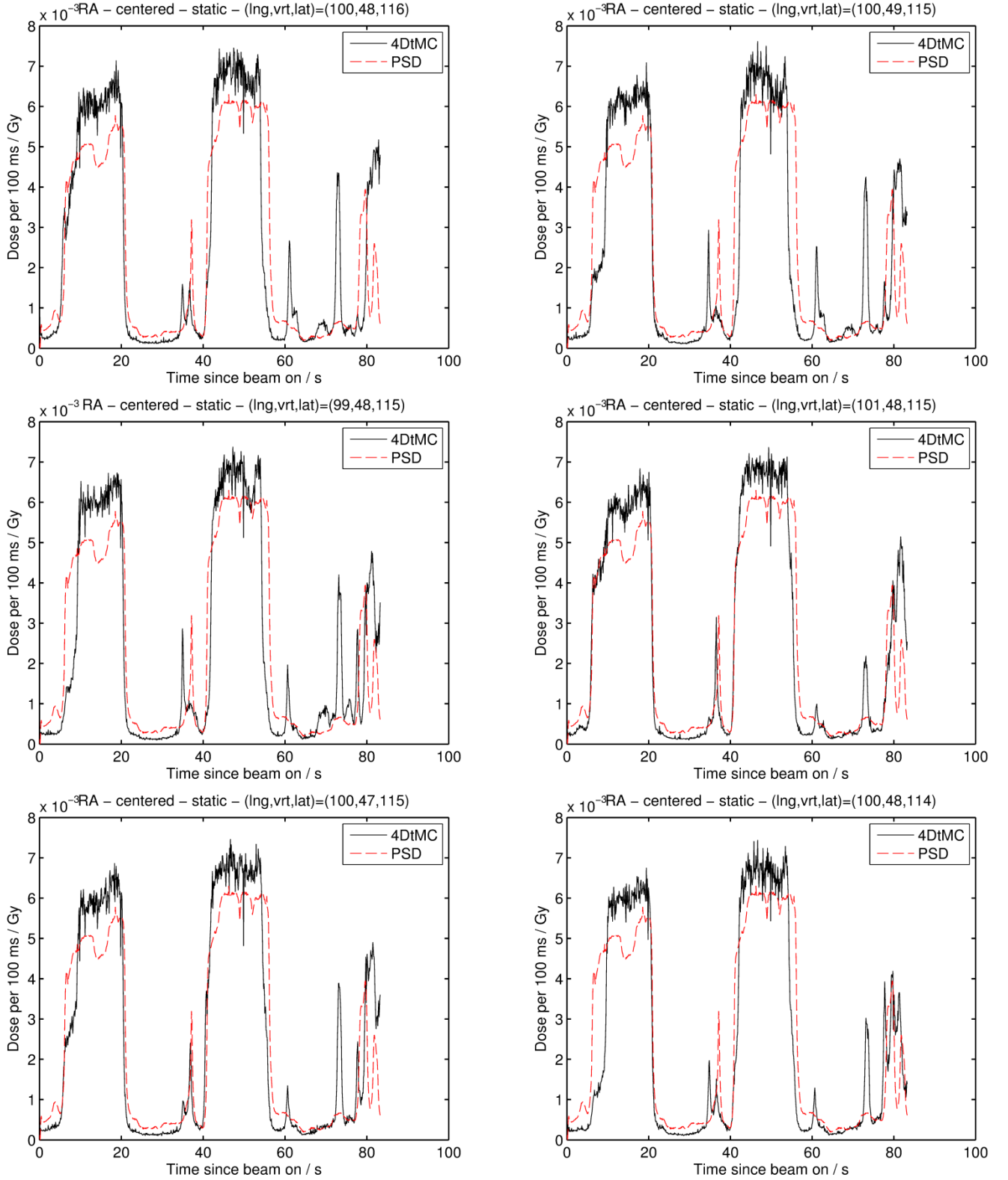
Figure 16. Comparison of the dose profiles between four-dimensional time-resolved Monte Carlo (4DtMC) simulations and plastic scintillator detector measurements. Dose recorded in the center of the tumor for a single half-arc RapidArc plan delivered to a static thorax phantom, with a PMMA tumor embedded into a balsa wood lung insert and the isocenter positioned in the center of the tumor. Results are presented for the six voxels (specified by their lng, vrt, lat coordinates) adjacent to the primary voxel at (100, 48, 115).

5 Conclusions

5.1 Summary

The work presented in this thesis has been carried out with the focus on improving methods for estimating and verifying the dose delivered to time-dependent geometries. The motivation lies in the challenging task of dose verification when using complex modern delivery techniques in radiotherapy of lung cancer. First of all inter-fractional variations, or more specifically anatomical changes in the form of density alterations, occur randomly over the course of treatment and by estimating the dosimetric effect a foundation for assessing the need for adaptation of the treatment plan was established. Furthermore, it is essential to manage uncertainties related to intra-fractional variations such as respiratory-induced tumor motion. This has been addressed by the development of tools for time-resolved measurements and accurate dose calculations. While the in-house developed tools for dose verification, based on time-resolved scintillator dosimetry in a dynamic thorax phantom and time-resolved Monte Carlo simulations, might be perceived as complex, the aim was also to make the methods accessible. Automating the workflow as much as possible in order to minimize the user interaction was therefore an important contribution from the work carried out.

A more detailed summary of the findings and there potential implications in quality assurance of lung cancer radiotherapy is presented in sections 5.1.1-5.1.3, together with the main conclusions in section 5.2 and future perspectives in section 5.3.

5.1.1 Managing anatomical changes in radiotherapy of lung cancer patients

Paper I was an investigation of the dosimetric effect of anatomical changes during modern radiotherapy of lung cancer patients, where modern radiotherapy refers to the inclusion of both standard fractionated and dose-escalated treatment plans delivered in either free-breathing or deep-inspiration breath-hold. Systematic introduction of simulated increase in pleural fluid and tumor shrinkage, in both phantom and patient geometries, served as a method to determine the levels of anatomical changes where an unacceptable change in dose to target or OARs occurred. Furthermore, a clinical case of appearing atelectasis was analyzed, which together with the simulated changes emphasized the challenges to handle anatomical changes in the thoracic region. The study therefore highlighted the fact that individualized treatment-specific assessment of the dosimetric effects caused by the anatomical changes is necessary in most cases. Such assessment can often be carried out shortly after the detection of change by applying the method used here of recalculating the original treatment and including the specific density alterations. Action levels below which treatment is always delivered are, however, applicable in many situations even though they require certainty in the data behind the threshold levels. This study contributes to the validity of using action levels for anatomical changes and thereby simplifying the online decision between continued treatment and re-planning.

5.1.2 Time-resolved dosimetry in time-dependent geometries

Paper II is a manuscript presenting the development and validation of an experimental solution for time-resolved dosimetry in a dynamic thorax phantom. Due to the previously demonstrated well-suited characteristics of the plastic scintillator detector for verification of dynamic treatment deliveries it was implemented also here with the main factor being the possibility to measure the dose per LINAC pulse with high accuracy. The in-house developed thoracic-like phantom was built in order to enable the use of the small scintillator detector inside a geometry mimicking the thorax of a lung cancer patient with similar dimensions and material properties. Most importantly, the study presents the development of a script controlling the motion of one of the phantoms lateral cylinders, including the lung insert with an embedded tumor holding a spot for the scintillator. This motion was driven by a linear stage distanced from the phantom using a rod wherein the fiber coupled scintillator also could slide in and be positioned in the center of the tumor. The setup was tested for sinusoidal motion and a high level of precision and repeatability was demonstrated.

However, the script was also built in order to facilitate any kind of imported motion, enabling future dose verification during patient-specific breathing patterns. With the temporal resolution of the plastic scintillator detector there is also the potential to resolve when during a delivery a possible dose deviation, otherwise only observable in the accumulated dose, has occurred. The combination of time-resolved scintillator dosimetry in a thorax phantom with respiratory-like motion is therefore unique and has the potential to take on an important role in dose verification of respiratory-guided treatment techniques.

5.1.3 Four-dimensional Monte Carlo solutions

Paper III and Paper IV are manuscripts focusing on the need to incorporate MC dose calculations as a tool in quality assurance of lung cancer radiotherapy. Focus was especially on the need to include the fourth dimension, time, in the equation since intra-fractional motion heavily contribute to uncertainties and possible errors in lung radiotherapy. Despite the increasing amount of 4D MC related publication, there is only a limited use of the technique in routine treatment planning or quality assurance and in many cases the solutions have simplifications and built in approximations limiting the usefulness. A recently developed 4D MC user code based on the reliable voxel warping technique was therefore incorporated into an automated workflow for MC based independent dose calculations. The aim was to enable MC simulations of synchronized dynamic beam configurations and patient motion with minimum user interaction. The workflow solution was built into a python based script consisting of a set of modules executing sequentially without user interaction. The script is triggered by the appearance of the necessary plan specific DICOM files, logfiles, deformation vector fields, and motion recordings, resulting in a TPS compatible MC calculated 3D dose distribution.

The fact that the original 4D MC workflow results in a 3D dose distribution implies that the dose is accumulated over all control points and that the temporal resolution is not utilized in the end. This issue was therefore addressed by adjusting the 4D MC code to enable dose output as a function of time. However, reporting the MC calculated dose with a high temporal resolution requires a monumental increase in computational time if similar statistical uncertainty is desired. A novel approach to variance reduction in a cubic voxelized phantom was therefore introduced together with the limitation of the reported dose to only one voxel. This voxel was chosen to correspond with the position of the plastic scintillator detector during measurement of dynamic treatment delivery to the in-house developed thorax phantom. Experimental validation of the time-resolved MC user code could thus be conducted. Comparison between measured and calculated temporal dose profiles demonstrated several regions of large dose differences despite the general similarities also observed. The study therefore only functions as an initial validation, showing that the code is fundamentally correct while still in need of further validation. Most importantly the time-resolved MC code was indicated to be useful as a tool to resolve when during treatment delivery a dose deviation has occurred. The role in lung radiotherapy quality assurance is therefore right now seen as a method for further investigation of a failed delivery as detected by deviations in accumulated doses, either measured or calculated. Such a tool can play an essential part for the mentioned dose verification of modern respiratory-guided treatment techniques applied in lung cancer radiotherapy.

5.2 Main conclusions

Based on the work in this study it can first of all be concluded that estimating the dosimetric impact of inter- and intra-fractional variations has been demonstrated essential in radiotherapy of lung cancer patients. Certain anatomical changes did to not require re-planning if below obtained action levels, while the majority of changes require individualized assessment. Furthermore, the in-house developed tools for time-resolved measurements and dose calculations have proven to have great potential in dose verification of respiratory-guided radiotherapy of lung cancer patients. The main conclusions from the manuscripts included in this thesis are listed below.

I. Simulated anatomical changes provided clinically relevant action levels supporting the decision between continued treatment and the start of an adaptive process. However, it can also be concluded that patient-specific assessment of the dosimetric effect of individual changes is necessary in most cases. This was concluded for both standard fractionated and dose-escalated treatment plans in DIBH as well as FB, despite potential superiority in DIBH with regards to anatomical changes in dose-escalated treatments.

II. A novel setup for time-resolved plastic scintillator in a dynamic thorax phantom during reproducible, respiratory-like motion was developed. The use of scintillator dosimetry in a thorax phantom during controlled motion can play an essential role in quality assurance of lung cancer radiotherapy, especially in revealing dose deviations due to the shortcomings of commercial treatment planning systems concerning issues related to tumor motion and heterogeneities.

III. An automated 4D MC workflow was developed and demonstrated to enable 4D dose verification with minimum user interaction. This has great impact for dynamic treatment delivery to time-dependent geometries, such as respiratory-guided radiotherapy of lung cancer patients. The tool was demonstrated to have high potential in making quality assurance of such nature readily available for any user.

IV. Time-resolved MC simulations were demonstrated to resolve steep dose gradients with good temporal agreement to scintillator measurements. Novel approach to variance reduction enabled development of a time-resolved MC user code, rendering in a dose output with relevant temporal resolution and acceptable statistical uncertainty. Further validation was, however, considered necessary.

5.3   Future perspectives

The thesis presents methods for estimating the dosimetric variations due to inter- and intra-fractional variations. The methods have here been applied to an extent of various treatment techniques while still being limited to a fraction of the delivery techniques available. As radiotherapy of lung cancer is increasing in complexity it would also be interesting to apply the developed methods for the most complex situations where the treatment delivery is being adjusted online, as e.g. in respiratory-guided tracking. Applying the time-resolved measurements and MC dose calculations in such a time-dependent situation would be ideal. However, it would be equally interesting to estimate the dosimetric impact of anatomical changes and the potential need for inter-fractional adaptation in the environment of online adaptive treatment.

In order to re-assure that the system can be used in clinically relevant scenarios, further investigation of the application of patient-specific breathing patterns to the phantom motion is desirable. This would preferably include normal breathing patterns but also irregular breathing patterns as well as e.g. breathing patterns from visually guided DIBH.

After the introduction of MR-linacs, respiratory-guided radiotherapy is no longer only limited to traditional LINACs. MR-linac systems enabling tumor tracking based on the internal motion are emerging and will most likely be available at many of the Danish radiotherapy centers in the near future. Testing and benchmarking of the scintillator dosimetry system for measurements of radiotherapy in magnetic fields is a field with great potential. Further development to enable controlled motion of the thorax phantom in an MR-linac could result in a valuable tool for time-resolved dose verification of respiratory-guided MR-linac treatments. In the same context, further development of the 4D MC and time-resolved MC codes in order to incorporate a magnetic field would serve as a similarly valuable tool. However, further experimental validation of the time-resolved MC user code is first of all necessary even for the more simple cases.

Finally, it will be crucial to keep the MC method as simple as possible in a workflow with minimum user interaction in order to ensure that the methods will be used as a routine part of the quality assurance in radiotherapy of time-dependent geometries.

Manuscripts

6 Paper I

Adaptation requirements due to anatomical changes in free-breathing and deep-inspiration breath-hold for standard and dose escalated radiotherapy of lung cancer patients

Patrik Sibolt[1,2], Wiviann Ottosson[2], David Sjöström[2], Christina Larsen[2] and Claus F Behrens[2]

[1]Center for Nuclear Technologies, Technical University of Denmark, DTU Risø Campus, DK-4000 Roskilde, Denmark

[2]Department of Oncology, Radiotherapy Research Unit, Herlev Hospital, University of Copenhagen, DK-2730 Herlev, Denmark

Person responsible for editorial correspondence:

Patrik Sibolt

Current address:

Center for Nuclear Technologies, Technical University of Denmark,

DTU Risø Campus, Fredriksborgvej 399, Building 201

DK-4000 Roskilde, Denmark

E-mail: pasi@dtu.dk

Abstract

Introduction: Radiotherapy of lung cancer patients is subject to uncertainties related to heterogeneities, anatomical changes and breathing motion. Use of deep-inspiration breath-hold (DIBH) can reduce the treated volume, potentially enabling dose escalated (DE) treatments. This study was designed to investigate the need for adaptation due to anatomical changes, for both standard (ST) and DE plans in free-breathing (FB) and DIBH.

Material and Methods: The effect of tumor shrinkage (TS), pleural effusion (PE) and atelectasis was investigated for patients and for a CIRS thorax phantom. Sixteen patients were CT imaged both in FB and DIBH. Anatomical changes were simulated by CT information editing and re-calculations, of both ST and DE plans, in the treatment planning system. PE was systematically simulated by adding fluid in the dorsal region of the lung and TS by reduction of the tumor volume.

Results: Phantom simulations resulted in maximum deviations in mean dose to the GTV-T ($<D>_{GTV-T}$) of -1% for 3 cm PE and centrally located tumor, and +3% for TS from 5 cm to 1 cm diameter for an anterior tumor location. For the majority of the patients, simulated PE resulted in a decreasing $<D>_{GTV-T}$ with increasing amount of fluid and increasing $<D>_{GTV-T}$ for decreasing tumor volume. Maximum change in $<D>_{GTV-T}$ of -3% (3 cm PE in FB for both ST and DE plans) and +10% (2 cm TS in FB for DE plan) was observed. Large atelectasis reduction increased the $<D>_{GTV-T}$ with 2% for FB and had no effect for DIBH.

Conclusion: Phantom simulations provided potential adaptation action-levels for PE and TS. For the more complex patient geometry, individual assessment of the dosimetric impact is recommended for both ST and DE plans in DIBH as well as in FB. However, DIBH was found to be superior over FB for DE plans, regarding robustness of $<D>_{GTV-T}$ to TS.

6.1   Introduction

Lung cancer is one of the most common cancer diseases worldwide[1,2,116]. Unfortunately lung cancer patients also suffer from a high mortality rate and the local control for patients undergoing radiotherapy as a part of their treatment is poor. Escalating the radiation dose to the tumor could lead to an increased cure rate[3]. Even if this statement is debatable in the light of the results of the RTOG0617 study[4,5],the idea of dose escalated (DE) radiotherapy of lung cancer patients is generally supported and emerging dose escalation studies, having higher focus on quality assurance and keeping the dose to normal tissues as low as for standard treatments, should proceed[6].

In radiotherapy of lung cancer patients, extensive margins are added to the tumor volume in order to account for uncertainties related to baseline shifts, delineation, organ motion and respiration[8,9]. This results in large irradiated volumes of adjacent normal tissue, limiting escalation of the dose to the tumor. Setup margins in the thorax region can be reduced by moving from bony match on the spine towards direct match on the soft-tissue of the lung tumor[10]. Further margin reduction is conceivable by synchronizing the radiation delivery with tumor motion[12]. Use of deep-inspiration breath-hold (DIBH) reduces the tumor motion and can potentially enable DE treatments of lung cancer patients, without increasing the severe radiation induced side effects of organs at risk (OARs)[117,118].

Radiotherapy of lung cancer patients is however also subject to uncertainties related to heterogeneities and anatomical changes. As margins are minimized and dose to the tumor is conformed and escalated, adaptation of the treatment plan due to anatomical changes could become more crucial. Previous studies demonstrate that changes in dose due to anatomical changes have the largest effect on the delivered dose to the tumor[15]. One reason being the lung density alteration that arises with the appearance of anatomical changes, such as atelectasis, pneumonitis, pleural effusion (PE) and tumor shrinkage (TS). While previous studies have investigated the effect of anatomical changes and need for adaptive strategies in standard fractionated treatment of lung cancer patients in free-breathing (FB)[15,28], there is a lack of studies investigating the potential need for adaptation in DE treatment of lung cancer patients in DIBH.

This study is designed to investigate the need for adaptation due to lung density alteration as a result of PE, TS or atelectasis, for both standard (ST) and DE plans in FB and DIBH.

6.2   Material and methods

6.2.1   Data and treatment preparations

In order to perform simulations in a reproducible, well-defined geometry, a three-dimensional CT (3DCT) of the CIRS thorax phantom (CIRS Inc., Norfolk, VA, USA) was acquired. Spherical gross tumor volumes (GTV-Ts) with a diameter of 5 cm were delineated in the anterior (A), central (C) and posterior (P) part of the left lung insert, and given Hounsfield units (HUs) corresponding to water. OARs, clinical target

volumes (CTV-Ts) and planning target volumes (PTV-Ts) were defined and ST plans were produced, for all situations.

Furthermore, sixteen locally advanced non-small-cell lung cancer (NSCLC) patients scheduled for curative radiotherapy, between December 2012 and July 2014, were enrolled. One four-dimensional computed tomography (4DCT) in FB and one 3DCT in DIBH, both with intravenous contrast, were acquired prior to, in the middle of and after the course of treatment. Target volumes and OARs, both in FB and DIBH, were delineated separately on each CT dataset by an oncologist in a treatment planning system (TPS) (Eclipse, Varian Medical Systems, CA, USA)[10]. Dose calculations of ST (utilized for treatment on Varian 2300 iX linear accelerators[119]) and DE volumetric modulated arc therapy (VMAT) plans were carried out in the same TPS, using the AAA calculation algorithm[120].

Additional information regarding the clinical protocol, patient characteristics, scanning procedures, delineations and treatment planning is provided in the supplementary material (available online).
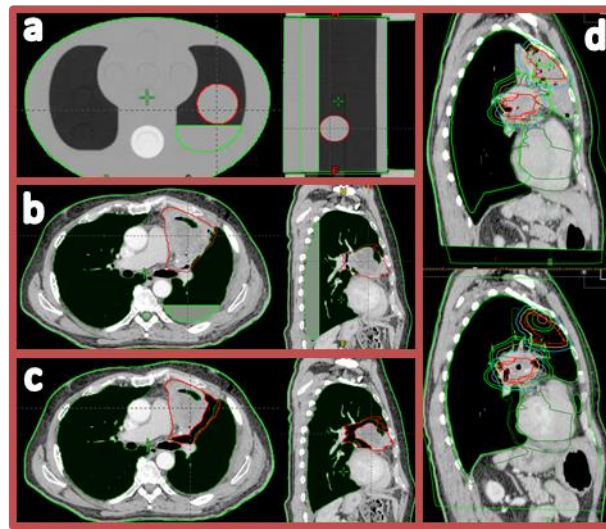
Figure 17. Examples of simulated anatomical changes; a) 3 cm pleural effusion for the centrally located tumor in the CIRS thorax phantom, b) 3 cm pleural effusion in a patient, c) tumor shrinkage in the form of 1 cm radius reduction in a patient, and d) large atelectasis disappearance between pre-treatment (upper) and post-treatment (lower) CT. Colors available online.

6.2.2 Pleural effusion

The dosimetric effect of PE was simulated for ST plans in FB and three different tumor locations in the CIRS thorax phantom (Figure 17a). Simulations of PE in patients were carried out on the pre-treatment CT scans by adding 1, 2 or 3 cm fluid in the dorsal region of the lung (patient in supine position) (Figure 17b), resulting in three new image sets per patient and scanning technique. Simulations were carried out by altering the HUs in the PE region to correspond to water. PE was realistically simulated in the sense that no adjustment was made to the fact that the posterior wall of the lung was not in the same vertical position for the entire longitudinal extension of the patient. This implies that the amount of fluid varied over the longitudinal length of the lung, including the tumor region and depending on the patients' lung geometry as well as tumor location. Original ST and DE plans were re-calculated on the new image sets, preserving the original monitor units (MU).

6.2.3 Tumor shrinkage

TS was simulated for ST plans and the three tumor locations in the CIRS thorax phantom. Simulations of TS in patients were carried out on the pre-treatment CT scans by reductions of the GTV-T radius of the tumor regions adjacent to the lung, both in FB and DIBH (Figure 17c). Thus, parts of tumor extending into the mediastinum, thoracic wall or adjacent to the spinal cord were not reduced. TS was simulated stepwise from a 0.5 cm to a 2.0 cm reduction, with a step size of 0.5 cm, by altering HUs in the subtracted volume to correspond to the surrounding lung tissue, resulting in 4 new image sets per patient and scanning technique. New CTV-Ts and PTV-Ts were re-generated in each new image set. One patient was excluded due to atelectasis at the time of pre-treatment CT. Furthermore, not all patients had GTV-Ts large enough to enable shrinkage in all steps. Original ST and DE plans were re-calculated on the new image sets, preserving the MU from the original plans.

6.2.4 Atelectasis

One patient had atelectasis enclosing the GTV-T at the planning stage (Figure 17d upper). The atelectasis regressed and finally disappeared during the course of treatment (Figure 17d lower). Pre-treatment FB 4DCT and DIBH 3DCT were rigidly registered to corresponding CTs acquired post-treatment, according to a soft-tissue tumor position verification procedure currently in practice at our clinic. OARs and target volumes were re-delineated on the post-treatment CTs. The dosimetric effect of atelectasis was investigated by re-calculation of the original ST and DE plans in FB and DIBH on the post-treatment CT scans, preserving the MU from the original plans.

6.2.5 Statistical analysis

Statistical analysis was carried out in MATLAB, including the Statistics Toolbox 8.3 (R2013b), (The MathWorks, MA, USA). The aim was to discover potentially statistically significant differences between the impacts of anatomical changes in DIBH and FB as well as between ST and DE plans. Bonferroni corrected two-sided Wilcoxon signed rank tests were applied to test the medians of the data, for each level of anatomical change. Results were considered statistically significant at $p \leq 0.004$ and $p \leq 0.003$, for PE and TS respectively.

6.3 Results

6.3.1 Pleural effusion

Phantom simulations resulted in a reduction of the mean dose to the GTV-T ($<D>_{GTV-T}$) with increasing amount of PE for all tumor positions (Figure 18), with a maximum decrease of 1.3% for the centrally located tumor. For anteriorly and centrally located tumors, this trend was also visible for the mean dose to the CTV-T ($<D>_{CTV-T}$) and the mean dose to the PTV-T ($<D>_{PTV-T}$). For the posteriorly positioned tumor only a slight decrease of the $<D>_{CTV-T}$ was observed, while the $<D>_{PTV-T}$ increased.

For the majority of the patients, simulated PE resulted in decreasing $<D>_{GTV-T}$ with increasing PE (Figure 19). Up to 2.8% decrease was observed for 3 cm PE in FB for both ST and DE plans (patient 6). For the largest amount of PE, median decrease in $<D>_{GTV-T}$ among patients was similar in DIBH (-0.3% for both ST [-2.4%;0.7%] and DE [-2.3%;0.6%] plans) and in FB (-0.3% [-2.8%;0.5%] for ST and -0.4% [-2.8;0.6] for DE plans). Some patients (9, 12 and 15) presented no change in $<D>_{GTV-T}$ with changing amount of PE, and for a few patients (7, 10 and 13) $<D>_{GTV-T}$ even increased with increasing amount of PE (Figure 19).

The Bonferroni corrected two-sided Wilcoxon signed rank test resulted in no statistically significant differences, when considering the effect of PE on $<D>_{GTV-T}$, between FB and DIBH or between ST and DE plans.

Additional results for the effect of PE on the maximum dose (D_{max}) to the spinal cord is provided in supplementary material (available online).
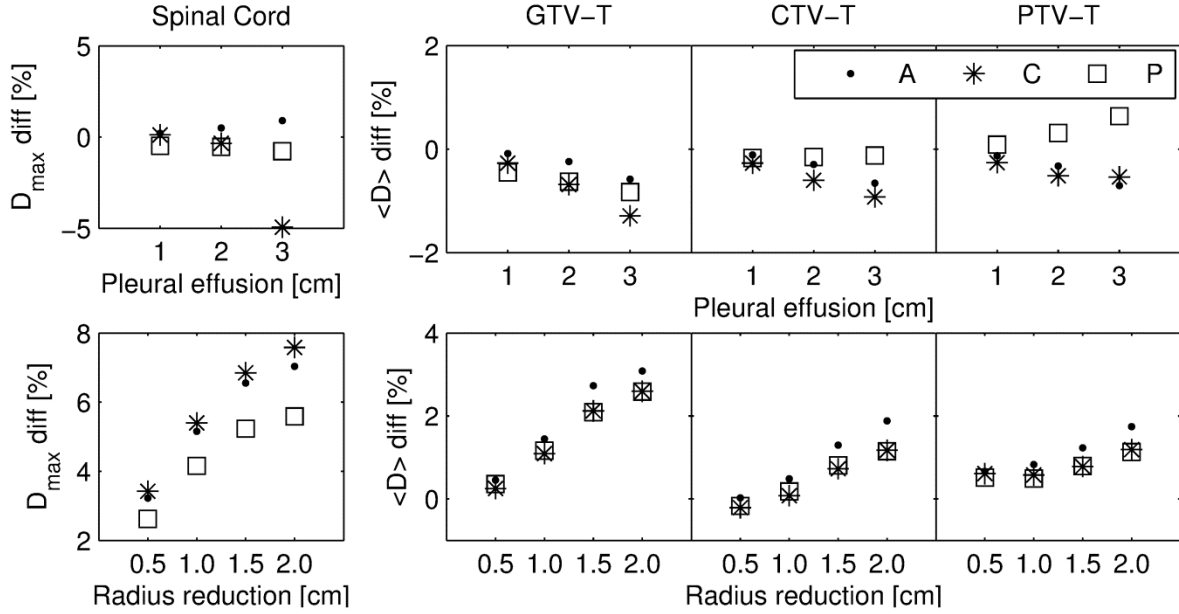
Figure 18. Impact of pleural effusion (upper row) and tumor shrinkage (lower row) on Dmax to the spinal cord as well, <D>GTV-T, <D>CTV-T and <D>PTV-T, for simulations carried out in a CIRS dynamic thorax phantom (locations: A=anterior, C=central, P=posterior).

6.3.2 Tumor shrinkage

Phantom simulations of TS resulted in increasing $<D>_{GTV-T}$, $<D>_{CTV-T}$ and $<D>_{PTV-T}$ with decreasing GTV-T, for all tumor locations (Figure 18). TS had less effect on the $<D>_{CTV-T}$ than on the $<D>_{GTV-T}$, and even smaller impact on the $<D>_{PTV-T}$. A maximum increase of the $<D>_{GTV-T}$ by 3.1% was observed for the anteriorly located tumor. A difference ≥1% in mean dose was reached at a radius reduction of 1 cm for the GTV-T, and 1.5 cm reduction for the CTV-T and PTV-T.

Similar to phantom simulations, increasing $<D>_{GTV-T}$ for decreasing tumor volume was observed for the majority of the patients, regardless of motion management technique and fraction dose (Figure 20), with a maximum increase of 10.4% (DE plan in FB for patient 3). For the largest amount of TS, median increase in $<D>_{GTV-T}$ among patients was smaller in DIBH (2.6% [0.8%;4.1%] for ST and 2.5% [-3.6%;6.9%] DE plans) than in FB (2.6% [0.6%;4.7%] for ST and 5.1% [1.6%;10.4%] for DE plans). In a few cases $<D>_{GTV-T}$ decreased with decreasing tumor volume (DE plan in DIBH for patient 6, 9 and 11, and ST plan in DIBH for patient 5 and 9).

For TS, Bonferroni corrected Wilcoxon signed rank testing on the percentage difference in $<D>_{GTV-T}$, resulted in statistically significant differences, at 0.5 cm radius reduction of the GTV-T, between ST and DE plans for both DIBH (p<0.001; median increase of 0.4% [-0.4%;1.1%] for ST and 1.1% [-0.2%;6.4%] for DE plans) and FB (p<0.001; median increase of 0.5% [0.0%;0.7%] for ST and 1.7% [0.0%;3.8%] for DE plans). However, for 1 cm radius reduction, statistical significance was only observed for corresponding differences in FB (p=0.002; median increase of 1.1% [0.4%;1.8%] for ST and 3.4% [0.6%;5.5%] for DE plans). For all other cases, no statistically significant differences were observed.

Spinal cord results for TS are provided in supplementary material (available online).
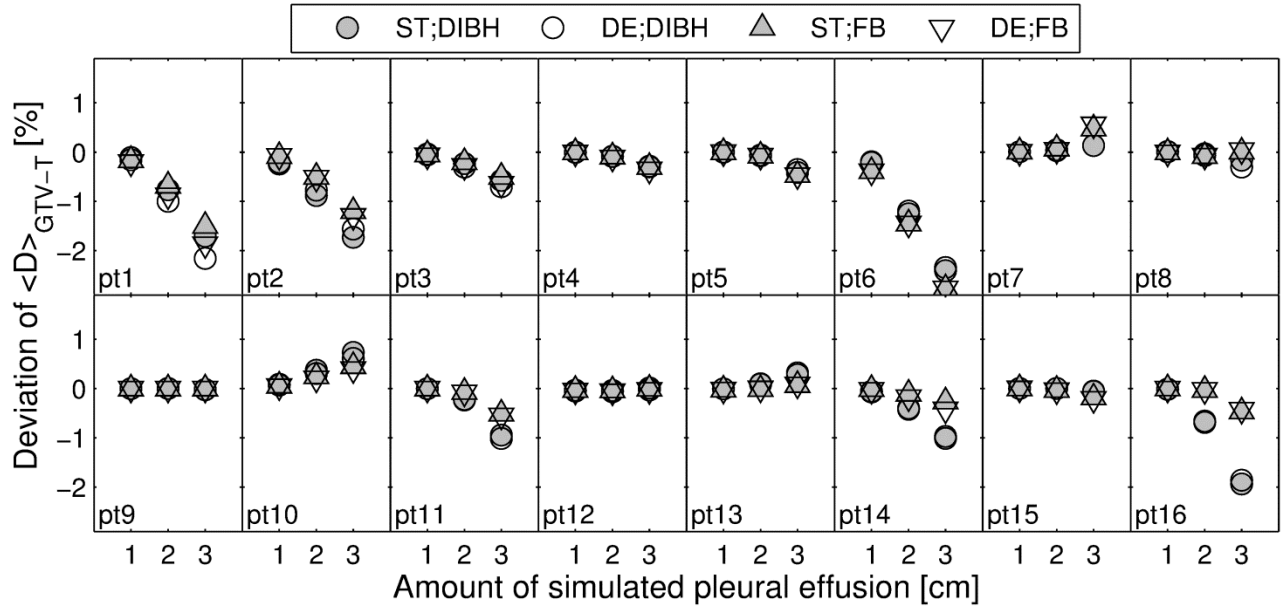
Figure 19. Impact of pleural effusion on $<D>_{GTV-T}$ for all 16 patients and combinations of scanning technique and fractionation.
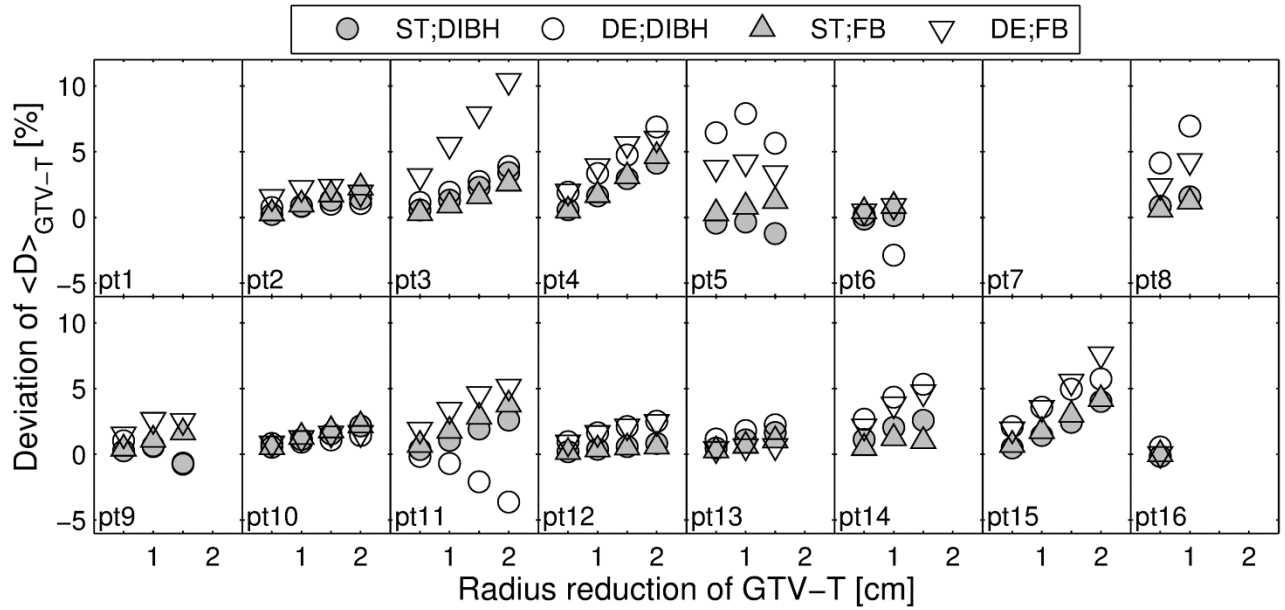
Figure 20. Impact of tumor shrinkage on $<D>_{GTV-T}$ for all 16 patients and combinations of scanning technique and fractionation.

6.3.3 Atelectasis

In addition to atelectasis reduction during the course of treatment for patient 1 (Figure 17d), the total GTV-T decreased by 43.8% and 24.8% for FB and DIBH, respectively. These changes increased the mean dose of the total GTV-T for the ST plan with 2.4% in FB and 0.2% in DIBH. Corresponding numbers for the DE plans were an increase of 1.9% and a decrease of 5.2% for FB and DIBH, respectively. A larger decrease in minimum dose to the target was observed in DIBH (45.3% for ST and 53.8% for DE plan) than in FB (0.1% for ST and 3.5% for DE plan). Spinal cord results are available in supplementary material (online).

6.4   Discussion

The dosimetric impacts of PE, TS and atelectasis on VMAT treatment of NSCLC patients were investigated, both for ST and DE treatments in FB as well as in DIBH. For the clinically realistic ranges of PE and TS considered in the current study, both phantom (Figure 18) and patient simulations (Figure 19 and Figure **20**, Supplementary figure 1 and Supplementary **figure 2**) indicate that TS have larger dosimetric impact than PE, when considering both targets and the spinal cord.

For the majority of the patients a decreasing $<D>_{GTV-T}$ was observed for increasing amount of PE, while spinal cord D_{max} increased. This general decrease in target dose is in concordance with previous studies [14, 15]. The exceptions from this are in most cases due to the location of the tumor. A posteriorly positioned tumor will in some cases get surrounded by fluid during PE, resulting in a build-up effect that is greater than the attenuating effect. This is e.g. indicated by the increase in $<D>_{CTV-T}$ and $<D>_{PTV-T}$ of the posteriorly located tumor in the phantom simulations. The few patient cases where almost no change in $<D>_{GTV-T}$ was present during PE simulations could be explained by the tumor being located in the superior region of the lung where no PE was present (located outside the photon beam). The variation in tumor shapes, sizes and locations of the patient cohort, do also to some extent explain the spread in the resulting deviations from the original $<D>_{GTV-T}$. No apparent difference was observed, when considering robustness to PE, in using DIBH or FB, neither for ST or DE plans, also supported by the lack of statistically significant differences, when considering $<D>_{GTV-T}$. Any conclusion regarding potential advantage, in terms of robustness to PE, in utilizing DIBH or FB when moving towards DE plans, would require larger data sets to strengthen the statistics.

TS mostly resulted in an increase in $<D>_{GTV-T}$ for decreasing tumor volume, complying with the finding of Schmidt et al.[15], who for ST plans observed increases of $<D>_{CTV-T}$ of up to 4.0% when TS occurred. Similarly, also spinal cord D_{max} increased with decreasing tumor volume for the majority of the patients. These effects were furthermore observed when simulating TS in a phantom, regardless of tumor location. However, phantom simulations were carried out by isotropic reduction of the tumor radius, while TS in patients was carried out by only altering the GTV-T adjacent to lung tissue. Furthermore, the patient population consisted of a variation of original GTV-T volumes and locations, affecting the tumor reductions and contributing to the observed inter-patient variation, regarding the differences in $<D>_{GTV-T}$. Original tumor volume can be of importance, as e.g. reduction of already small tumors surrounded by lung tissue will increase the effect of lack of charged particle equilibrium. However, a larger patient cohort is necessary in order to make a statistically significant statement regarding this dependency. Alternatively, actual anatomical changes appearing during the course of treatment could be utilized, as in previous studies[15,28]. Nevertheless, statistically significant differences in $<D>_{GTV-T}$ were observed between ST and DE plans for 0.5 cm and 1 cm simulated TS when treating in FB. For DIBH, statistical significance between ST and DE plans was only observed for a 0.5 cm reduction. This indicates that (i) DE plans are potentially inferior to ST plans in terms of robustness to TS, when considering $<D>_{GTV-T}$, and (ii) DIBH potentially can reduce the impact of TS for DE treatments. This could be explained by the smaller original GTV-T volume when utilizing DIBH, compared to FB[118].

The low variation in the effect on the $<D>_{GTV-T}$ for TS <1 cm radius reduction could explain the statistically significant differences observed when comparing ST and DE plans. The same variation generally increases with increasing anatomical changes and was observed to be larger in comparisons between motion management techniques than fractionation schemes. However, for both PE and TS, statistical analysis of the difference between DIBH and FB resulted in decreasing p-values with increasing anatomical changes, even if never reaching statistical significance, and smaller p-values were generally observed for DE than for ST plans. The median deviations in $<D>_{GTV-T}$ for the largest anatomical changes indicate that DIBH has a

potential superiority when considering TS (Figure 20), while similar responses to PE were observed (Figure 19).

When considering atelectasis, varying results regarding changes in doses to the GTV were observed amongst the different scanning techniques and fractionations in the one patient where atelectasis disappeared during treatment. However, GTV-T also decreased during the course of treatment and (larger decrease observed in FB than in DIBH). Together with registration and delineation uncertainties, this could explain the dosimetric variations observed.

In general, the present study indicates a potential benefit in utilizing DIBH instead of FB during DE radiotherapy of NSCLC patients, regarding robustness to anatomical changes. However, it does not take into account any differences in inter- or intra-fractional uncertainties during setup and delivery of VMAT treatment in DIBH or FB. Furthermore, as positron emission tomography (PET) is necessary for DE treatment, adaption of treatment plans may require a new PET[121]. In addition to the PET signal being sensitive to tissue response after radiotherapy, performing a reproducible PET at the stage of adaption may be a challenge, and is not trivial, since the PET-active volume may be deformed, systematically moved, or new PET-active volumes may be present[122]. The patients enrolled in the current study were only PET imaged in FB. Thus, in order to minimize the bias between DE plans in FB and DIBH, the dose escalation was applied to the entire GTV-T volume in both image sets. The impact of this on the results in the current study is considered small.

Standard action-levels are difficult to define. If 1 % change in $<D>_{GTV-T}$ would be considered as the action-level required, phantom data indicate that action should be taken for PE of ≥3 cm thickness and TS of ≥1 cm radius reduction. This was not confirmed by the patient data, where a larger variation in changes with PE and TS was observed. However, PE results are in concordance with Møller et al.[28], who observed PE for 13 out of 163 studied patients and deviations in $<D>_{PTV-T}$ ≥1% in four cases with ≥2 cm PE.

Randomly occurring anatomical changes of the sort presented in this study can most likely not be accounted for by extending margins. Thus, an adaptive strategy is necessary where the changes during the course of treatment are monitored for each patient individually. Møller et al.[28] have presented results of a random pattern in the appearance and disappearance of anatomical changes supporting this statement. Rapid adaption to anatomical changes (e.g. daily adaptive plan selection) has previously been proven beneficial for normal tissue sparing in sites such as bladder[123]. A similar approach, together with the reduction in treatment volume from utilizing DIBH, is appealing for sparing normal tissue in lung cancer radiotherapy. Similarly to the current study, an approach of density alterations, based on daily CBCT image information, could be utilized in order to alter the original CT, on which re-calculation of the original treatment plan could be carried out. Preferably, deformable image registration would be utilized in order to transfer anatomical information from the CBCT to the original CT image. However, there are known issues required to be solved before having a reliable deformable image registration tool effective for evaluating lung cancer radiotherapy over the course of treatment[124]. It should be mentioned that there are limitations in the AAA calculation algorithm when calculating dose in heterogeneous situations[60,63,64], and Monte Carlo simulations could potentially render different results[125].

In conclusion, phantom simulations have provided information about potential action-levels for when adaptation to appearance of either PE or TS is required. However, for the more complex patient geometry, also tumor volume and location needs to be taken into consideration. Individual assessment of the dosimetric impact should rather be carried out instead of applying standard action levels. This is the recommendation for both ST and DE treatment plans in DIBH as well as in FB, even if the current study suggests a potential superiority in DIBH, regarding the robustness in $<D>_{GTV-T}$ to anatomical changes in DE treatment.

Acknowledgment

6.5 Supplementary material

6.5.1 Supplementary Material and Methods

The clinical protocol was approved by the Copenhagen Regional Committee on Health Research Ethics (protocol no. H-4-2012-066) and the Danish Data Protection Agency (ID. nr.: 2007-58-0015 / HEH.750.24-61). Every patient gave informed consent to the work before inclusion. Patient characteristics are summarized in Supplementary table 1. Patients had varying number of primary tumors and lymph nodes involved as well as spread in the location of the primary tumor.

A marker-based optical breathing signal (RPM, Varian Medical Systems, CA, USA) was utilized both for phase sorting into 10 breathing phases during 4DCT and for visual patient guidance in DIBH 3DCT. During DIBH imaging, patients were audio-visually guided to hold their breath within a pre-defined amplitude level and a gating window 2-3 mm width.

In FB, the primary GTV-T was delineated using the maximum intensity projection (MIP) method, resulting in a primary gross tumor volume including internal margins [10]. In DIBH, GTV-T was delineated directly on the 3DCT. CTV-T was rendered by adding a 5 mm isotropic margin to the GTV and shaping it to boundaries of non-involved tissue, such as bone and vessels. Furthermore, a PTV-T was created by adding 5mm isotropic margin to the CTV-T.

Supplementary table 1. Summary of patient characteristics, including age, gender, TNM stage, tumor location, TMI and original GTV-T volume [cm^3] in DIBH and FB, respectively. Note, for patient 12, that the mentioning of two lung lobes indicates the single tumor extending through both lobes.

Patient	Age	Gender	TNM	Tumor location	TMI	DIBH GTV-T [cm^3]	FB GTV-T [cm^3]
1	77	M	T4N0M0	LUL	N	54	72
2	54	F	T4N2M0	LUL	Y	70	83
3	71	M	T4N0M0	LUL	Y	249	281
4	73	F	T4N0M0	LUL	Y	183	205
5	64	M	T2aN2M0	RUL	Y	38	46
6	67	M	T2aN2M0	RLL	N	33	54
7	74	M	T1aN2M0	LUL	N	2	4
8	65	M	T3N2M0	RUL	N	58	132
9	77	M	T2aN2M0	LUL	N	46	53
10	66	M	T3N2M0	LLL	Y	208	248
11	58	F	T3N2M0	RUL	N	114	143
12	58	F	T3N1M0	RUL˙RML	Y	791	806
13	56	M	T4N1M0	LLL	N	383	437
14	59	M	T3N2M0	RLL	Y	91	140
15	70	M	T3N3M0	RUL	Y	151	170
16	64	F	T1bN3M0	LLL	Y	9	17

M, Male; F, Female; TNM, Tumor-Node-Metastasis staging; L/R-UL, Left/Right-Upper Lobe; L/R-LL, Left/Right-Lower Lobe; RML, Right Middle Lobe; TMI, Tumor Mediastinal Involvement; N, No; Y, Yes.

For treatment planning in FB, the untagged reconstruction of the 4DCT was utilized. Treatment planning was carried out for ST and DE treatment plans in FB and DIBH, using multiple half-arc volumetric modulated arc therapy (VMAT) (RapidArc, Varian Medical Systems, CA, USA), resulting in a total of 64 original plans for the 16 patients. The ST plans were utilized for treatment in FB on Varian 2300 iX linear accelerators [16] in 33 fractions (fx), to a total dose of 66 Gy (2 Gy/fx, 5 fx/week). DE plans were achieved by increasing the ¡D¿GTV-T to a maximum of 95 Gy (33 fx), while maintaining normal tissue doses similar to the ST plans (limited by dose to the lungs and to the spinal cord).

6.5.2 Supplementary results

Pleural effusion

For phantom simulations, introduction of 1 cm or 2 cm pleural fluid had little effect on the spinal cord Dmax (Figure 18). However, introduction of 3 cm pleural fluid resulted in a decreased D_{max} of 4.9% for the centrally located tumor. An increase (0.9%) in the D_{max} was only observed for the anteriorly located tumor and 3 cm fluid.

Furthermore, only for a few patients (patient 1 for ST plan in DIBH, patients 3 and 4 for DE plans in DIBH, patient 6 for DE plans in DIBH and FB, patient 7 for ST plan in DIBH and patient 13 for ST plan in FB) gave the introduction of PE rise to changes in D_{max} to the spinal cord of ≥1%, with a maximum of 1.4% increase (patient 3 for 3 cm PE and DE plan in DIBH) (Supplementary figure 1).

Tumor shrinkage

For patient simulations, a 2 cm reduction of the tumor radius resulted in an increase in D_{max} to the spinal cord of 7.6% for the centrally located tumor (Figure 18). Even the smallest radius reduction of 0.5 cm resulted in an increase of ≥2% for the Dmax of the spinal cord, regardless of tumor location.

For the patient population, TS had an impact on the Dmax to the spinal cord of ≥1% increase at 1 cm radius reduction for the majority of the patients, and a maximum increase of 9.9% (DE plan in FB for patient 12) (Supplementary figure 2). However, some patients (patient 10 and ST plans in FB for patient 4 and 8) had a small decrease in D_{max} of the spinal cord with decreasing tumor volume.

Atelectasis

For the spinal cord, atelectasis resulted in increments of 9.6% and 7.1% of the Dmax in DIBH for ST and DE plans, respectively. Corresponding numbers for FB were 9.2% and 11.1% for ST and DE plans, respectively.
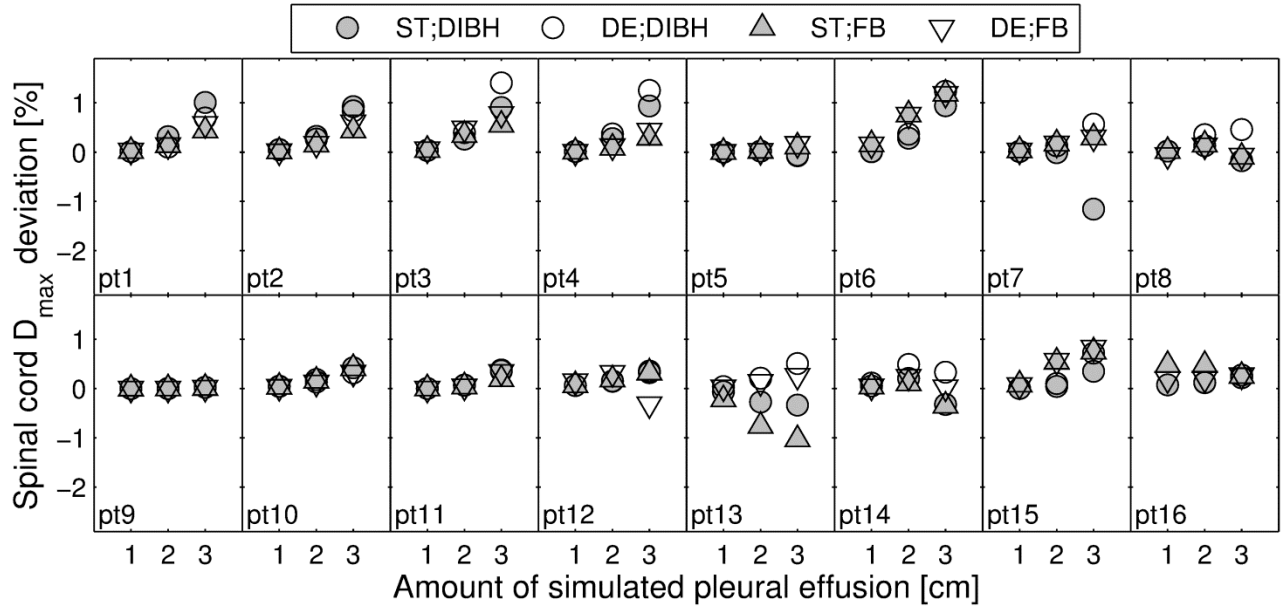
Supplementary figure 1. Impact of pleural effusion on Dmax to the spinal cord for all 16 patients and combinations of scanning technique and fractionation.
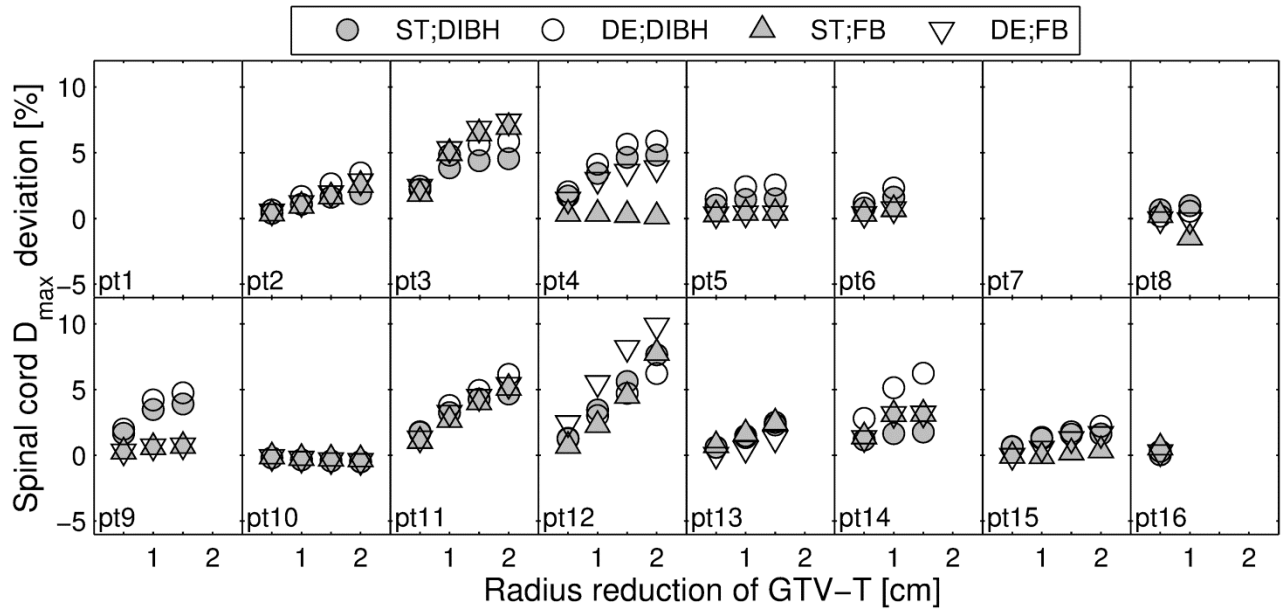
Supplementary figure 2. Impact of tumor shrinkage on Dmax to the spinal cord for all 16 patients and combinations of scanning technique and fractionation.

7 Paper II

Time-resolved plastic scintillator dosimetry in a dynamic thorax phantom

Patrik Sibolt[1,2,†], Claus E. Andersen[1], Wiviann Ottosson[2] and Claus F. Behrens[2]

[1]Technical University of Denmark, Center for Nuclear Technologies, Risø Campus, Frederiksborgvej 399, DK-4000, Roskilde, Denmark

[2]Herlev Hospital, Radiotherapy Research Unit, Herlev Ringvej 75, DK-2730, Herlev, Denmark

[†]Corresponding author: pasi@dtu.dk

Abstract. Motion managed and dynamic radiotherapy of lung cancer patients is increasingly complex and subject to challenges related to respiratory motion and heterogeneous tissue densities. This puts high demands on methods for quality assurance and especially time-resolved dose verification of the treatment delivery. The aim of this study was to develop a novel dynamic thorax phantom for time-resolved plastic scintillator dosimetry. The in-house developed phantom has a well-known geometry mimicking a lung cancer patient with a reproducible (within 0.04 mm), respiratory-like motion of a tumor embedded in a lung. The phantom motion was controlled by a script in-house developed using LabVIEW (National Instruments) and synchronized with the in-house developed ME40 scintillator dosimetry system (DTU Nutech). The dose in the center of the tumor was measured, using a BCF-60 plastic scintillator detector (Saint-Gobain Ceramics & Plastics Inc.), during dynamic 6 MV half-arc treatments on a TrueBeam linear accelerator (Varian Medical Systems). Deviations of ˜2% from the corresponding dose calculated by the treatment planning system (TPS) were detected. The results emphasize the shortcomings of commercial TPSs to handle respiratory motion and lack of lateral charged particle equilibrium, motivating quality assurance based on a system like the one presented in this study. It has specifically been demonstrated that reliable time-resolved scintillator dosimetry in a dynamic thorax phantom can play an essential role in dose verification of lung cancer radiotherapy.

7.1 Introduction

Dynamic radiotherapy of lung cancer patients is subject to challenges related to breathing motion and heterogeneities. The report of AAPM Task Group 76 presents recommendations on respiratory motion management during radiotherapy[13]. The report includes guidelines motion-encompassing methods, respiratory gated techniques, breath-hold techniques, and respiration-synchronized techniques and it moreover stresses the need for quality assurance (QA) of the devices and methods. The demands on reliable QA methods are increasing, as for example gating and tracking methods are becoming more and more complex. It is furthermore known that commercial treatment planning systems (TPSs) have difficulties with accounting for lack of charged particle equilibrium (CPE) in volumes of the body encompassing heterogeneities such as lung, air cavities and bone[14,57–59]. Thus, reliable verification of dose calculation and delivery is critical. Not only is the accumulated dose of relevance but for motion managed radiotherapy the dose delivered as a function of time should be considered. This is especially the case if one is interested in finding the underlying cause of a failed treatment delivery. The benefit of time resolved dosimetry over accumulated dose measurements lies in the increased likelihood of separating errors due to for example MLC motion, gantry

motion and interplay effects. Such methods for time-resolved dose verification has previously been presented based on the use of electronic portal imaging device (EPID)[68–70], fiber-coupled aluminum oxide crystals[71], as well as the Scandidos Delta[4] diode array[72]. However, to the authors' knowledge, there is a lack of systems providing time-resolved measurements in a geometry mimicking the heterogeneous anatomy and respiratory motion of the thoracic part of a patient. A detector suitable for dosimetry in that kind of complex geometry is the fiber-coupled plastic scintillator detector (PSD) as its characteristics make it suitable for time-resolved radiation dosimetry in small, complex and dynamic megavoltage (MV) photon beams[74–77]. This study aimed to develop a novel dosimetry system, combining and synchronizing an in-house developed dynamic thorax phantom with an in-house developed PSD dosimetry system. It furthermore aimed to verify the reliability of the system and to test its applicability on clinically relevant dynamic arc treatments.

7.2 Material and Methods

7.2.1 Dynamic thorax phantom

Phantom description

The dynamic thorax phantom was developed to enable time-resolved dosimetry of complex dynamic radiotherapy using an organic plastic scintillator detector (PSD) in a geometry resembling a lung cancer patient. The phantom design has previously been described, why only a brief description is given here[80]. A thorax phantom, mimicking a lung cancer patient, was designed and built with a well-defined geometry consisting of a PMMA body (34 cm in width, 23 cm in height, 40 cm in length) with three hollow cylinders (50 cm in length, 10 cm in diameter) (Figure 6). The cylinders can be filled with various inserts in order to simulate either hetero- or homogeneous geometries. The inserts mimicking bone, lung or soft tissue are constructed out of high density delrin, low density balsa wood, and PMMA, respectively. The dimensions of the inserts were chosen based on data on the human anatomy and PMMA spheres of various diameters ($1 - 8$ cm) were embedded inside the lung inserts (15 cm in length and 9 cm in diameter) in order to simulate tumors in the lung . The design of the inserts enables PSD measurements in the center of the tumor.
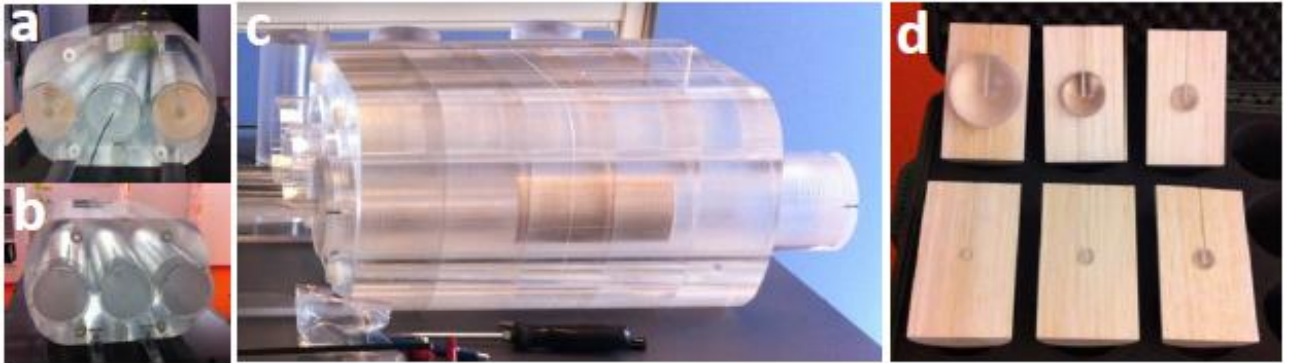
Figure 21. a) A heterogeneous setup where the two lateral cylinders are filled with balsa wood inserts. b) A homogeneous setup with everything in PMMA. c) The heterogeneous setup described in a) viewed from the side. d) Balsa wood lung inserts with associated tumors. (Figure adopted with permission from Ottosson et al.,[80])

Dynamic motion of the phantom

In order to replicate the respiratory motion of a lung cancer patient, the thorax phantom, described in section 2.1.1., was connected to a motorized linear stage (A-LST0250B-C, Zaber Technologies Inc.) (Figure 22). The connection was constructed using a PMMA rod mounted to the stage and attached to the end wall of one of the lateral cylinder inserts. This enabled one dimensional motion of the cylinder through the length of the body of the thorax phantom. In order to simulate a complex realistic dynamic breathing motion of the tumor

and lung insert, a script for controlling the motion of the linear stage was in-house developed using LabVIEW (National Instruments). This was partly based on a library of LabVIEW instrument drivers provided by the stage vendor. Communication between the script (local PC) and the linear stage was conducted through a 115200 baud RS232 serial port. The script operates by first moving the cylinder insert to the center position for an optimal position of the lung insert and tumor before initiating the accelerator beam and scintillator measurements. It thereafter requires an input file describing the desired motion of the cylinder. This motion input should include the expected position as a function of time and can be either manually generated or for example based on monitored respiratory motion of a lung cancer patient using a respiratory monitoring/gating system. As the linear stage is set in motion the script starts to acquire the position of the stage in real-time. Knowing the actual and expected position, the script continuously updates the velocity of the stage in order to continue along the desired motion pattern.
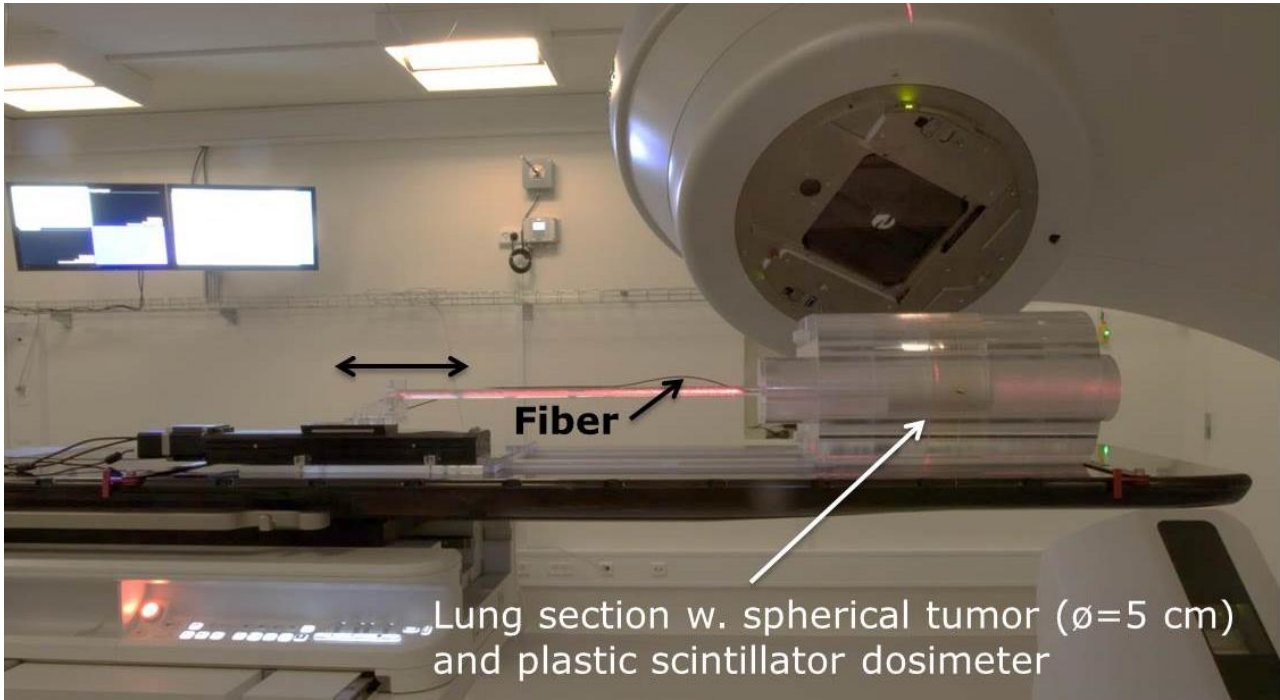
Figure 22. The setup of the dynamic thorax phantom with the motorized linear stage connected through a rod with one of the lateral cylinders. The plastic scintillator detector is placed in the center of the spherical tumor (diameter of 5 cm), located in the center of the balsa wood lung insert.

7.2.2 Time-resolved fiber-coupled plastic scintillator dosimetry

In order to use the PSD measured radiation dose for time-resolved verification of the treatment, the motion of the phantom was required to be linked to the measured dose as a function of time. The motion of the phantom was therefore synchronized with the in-house developed ME40 scintillator dosimetry system (DTU Nutech)[75] using an external 10 V ramp signal (period: 6 s) which was simultaneously recorded by both systems. The synchronization between measurements and phantom motion furthermore imply a synchronization with the linear accelerator log files as the ME40 system is triggering on the sync pulse from the linear accelerator. It is therefore, for example, possible to use the described dynamic thorax phantom dosimetry system as an input to four-dimensional Monte Carlo simulations, opening up for a solid solution for complete quality assurance of complex lung cancer radiotherapy.

All measurements in this study were carried out using a BCF-60 PSD (Saint-Gobain Ceramics & Plastics Inc.), with a diameter of 1 mm and a length of 2 mm. The system has previously been described and further studied for its potential use in time-resolved verification of dynamic radiotherapy [75,77]. With 0.1 ms readout and mm spatial resolution it is well suited for detailed time-resolve quality assurance of small dynamic

radiotherapy dose increments. Chromatic removal calibration of the PSD was conducted according to the procedure (method C) described by Guillot *et al.* [78] in a solid water calibration phantom.

7.2.3   Experimental setup

A PMMA sphere of 5 cm diameter (tumor) embedded in a lung insert was laterally positioned in the thorax phantom. The dynamic motion of the phantom was performed using the motorized linear stage controlled by the in-house developed script as described in section 2.1.2. During CT-scans and irradiations the cylinder with the tumor embedded in the lung insert was set in a respiratory-like sinusoidal motion with a frequency of 0.25 Hz, corresponding to a clinically relevant breath-rate of 15 breaths per minute, and peak-to-peak amplitude of 20 mm. The dynamic phantom was scanned in a 16 slice Philips Brilliance CT Big Bore scanner (Philips Medical Systems, Cleveland, OH) according to a clinically used four-dimensional CT (4DCT) protocol[29]. From the acquired 4DCT images an UnTagged image reconstruction was obtained. The UnTagged image set is a time weighted reconstruction with a true Hounsfield unit representation, used for treatment planning and dose calculation. Two 6 MV half-arc RapidArc plans were optimized and calculated using the Anisotropic-Analytical-Algorithm (AAA) in Eclipse TPS (Varian Medical Systems) to yield 1 Gy (plan 1) and 2 Gy (plan 2) mean target dose. The target was defined as the tumor without any additional margin. Treatment plan delivery was performed using a Varian TrueBeam linear accelerator and time-resolved (resolution: 3.3 ms) measurements (n=6 per plan) were conducted with the PSD positioned centrally in the tumor (Figure 22). The start of each irradiation (beam on) was not synchronized with the tumor position, i.e. the tumor position at beam on was random, in order to simulate a clinically relevant situation.

7.3   Results and discussion

7.3.1   Phantom motion reproducibility

The script designed to control the phantom motion resulted in an average update interval of 29 ms, corresponding well with the 20 ms time interval between linear accelerator pulses as well as control points in the log files, received for the Varian TrueBeam accelerator. The update frequency of the motion controlling script depends on the desired motion of the phantom. A more complex motion will generally require more frequent velocity updates compared with less dynamic motion patterns. There is, however, a limit to the update frequency depending on the specification of the computer as well as the communication method used to control the linear stage. The acquired motion profiles resulted in a mean and standard deviation (1 SD) of the phantom motion peak amplitude (n=116) of 10.04 mm and 0.05 mm, respectively (Figure 23). The control system for the linear stage can therefore be considered reliable and reproducible, securing a well-known position of the tumor insert as well as PSD. It should however be noted that this initial study is performed for simple sinusoidal motions and that patient-specific analysis of motion reproducibility could be needed, despite the promising results presented here. The possibility to adjust the script depending on the motion input and requirements of the user is an additional feature and one of the major benefits of an in-house developed phantom and control system.
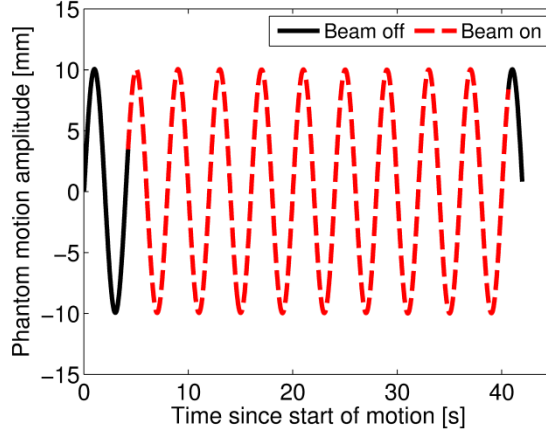
Figure 23. Graph of one movement of the linear stage connected to the lateral cylinder with the spherical tumor insert inside the balsa wood lung insert. The red part of the curve indicates that the linear accelerator beam was turned on, demonstrating the synchronization between the system controlling the motion of the dynamic thorax phantom and the ME40 scintillator dosimetry system.

7.3.2 Plastic scintillator detector measurements of dynamic treatments

The PSD measurements in the center of the tumor resulted in average accumulated doses of 1.056 Gy and 2.113 Gy (relative SD ≈ 1%; n = 6 per plan), deviating by -1.6 % and -2.8 % from the equivalent TPS doses (point dose in center of tumor) for plan 1 and plan 2, respectively. Deviations between PSD and TPS doses were expected due to known calculation challenges for the TPS in heterogeneous geometries, where lack of lateral CPE can exist. The detected deviations correspond well with previously reported results for static measurements[80], indicating that the effect of the motion of the tumor is most likely insignificant in the center of the tumor and for the simple sinusoidal case presented in this study. It also demonstrates that the motion of the phantom is well-behaving as the expected deviations are due to known calculation difficulties and not related to any discrepancies in the expected motion of the phantom. However, it is interesting to note that the measured dose as a function of time displays a variation in how the dose is delivered during the irradiations (Figure 24). This variation is most likely due to the random position of the tumor at beam on (average = 2.91 [-9.28; 10.02] mm), as interplay effects caused by the unsynchronized motion of the tumor and the dynamic beam configuration will manifest differently for different motion patterns. Interplay effects have, however, been reported to be mostly relevant if dynamic treatment delivery is given with very few arcs in very few fractions[25,126] and that it averages out if given over a large number of fractions[127]. The detected variation can also partly be explained by variations in how the machine performs from treatment to treatment. However, initial 4D Monte Carlo simulations of these measurements do not indicate any deviations greater than 0.1% in accumulated dose between calculations based on the expected treatment delivery and the actually delivered treatment as seen in the accelerator log files [128].
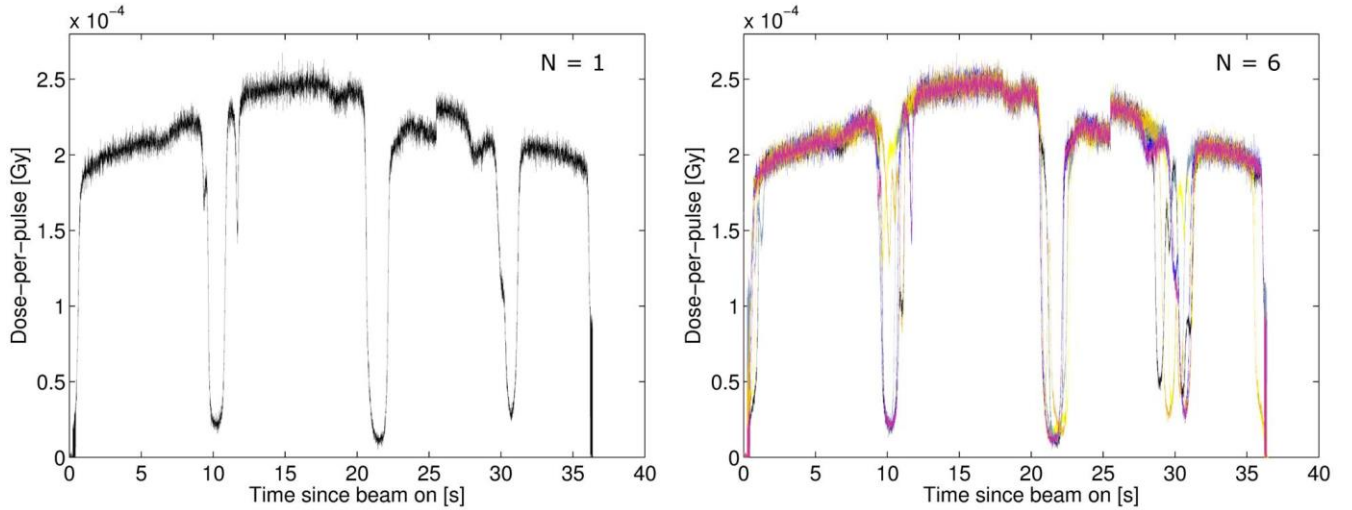
Figure 24. The PSD measured dose as a function of beam-on time for plan 2, presented for a single irradiation (left) as well as for all six irradiations (right). Note how the dose per pulse varies between the repeated measurements, especially around 30 s beam on time, but also around 10 s, 20 s and at the time of beam on and beam off.

7.4 Conclusions

A novel dynamic thorax phantom was developed, enabling time-resolved PSD dosimetry during reproducible, respiratory-like, motion of a lung tumor. This study stresses the challenges in commercial TPSs to correctly calculate dose in heterogeneous geometries. It furthermore suggests that how the dose is deposited as a function of time potentially depends on the position of the tumor at beam on (interplay effects). It has been demonstrated that reliable PSD dosimetry in a dynamic thorax phantom can play an essential role in dose verification of lung cancer radiotherapy. Furthermore, the shortcomings of commercial TPSs to handle respiratory motion and lack of CPE motivate quality assurance with the use of a system like the one presented in this study, preferably in combination with a solution for 4D Monte Carlo simulations.

Acknowledgements

8 Paper III

Automated four-dimensional Monte Carlo workflow using log files and real-time motion monitoring

P Sibolt[1,2,†], R O Cronholm[3], E Heath[4], C E Andersen[1] and C F Behrens[2]

[1]Center for Nuclear Technologies, Technical University of Denmark, Roskilde, Denmark

[2]Radiotherapy Research Unit, Herlev Hospital, Herlev, Denmark

[3]Department of Radiation Physics, Skåne University Hospital, Lund, Sweden

[4]Carleton Laboratory for Radiotherapy Physics, Carleton University, Ottawa, Canada.

[†]Corresponding author: pasi@dtu.dk

Abstract. With emerging techniques for tracking and gating methods in radiotherapy of lung cancer patients, there is an increasing need for efficient four-dimensional Monte Carlo (4DMC) based quality assurance (QA). An automated and flexible workflow for 4DMC QA, based on the 4DdefDOSXYZnrc user code, has been developed in python. The workflow has been tested and verified using an in-house developed dosimetry system comprised of a dynamic thorax phantom constructed for plastic scintillator dosimetry. The workflow is directly compatible with any treatment planning system and can also be triggered by the appearance of linac log files. It has minimum user interaction and, with the use of linac log files, it provides a method for verification of the actually delivered dose in the patient geometry.

8.1 Introduction

Motion management in external beam radiotherapy is becoming increasingly sophisticated and the demands on quality assurance (QA) of advanced radiotherapy are therefore also increasing. One interesting example is the need for QA of emerging techniques for tracking and gating methods in radiotherapy of lung cancer patients. Many commercial treatment planning systems (TPS) have recognized difficulties to accurately calculate dose for dynamic treatments due to challenges related to breathing motion and heterogeneities. This has for example been shown for deep-inspiration breath-hold (DIBH) intensity-modulated radiotherapy (IMRT) of lung cancer patients, where Monte Carlo (MC) calculations revealed large inaccuracies in the dose calculated by the TPS [14]. Monte Carlo is considered to be the gold standard among dose calculation algorithms and the use of MC-based QA (MCQA) for verification of external beam radiotherapy is widely recommended, especially in the case of four-dimensional treatments [129]. However, implementation of MCQA often involves procedures including several steps of manual interaction or its integration into one specific TPS using a designated interface. An automated MCQA workflow with minimum user interaction is much more desirable. Preferably this MCQA workflow would enable four-dimensional Monte Carlo (4DMC) which models synchronously the dynamic beam configurations and the motion and deformation of the patient anatomy.

The purpose of this study was to incorporate a solution for 4DMC into an automated MCQA workflow with the possibility to use linear accelerator (linac) log files and motion monitoring signals for both pre-treatment and per-fraction dose verification.

8.2 Material and Methods

8.2.1 Workflow for four-dimensional Monte Carlo

In order to incorporate the synchronization between the dynamic beam configuration and the motion of the patient anatomy, MC simulations were carried out using 4DdefDOSXYZnrc. The 4DdefDOSXYZnrc code is an altered version of the EGSnrc [85] user code defDOSXYZnrc, where dose deposition is tracked in a

deformed anatomy without altering the voxel grid[100,107]. It makes use of the source 20 of DOSYZnrc for simulation of continuously varying beam configurations [87]. The 4DdefDOSXYZnrc user code samples a new geometry for each incident particle, which enables simulation of a continuously moving anatomy. The geometries are sampled by linearly interpolating a deformation vector field, determined from image registration between the reference phase and an extreme phase of the 4DCT, using the motion signal measured during treatment.

The use of linac log files, deformation vector fields, and motion monitoring signal as an input for the 4DMC simulations is incorporated within a workflow solution for automated MCQA. The workflow is built up of a number of different modules, all written in python, which are executed sequentially without user interaction (Table 2). The automation of the workflow depends on each module, at the end of execution, leaving data for the next module to process. The workflow is connected to the TPS by means of exports and imports done in the TPS. This implicitly means that the workflow is portable between TPSs. The first module reads and processes TPS exported DICOM files and the last module writes the resulting dose distributions as DICOM files. In addition to the original TPS DICOM files, the 4D workflow requires access to the deformation vector field and the motion monitoring signal. This access can be configured differently depending upon the deformable image registration software and motion monitoring system in use. Furthermore, the workflow can be initiated by the appearance of linac log files, which are used to write the DICOM input files needed to trigger the start of the workflow.

Table 2. A brief description of the different modules that constitutes the modified workflow enabling four-dimensional Monte Carlo based quality assurance.

Module	Brief description
I	Generates BEAMnrc/4DdefDOSXYZnrc input files replicating all plan and motion specific parameters. Initiates module II if CT data and RT Structure Set are exported from the TPS.
II	Builds a voxalized phantom based on the CT data and information form the RT Structure Set. The module is based on CTC-ask [130]. The distinct differences being that it is written in python, automated and includes patient support structures. Media selection rules are predefined by the user and can be differentiated for various structure types. Also handles the motion input and writes the vector field in the correct format for further use in the simulations.
III	Initiates treatment specific BEAMnrc simulation starting from a previously generated phase space scored above collimating devices.
IV	Concatenates phase spaces files (if parallel simulation). Computes number of histories required in order to achieve a fixed level of uncertainty. Initiates 4DdefDOSXYZnrc simulations.
V	Deletes auxiliary files (e.g. phase spaces)
VI	Converts to absolute dose. Writes DICOM RT objects using the exported files as templates.

One of the aims of the proposed workflow is that no simulation parameters should be hardcoded. Instead, the workflow uses initial phase space files together with templates, where only treatment specific parameters are overwritten. The workflow is controlled by extracting information from the provided DICOM RP files together with data from a global and a machine specific configuration file written in plain text. This makes the workflow flexible and independent of vendor, energy and fluence mode.

Sending a treatment plan through this workflow results in a set of DICOM RT objects (plan and dose), which are written using the TPS exported files as templates. This enables direct import to any TPS with automatic connection to the correct study.

8.2.2 Example with an in-house developed moving thorax phantom

A time-resolved plastic scintillator detector (PSD) dosimetry system was combined with a dynamic thorax phantom (both in-house developed), containing a PMMA sphere (tumor, ø = 5 cm) embedded in a balsa wood insert (lung) and laterally position in a hollow cylinder [80]. During irradiations, the cylinder containing the tumor was set in a controlled respiratory-like sinusoidal motion with a frequency of 0.25 Hz and peak-to-peak amplitude of 20 mm (corresponding to a clinically relevant motion with 15 breaths per minute). PSD measurements were performed in the center of the tumor for two half-arc 6 MV RapidArc plans (plan 1 and 2 optimized to give mean tumor doses of 1 Gy and 2 Gy, respectively) on a Varian TrueBeam linac. Trajectory log files and phantom motion profiles were obtained during the measurements and thereafter used for generating 4D MC input files. Deformation vectors corresponding to the phantom cylinder motion during treatments were manually generated and applied to the voxel grid at a reference phase. Monte Carlo simulations in the deformed anatomy were carried out, according to the workflow described above, with a calculation time of less than 24 hours on a standard CPU based cluster for a statistical uncertainty below 0.2 %. 4D MC input files were based on both the treatment plan beam configurations as planned in the TPS as well as the actually delivered dynamic beam configuration as extracted from the linac log files. A comparison between planned and delivered dose was conducted.

8.3 Results

8.3.1 Example with an in-house developed thorax phantom
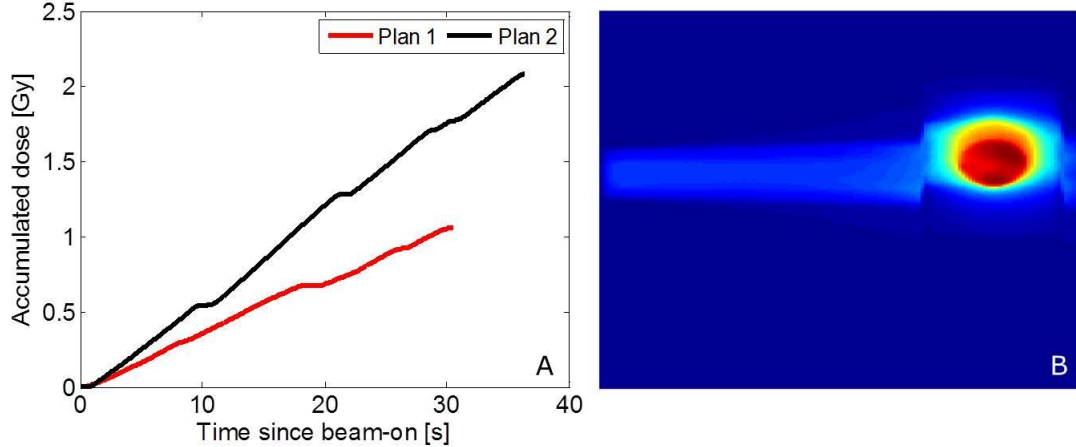
Figure 25. (A) The accumulated dose over time measured by the PSD in a dynamic thorax phantom for plan 1 and 2 and (B) the corresponding 4Ddefdosxyznrc calculated accumulated dose based on the actually delivered beam configuration obtained from the linac log file, presented for a slice centrally located in the tumor.

The time-resolved PSD measurements resulted in average accumulated doses (relative standard deviation of ˜1 %; n = 6 per plan) deviating from corresponding TPS isocenter doses with -1.6 % and -2.8 % for plan 1 and 2, respectively (figure 1A). The hypothesis was that the deviations between measured and TPS calculated doses were true deviations as a result of the tumor motion and the difficulties for the TPS to accurately account for the lack of charged particle equilibrium (CPE). This was verified by the 4D MC simulations (figure 1B). Simulations based on expected and actual beam configuration information resulted in differences in extracted accumulated tumor center doses of approximately 0.1 %, confirming that PSD measured and TPS calculated doses did not differ due to treatment delivery uncertainties.

8.4   Conclusions

An automated and flexible workflow for four-dimensional Monte Carlo QA, based on the EGSnrc user code 4DdefDOSXYZnrc, has been developed. The workflow is initiated from the TPS via export of files and thus directly compatible with any TPS. It can also be triggered by the appearance of linac log files. Enabling 4DMC requires an extra user interaction compared to 3D simulations due to the need for deformation and motion information. The end product is a set of DICOM RT objects that can be imported into, and analyzed in, the TPS. The major benefits of a solution for 4D dose verification like the one proposed here are the resource effectiveness, the fact that it requires no beam time and results in a dose in the patient geometry. Additionally, with the use of linac log files it provides a method for verification of the actually delivered dose.

9 Paper IV

First validation of a user code for time-resolved Monte Carlo simulations of dose delivered to a dynamic thorax phantom using plastic scintillator dosimetry

P Sibolt[1,2,†], C E Andersen[1], C F Behrens[2], R O Cronholm[3], and E Heath[4],

[1]Center for Nuclear Technologies, Technical University of Denmark, Roskilde, Denmark

[2]Radiotherapy Research Unit, Herlev and Gentofte Hospital, Herlev, Denmark

[3]Department of Radiation Physics, Skåne University Hospital, Lund, Sweden

[4]Carleton Laboratory for Radiotherapy Physics, Carleton University, Ottawa, Canada.

[†]Corresponding author: pasi@dtu.dk

9.1 Introduction

Intra-fractional motion is one of the major challenges in radiotherapy in the abdominal and thoracic region of cancer patients. Due to the respiratory movement, large margins are in general applied in order to ensure correct target dosage[8,11,13]. However, adding large margins increases the irradiated volume and thus also the risk of normal tissue complication. In stereotactic body radiation therapy (SBRT) of lung cancer patients, where large doses are delivered in fewer fractions than conventional radiotherapy, this has for a long time been acknowledged as a major limitation[13,131]. Furthermore, with the introduction of dose escalation to targets otherwise subject to standard fractionation, the need for minimizing the irradiated volume is increasing also for conventional lung cancer radiotherapy[3,5,121]. Methods that have been applied in order to reduce the normal tissue toxicity due to large irradiated volumes include various implementations of respiratory-gated radiotherapy[11,14,117,118,132] and tracking[37,38,131,133,134]. Deep-inspiration breath-hold has e.g. been proven feasible and also potentially superior to free-breathing in dose-escalated lung cancer radiotherapy[135], while tracking can be more time-efficient and significantly increase the rather poor duty cycle[13]. Furthermore, real-time tumor tracking using MRI-guided radiotherapy is emerging[47–50] and will contribute to the increased complexity of lung cancer radiotherapy and the need for advanced dose calculation solutions, both for treatment planning but also for independent quality control. Common for all levels of complexity in lung cancer radiotherapy is, however, the presence of time-dependent dose uncertainties. Dose blurring[13,136], localized deformations in the dose distribution[136,137] as well as interplay effects[26,27] are all contributing to the uncertainties and errors in the calculated and delivered dose. The major reason for these effects is the limitation in using a 3D representation of the treated geometry while delivering the dose in a 4D setting. By using all information acquired from 4DCT imaging and respiratory monitoring, many previous studies have emphasized the need for 4D dose calculation approaches in order to improved accuracy in these settings. Methods applied have included convolution of the dose or the incident beam fluence by a probability density function describing the breathing pattern[89–92], and accumulation of dose calculated on multiple respiratory phases with or without the use of deformable image registration[94–97]. Several of these studies also utilized the superior accuracy in Monte Carlo simulations for use in heterogeneous anatomies. However, all of the methods referenced above suffer from assumptions and limitations; ranging from inaccuracies at tissue boundaries and inability to include interplay effects or take anatomical deformations into account to lack of conservation of the dose calculation grid. Therefore, energy/mass transfer[101–105] and voxel warping[100,106] methods were introduced as solutions conserving the mass and energy deposited for each point in time. Despite the improved accuracy in the latter solutions, they are still dose accumulation methods that do not provide the dose as a function of time. The time-dependent accuracy of treatment

delivery is therefore rarely known, making it difficult to locate the underlying cause of a potentially failed delivery, as concluded from the total dose. Recently a Monte Carlo based 4D dose accumulation solution, using the voxel warping approach, has been developed, tested and validated for dynamic dose delivery to a lung motion phantom[108]. The tool has also been included into an automated workflow using synchronized respiratory motion and treatment logfiles to trigger the process of providing 4D Monte Carlo simulations of dynamic beam delivery and the actual respiratory movement during irradiation[128]. By a novel approach to variance reduction the aim of this study was to further develop this 4D Monte Carlo approach in order to generate time-resolved 4D MC (4DtMC) dose calculations and to experimentally validate this method by using a plastic organic scintillator detector (PSD) for time-resolved dosimetry in a dynamic thorax phantom.

9.2   Material and Methods

9.2.1   In-house developed dynamic thorax phantom

In order to carry out the experiments in a geometry similar to a lung cancer patient, an in-house developed dynamic thorax phantom was used throughout this study. The phantom mimics the thorax of a patient both in dimensions and choice of material, with a body of PMMA, cylindrical lung inserts of balsa wood and spherical tumor inserts of PMMA (Figure 26). The design of the phantom has previously been described in detail[80]. In this study the focus was not to make use of the flexibility in geometrical setup but rather to simplify the geometry by maintaining a tumor size of 5 cm in diameter, positioned in one of the two lateral lung inserts. Furthermore, the columna was here mimicked by using a cylindrical insert of delrin in order to fully simulate the heterogeneous setup which is the case for radiotherapy of lung cancer patients. The dynamic in this study was, however, focused towards treatment planning and most of all the presence of motion or not. By connecting a motorized linear stage to the thorax phantom the respiratory motion of a lung cancer patient could be replicated in a reliable and reproducible manner. The construction enabling a one-dimensional motion of the cylinder encompassing the tumor embedded in a lung insert using an in-house developed LabVIEW (National Instruments) based script has been described elsewhere[138]. The position of the phantom over time is recorded with a resolution of 2-3 ms, corresponding well with the linear accelerator pulse interval. The result of the design on this dynamic thorax phantom is the possibility to perform time-resolved plastic scintillator dosimetry in a moving lung tumor as the phantom is manufactured in order to fit the sensitive volume of the fiber-coupled scintillator in the center of the tumor.
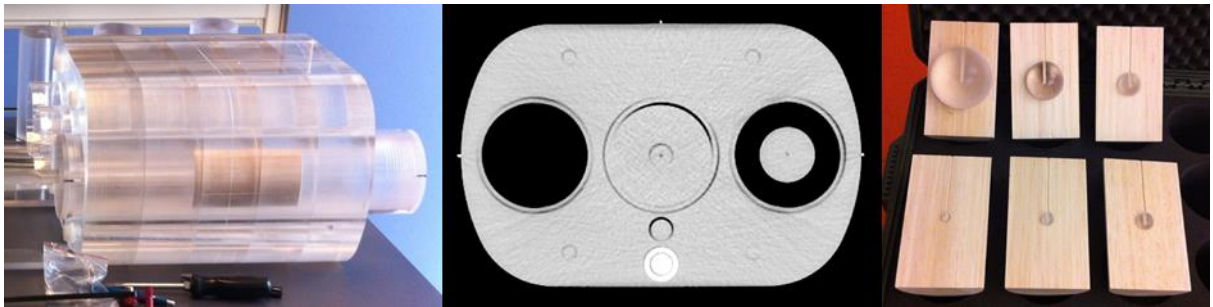
Figure 26. Illustration of the phantom design together with a transversal slice of the CT scanned phantom and a visualization of the flexibility in the various choices of tumor size.

9.2.2   Image acquisition and treatment preparation

The thorax phantom was scanned using a 16 slice Philips Brilliance CT Big Bore scanner (Philips Medical Systems) according to a clinically used thorax 3DCT protocol. The images were acquired with the phantom static in a position corresponding to the central position of the motion to be used during irradiation (Figure 26). Delineation of relevant structures (body, lungs, spinal cord and tumor) were carried out in the Eclipse treatment planning system (Varian Medical Systems), where also all treatment planning was performed. One conventional plan with a single lateral open field (90°) and one single half-arc RapidArc plan were optimized

and calculated using the Anisotropic-Analytical-Algorithm (AAA). Both the conventional and the RapidArc plans were calculated for a 6 MV beam and normalized to give a mean dose to the target of 2 Gy (227 MU and 698 MU, respectively). In this case the target was defined as the spherical tumor (GTV) with no additional safety margins (GTV = PTV). In order to simulate a gross positional error, both treatment plans were copied and recalculated using the same number of MU but with the isocenter shifted by 2.5 cm in the caudal (longitudinal) direction. In addition to the isocenter shift, as the motion of the phantom was not included in the treatment preparations (static 3DCT and no extra margins to encompass the motion), any motion during treatment deliver will simulate an unexpected event during treatment.

9.2.3 Fiber-coupled plastic organic scintillator dosimetry

Treatment plans were delivered on a TrueBeam (Varian Medical Systems) after setup of the phantom using a cone-beam CT with the phantom static in the same position as during the reference CT. Measurements of the four treatment plans were conducted using the in-house developed ME40 Scintillator Dosimetry System (DTU Nutech) for fiber couple plastic organic scintillator dosimetry. The ME40 Scintillator Dosimetry System has previously been well characterized and has also been used in multiple radiation dosimetry situations[75,77,80,138,139]. The system was here used in combination with the BCF-60 plastic scintillator detector (Saint-Gobain Ceramics & Plastics Inc.), enabling pulse-resolved measurements with a suitable spatial resolution (length of 2 mm and a diameter of 1mm). Chromatic removal calibration was carried out, as described in Method C by Guillot et al.[78], in a solid water calibration phantom, where also dosimetric calibration with a Farmer type FC65-G ionization chamber (Scanditronix / Wellhöfer) as reference was performed at an SSD of 100 cm and a depth of 10 cm. Six repeated scintillator measurements were conducted for each plan, both for a static phantom and with the phantom in motion with a randomly chosen starting position and sinusoidal motion with a peak-to-peak distance of 20 mm around the position during reference CT. This resulted in a total of 48 measurements of eight different more or less complicated radiotherapy scenarios. The complexity ranged from the simplest case with a static phantom and a single open conventional treatment field to a similar plan with an isocenter shift of 2.5 cm in the caudal direction delivered to a moving phantom and finally to a dynamic RapidArc delivery (Table 3). This range of complexity rendered a large set of various dose profiles over time which facilitated as a solid ground for testing of the time-resolved Monte Carlo simulations. In order to apply measured dose profiles as reference for Monte Carlo simulations, the pulse-resolved measurements were synchronized with the phantom positional readings. This was achieved by the use of an external 10 V ramp signal (period of 6 s) read out by both the phantom motion controller and the scintillator dosimetry system. Thereby, the motion of the phantom as well as the pulse-resolved measurements were connected and synchronized to the linear accelerator trajectory log files, holding the information necessary to conduct pulse-resolved Monte Carlo simulations based on the actually delivered treatment.

Table 3. The set of five different treatment scenarios investigated described based on the notation used for reference, the treatment plan delivery typ, isocenter location and phantom mode.

Denotation	Plan type	Isocenter location	Phantom mode
SF,c,St	Single open field (90° gantry angle)	Center of tumor	Static
SF,c,Dy	Single open field (90° gantry angle)	Center of tumor	Dynamic sinusoidal motion (25 Hz, 20 mm)
SF,s,St	Single open field (90° gantry angle)	Shifted 2.5 cm (caudal direction)	Static
SF,s,Dy	Single open field (90° gantry angle)	Shifted 2.5 cm (caudal direction)	Dynamic sinusoidal motion (25 Hz, 20 mm)
RA,c,St	Half-arc RapidArc (180°-0° gantry rotation)	Center of tumor	Static

9.2.4 Time-resolved Monte Carlo simulations

All Monte Carlo simulations were conducted using EGSnrc[140] (National Research Council of Canada). Particle transport through the linear accelerator head was simulated using the BEAMnrc user code[86]. The upper static part of the TrueBeam accelerator head was not explicitly modelled. Instead a vendor-provided standard phase space file (Varian Medical Systems) was used. For the dynamic part of the beam configuration, the trajectory logfiles and motion profiles acquired during scintillator measurements served as basis for the generation of input files for the Monte Carlo simulations. As synchronization between phantom motion and the dynamic beam configuration was necessary, the input files were created in order to exploit Source 21 and also the SYNC version of the MLC[87]. By sampling the beam configuration parameters using a common, randomly generated MU index, in the range between 0 and 1, the dose calculation geometry was synchronized with the jaws, MLC and gantry for each particle history. The voxelized dose calculation geometry (egs4phant) was created, based on the 3DCT of the in-house developed dynamic thorax phantom as well as information from the RT Structure Set, using the CTCask software[130]. While voxel densities were assigned according to the CT Hounsfield Unit calibration, the known materials of the delineated regions (PMMA or Balsa wood) were assigned accordingly and the region outside the phantom was defined as air with standard density. Furthermore, the created MC phantom was resampled in order to have a dose calculation geometry corresponding to the TPS dose calculation matrix (Figure 27.).
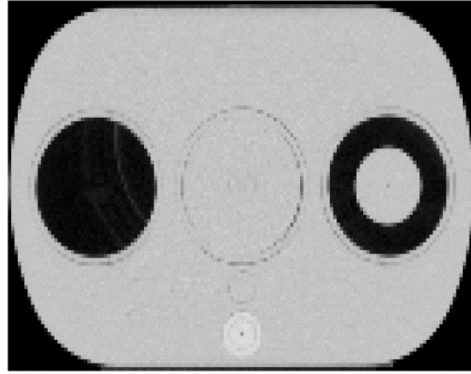

Figure 27. The MC compliant voxelized phantom created using CTC-ask based on 3DCT images of the thorax phantom in static mode.

As for all input file generation, the generation of the MC phantom was incorporated into an in-house developed automatic workflow based on the Skåne Automatic Monte Carlo package written in python[128]. This automatic workflow also included the generation of the input files needed for the simulation of particle transport through the moving phantom. These simulations were based on the 4DdefDOSXYZnrc user code, which enables dose calculation in continuously moving geometries by sampling a new geometry for each incident particle[108]. More specifically the code originates from an alteration of DOSXYZnrc called defDOSXYZnrc, which models the motion in the phantom by applying so called displacement vectors in order to displace the voxel nodes of the reference calculation geometry[100,106]. Throughout this work the displacement vectors were defined based on the expected motion of the dynamic thorax phantom, but can in general be created based on deformable image registration or any motion model. In addition to the general displacement vector the 4DdefDOSXYZnrc code includes a displacement vector scaling factor as a function of MU index, which describes the actual motion of the phantom as recorded during irradiation. During simulation, the randomly sampled MU index is therefore also used for determining a scaling factor to be applied to the displacement vector, giving the full synchronization between phantom deformation and beam delivery. The voxels are deformed accordingly and new densities are calculated for each deformed voxel to ensure conservation of mass (Figure 28). Particle transport and energy deposition is thereafter carried out in the deformed voxel.
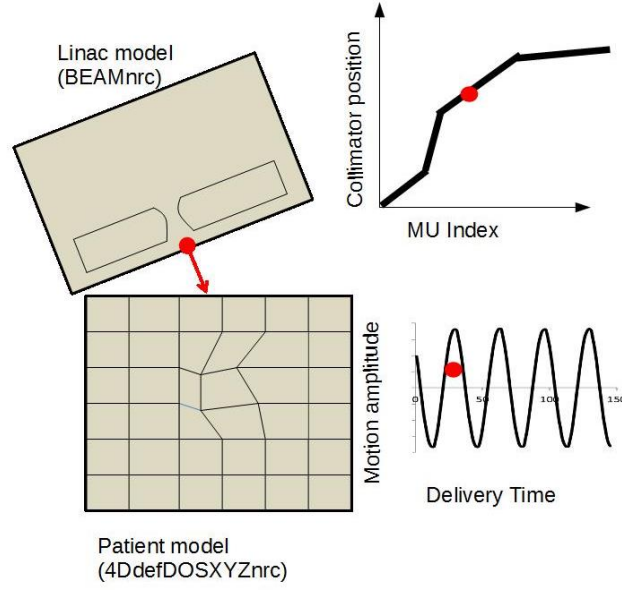
Figure 28. Illustration of the synchronization between beam parameters and patient deformation, using the monitor unit index to determine the dynamic collimator settings as well as motion state of the patient/phantom model.

The resulting dose is automatically accumulated in the reference geometry and eliminating the need for any mapping of dose between geometries. Additionally, the voxel warping approach described here will result in statistical uncertainties in the same order of magnitude as traditional 3D MC calculations with similar amount of histories. However, when advancing to presenting the resulting dose distribution as a function of time a completely different amount of histories will be required if the same statistical uncertainty is sought. The trajectory logfiles were set to a temporal resolution of 20 ms, in this study, rendering three order of magnitude more beam configurations to be simulated in the time-resolved MC simulations than in the standard accumulated 4D simulations. As increasing the number of histories with several orders of magnitude was not feasible the approach was here to modify the 4DdefDOSXYZnrc code in order to score the dose in a pre-defined limited amount of voxels for the given temporal resolution. This adjustment was carried out in order to implement cross-section enhancement as a variance reduction technique, which basically is a method similar to photon splitting but focused in a much smaller volume [114]. For all time-resolved simulations in this study the cross-section was enhanced by a factor of 8 in a region stretching 1 cm in each direction from a single voxel of interest corresponding to the position of the plastic scintillator detector. For 1 billion histories that would for the case of the simulations in this study result in a mean relative statistical uncertainty of 5% in the high dose regions. Furthermore, the photon cutoff energy and electron cutoff energy were set to 0.01 MeV and 0.7 MeV, respectively. All scenarios corresponding to the measured data were simulated using the time-resolved version of the 4DdefDOSXYZnrc code, from here on referred to as 4DtMC. The resulting 4DtMC calculated doses per number of incident particles were converted to absolute dose by multiplying with a calibration factor and the number of MU for the given treatment plan. The calibration factor was derived by simulation of four reference fields with known measured doses (6x6, 10x10, 20x20, and 30x30 cm^2, 100 cm SSD, 10 cm depth). Extracting the dose per incident particle and per MU for each field and calculating the average of those factors resulted in a calibration factor applicable to the range of field sizes of interest for this study.

9.2.5 Comparisons between Monte Carlo simulations and measurements

The dose profiles, i.e. the absolute doses as a function of time, were extracted for the 4DtMC simulations and compared to corresponding dose profiles retrieved from the scintillator measurements. By binning both the measured and simulated data to a resolution of 100 ms a statistical uncertainty in the MC data of

approximately 2-3 % was achieved in the high dose regions. Comparison of the binned data was focused on qualitatively determining if the measured and simulated data presented similar trends in dose gradients over time for the cases of varying complexity. However, quantitative analysis was carried out and first of all accumulated doses were compared. Furthermore, 1D global gamma analysis[141] of the time-resolved dose profiles was performed with an in-house developed MATLAB script, replacing the traditional distance to agreement with a time-difference value, using a 3% dose-difference and 100ms (corresponding to approximately 3 mm respiratory-induced longitudinal motion) time-difference criteria. Additional gamma criteria, acknowledging the uncertainties in the measured and simulated doses, were also tested. All gamma pass rates were calculations of global gamma and calculated for two different dose threshold (5% and 50% of dose maximum) in order to eliminate effects of increased uncertainties in low dose areas.

9.3   Results

The conventional single field plan delivered to a static phantom with the tumor centered in the field resulted in good agreement between the dose as a function of time measured with the plastic scintillator and calculated by the 4Dt MC code (Figure 29). This is also the plan with highest gamma passing rate of up to 83% for the 5%/0.2s criteria (independent of dose threshold) (Table 4). However, for the toughest gamma criteria of 3%/0.1s the passing rate drops down to 59% even for this most simple case. This stems from the slightly higher 4DtMC calculated dose which is readily observed. This is also reflected in the accumulated dose which for the 4DtMC simulation is calculated to be 2.7% higher than the measured dose (Table 4).

When introducing motion to the single conventional field plan with the isocenter in the center of the tumor, the 4DtMC dose was again observed to generally be higher than the PSD dose across the time-resolved profile (Figure 29). However, a difference in the shape of the profiles can be observed where the PSD dose profile has peaks and valleys correlated with the motion pattern. That indicates that the dose measured by the scintillator reveals changes in the delivery as the center of the tumor travels back and forward towards the edges of the treatment field, while the 4DtMC is not sensitive to these changes. The accumulated doses are similar for the single field plan with and without motion, with a 3.2% higher dose in the 4DtMC calculation than the PSD measurement for the dynamic case (Table 4). However, due to the motion-influenced shape of the PSD dose profile the gamma passing rates are below 75% for all gamma criteria.

Shifting the isocenter 2.5 cm towards the edge of the tumor increases the complexity of the situation. The shifted conventional single-field plan on the static phantom resulted in similar deviations between the 4DtMC and PSD dose profiles (Figure 29) and the accumulated dose difference was in the same order of magnitude. However, in contrast to the centered plan, shifting the isocenter resulted in an accumulated 4DtMC dose 4.6% lower than the PSD measured dose (Table 4). Adding the motion of the phantom to this shifted plan rendered in the center of the tumor moving in and out of the field. The effect of the scintillator detector and the dose calculation voxel moving in and out of the field can be observed in the 4DtMC and PSD dose profiles, respectively (Figure 29). The comparison between the measured and calculated dose profiles indicate that the timing of the two are correct as the drops in dose rate are occurring simultaneously. However, the dose is constantly greater in the PSD measurements, also resulting in the 4DtMC accumulated dose being 15% lower than the accumulated PSD dose. Consequently, the shifted plans with and without motion resulted in gamma comparisons with fewer points meeting the criteria (all below 65% gamma passing rate) (Table 4). It can be noted that the gamma passing rate for the shifted single field plan during motion increased from 52% to 62% when the dose threshold was raised from 5% up to 50%, indicating that the majority of the failed points are in the low dose regions.

Finally, comparison for the RapidArc plan on the static phantom increases the complexity of the dose profiles even further. Comparison reveals similar shapes of the dose profiles for the 4DtMC calculation and PSD measurement, but does also present large differences both in high and low dose regions (Figure 30). Despite the accumulated dose deviation being 3%, and therefore not far from the corresponding value for the conventional fields, the gamma analysis reveals large discrepancies in the dose profiles for the RapidArc plan

(Table 4). The gamma passing rates for this plan are all below 40% but also drop down to as low as 3% for the 3%/0.1s criteria, indicating that the majority of the failing points are in the high dose region for this plan.

Figure 29. Comparison of the dose profiles between four-dimensional time-resolved Monte Carlo (4DtMC) simulations and plastic scintillator detector (PSD) measurements. Results in this figure represents the dose in the center of the tumor as a function of time for the conventional single-field (SF) plan delivered to a static or dynamic phantom, with a PMMA tumor embedded into a balsa wood lung insert and the isocenter either centered or shifted.
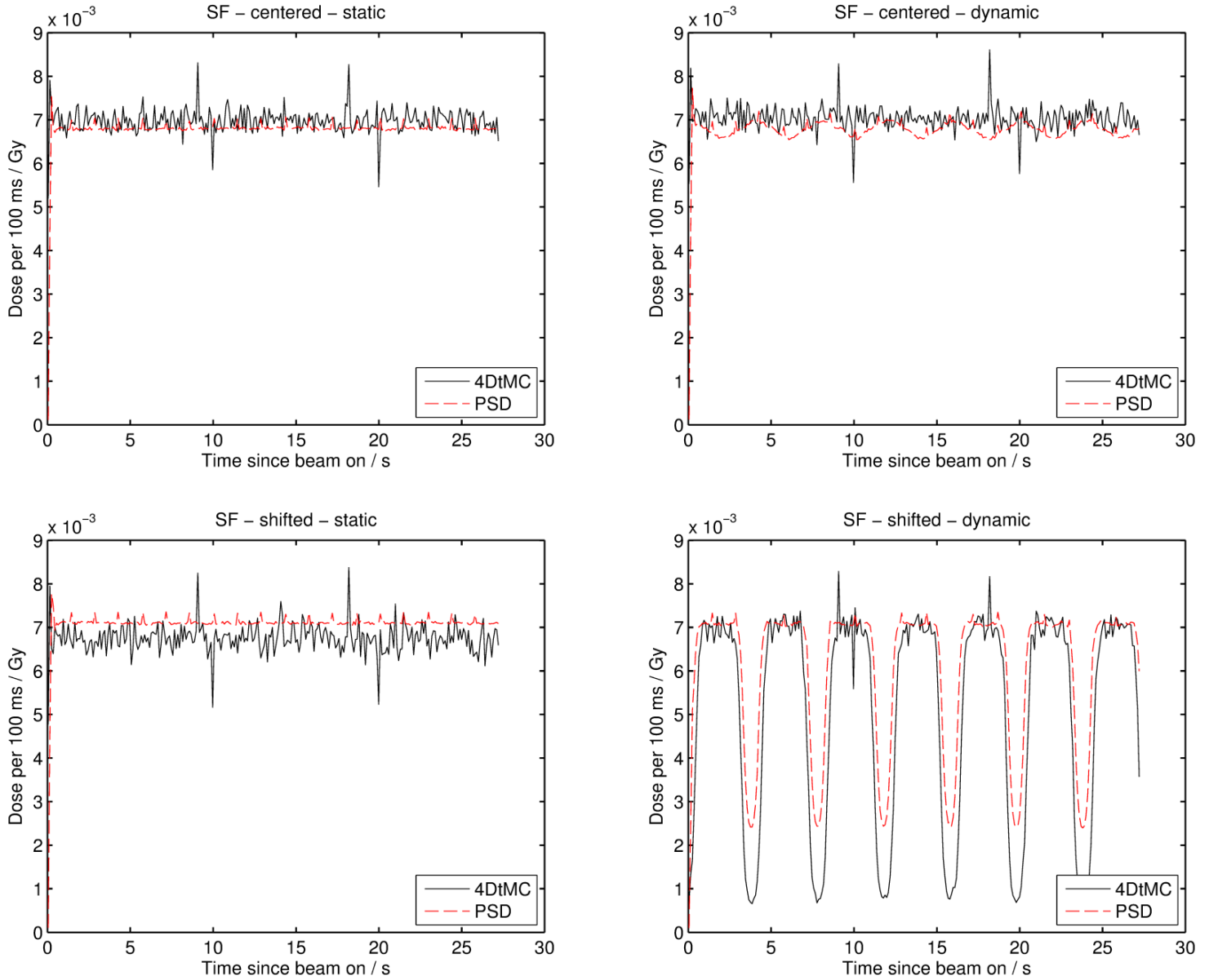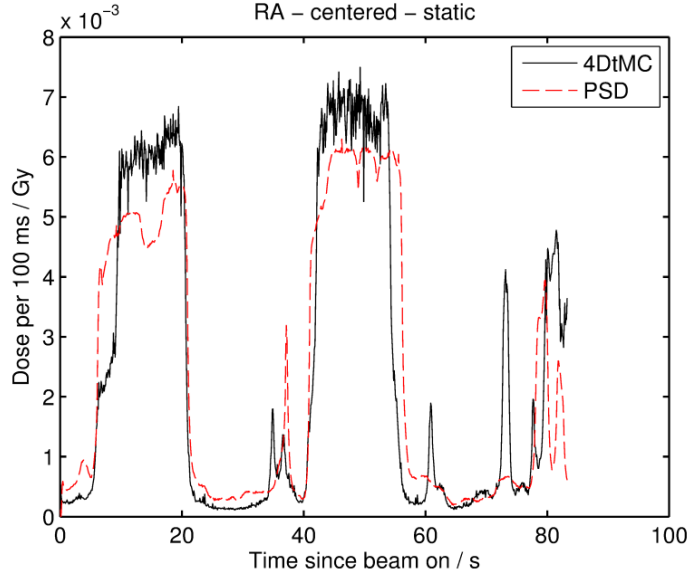
Figure 30. Comparison of the dose profiles between four-dimensional time-resolved Monte Carlo (4DtMC) simulations and plastic scintillator detector (PSD) measurements. Results in this figure represents the dose in the center of the tumor as a function of time for the single half-arc RapidArc plan delivered to a static thorax phantom, with a PMMA tumor embedded into a balsa wood lung insert and the isocenter positioned in the center of the tumor.

Table 4.Comparison of 4DtMC simulations and plastic scintillator detector (PSD) measurements for a range of plans with varying complexity, denoted as SF=single field or RA=RapidArc, c=centered or s=shifted, and St=static or Dy=dynamic. Accumulated doses and percentage dose differences are presented. Uncertainties are calculated based on a statistical uncertainty of 2% in the MC dose and an experimental uncertainty of 1.6% in the PSD measured dose[115]. Additionally, the passing rates for the gamma comparison between the dose profiles are presented for a set of four different gamma criteria.

	Accumulated dose [Gy]			Gamma passing rates			
Plan	4DtMC	PSD	Diff [%]	3%/0.1s/5%th	3%/0.1s/50%th	5%/0.2s/5%th	5%/0.2s/50%th
SF,c,St	1.90 ± 0.04	1.84 ± 0.03	3 ± 3	59.4	59.4	82.7	82.7
SF,c,Dy	1.91 ± 0.04	1.84 ± 0.03	4 ± 3	47.2	47.2	74.9	74.9
SF,s,St	1.83 ± 0.04	1.93 ± 0.03	-5 ± 2	29.2	29.2	55.4	55.4
SF,s,Dy	1.40 ± 0.03	1.65 ± 0.03	-15 ± 2	33.6	39.6	52.4	62.1
RA,c,St	2.03 ± 0.04	1.99 ± 0.03	2 ± 3	24.0	3.2	38.9	7.9

9.4 Discussion

The purpose of this study was to re-develop the 4DdefDOSXYZnrc code in order to provide a method for time-resolved MC simulations based on the voxel warping approach and to experimentally validate the new user code by comparisons to PSD measurements in an in-house developed dynamic thorax phantom. A set of treatment plans of varying complexity was delivered to the thorax phantom while in motion or stationary. The motion of the phantom was synchronized with the PSD measurements as well as the linac logfiles and thereby also with the MC simulations as the input files were generated based on the same motion files and logfiles.

In general, a good agreement between the shapes of the dose profiles was observed when comparing the PSD measured and 4DtMC calculated doses. The majority of the major dose gradients, due to dynamic beam

delivery as well as the dose point of interest moving in and out of the field, were observed for both methods. They were furthermore observed at the same points in time, indicating that the time-related synchronization between the motion, the measurements and the simulations were in order. The visual analysis of the dose profiles does, however, expose deviations between simulation and measurements and in some regions these deviations are rather large. This has also been confirmed by the quantitative analysis carried out as the difference in accumulated dose and the gamma passing rate ranges from -15% to 4% and 3% to 83%, respectively. In general it can be noted that the gamma passing rate is decreasing as the treatment plan complexity increases. The plans with shifted isocenter indicate a sensitivity of the system towards having the point of interest near the edge of the field or even outside of the field; i.e. regions of low dose. With exception of these shifted plans the difference in accumulated dose between 4DtMC and PSD is less than 4%. When relating this to the statistical and experimental uncertainty of around 2% in the 4DtMC calculations (high dose regions) and the PSD measurements, respectively, it is an indication of that the user code is performing correct on a large scale. However, the most complex dynamic beam deliveries also suffer from large deviations, especially in regions with steep dose gradient making the 4DtMC user code less reliable in its current state.

The fact that the majority of the deviations are located in low dose regions or in regions with steep dose gradients can be related to the higher statistical uncertainty in these regions. When dropping the dose approximately one order of magnitude the statistical uncertainty increases to up to above 20% in some cases. This is mainly a drawback related to the lack of computational power as increasing the number of histories in a simulation would decrease the statistical uncertainty but in the same time also increase an already rather long computational time. This is a limitation even for the current implementation with a temporal resolution of 100 ms and would be an even larger issue if aiming at calculating dose with a temporal resolution of around 3 ms to match the measurement resolution. As the deviations occur when the point of interest is close to the edge of the open field or subject to complex multi leaf collimator (MLC) movement there is also a chance that a part of the reason for the large deviations is the modelling of the collimator jaws and the MLC. These components have been validated previously in a 3D setting looking at the accumulated doses, but the time-resolved MC solution might be more sensitive to these factors. Finally, it is necessary to mention that the measurement system used in this study is also subject to uncertainties, where the stem and absolute dose calibrations are major contributors. Further investigation of the sensitivity of these calibrations to e.g. the amount of fiber in the treatment field might be needed. The scintillator sensitive volume is cylindrical and does not perfectly match the cubic calculation voxel in size. Positional uncertainty during measurement is also a minor contributor to the uncertainty and the agreement between the experimental and simulation point of interest is crucial.

Quantitatively the comparative results in this study are not a complete validation of the developed 4DtMC solution. However, quantitatively the results are an indication of a user code with potential to help resolve when in time a given deviation in the accumulated dose might have occurred. The timing of the dose gradients are generally in place and most likely a comparison of the expected and actually delivered dose, both calculated by the presented solution for time-resolved Monte Carlo calculations is the method closest to implementation in a routine patient-specific quality assurance system.

9.5 Conclusions

A novel user code for time-resolved Monte Carlo calculations of dose delivered to a moving anatomy was developed and qualitatively validated. Quantitatively there is a need for further validation despite indications of temporal agreements in detecting dose gradients with experimental data using the ME40 plastic scintillator system in an in-house developed thorax phantom. Implementation of the user code in an automated workflow was feasible and the solution has high potential in assisting in the detection of underlying causes to deviations detected in the accumulated dose, possibly best in combination with the scintillator dosimetry system. Future perspectives include further quantitative validation and testing in more clinically relevant cases with irregular respiratory movement as well as deforming anatomies. This development could make the time-resolved MC and dosimetry system serve as a valuable tool for quality assurance in environments with online adaptive treatments.

10 Bibliography

[1]   Ferlay J, Soerjomataram I, Ervik M, Dikshit R, Eser S, Mathers C, et al. GLOBOCAN 2012 v1. 0, Cancer Incidence and Mortality Worldwide: IARC CancerBase No. 11. Lyon, France, 2013. Available from: http://globocan.iarc.fr. Accessed on: 18/03/2015. 2012.

[2]   Engholm G, Ferlay J, Christensen N, Kejs A, Johannesen T, Khan S, et al. NORDCAN: Cancer Incidence, Mortality, Prevalence and Survival in the Nordic Countries, Version 7.0 (17.12.2014). Association of the Nordic Cancer Registries. Danish Cancer Society. Available from: http://www.ancr.nu. Accessed on: 18/03/2015. 2014.

[3]   Rengan R, Rosenzweig KE, Venkatraman E, Koutcher LA, Fox JL, Nayak R, et al. Improved local control with higher doses of radiation in large-volume stage III non-small-cell lung cancer. Int J Radiat Oncol Biol Phys, 2004;60:741 –7.

[4]   Bradley JD, Paulus R, Komaki R, Masters G, Blumenschein G, Schild S, et al. Standard-dose versus high-dose conformal radiotherapy with concurrent and consolidation carboplatin plus paclitaxel with or without cetuximab for patients with stage IIIA or IIIB non-small-cell lung cancer (RTOG 0617): A randomised, two-by-two factorial p. Lancet Oncol, 2015;16:187 –99.

[5]   Faivre-Finn C. Dose escalation in lung cancer: Have we gone full circle? Lancet Oncol, 2015;16:125 –7.

[6]   Belderbos J, Walraven I, van Diessen J, Verheij M, de Ruysscher D. Radiotherapy dose and fractionation for stage III NSCLC. Lancet Oncol, 2015;16:e156 –7.

[7]   Møller DS, Nielsen TB, Brink C, Hoffmann L, Lutz CM, Drøgemüller Lund M, et al. Heterogeneous FDG-guided dose-escalation for locally advanced NSCLC (the NARLAL2 trial): Design and early dosimetric results of a randomized, multi-centre phase-III study. Radiother Oncol, 2017;124:311 –7.

[8]   Van Herk M, Remeijer P, Rasch C, Lebesque J V. The probability of correct target dosage: Dose-population histograms for deriving treatment margins in radiotherapy. Int J Radiat Oncol Biol Phys, 2000;47:1121 –35.

[9]   Juhler-Nøttrup T, Korreman SS, Pedersen AN, Persson GF, Aarup LR, Nyström H, et al. Interfractional changes in tumour volume and position during entire radiotherapy courses for lung cancer with respiratory gating and image guidance. Acta Oncol (Madr), 2008;47:1406 –13.

[10]   Ottosson W, Baker M, Hedman M, Behrens CF, Söjström D. Evaluation of setup accuracy for NSCLC patients; Studying the impact of different types of cone-beam CT matches based on whole thorax, columna vertebralis, and GTV. Acta Oncol (Madr), 2010;49:1184 –91.

[11]   Ottosson W, Rahma F, Sjöström D, Behrens CF, Sibolt P. The advantage of deep-inspiration breath-hold and cone-beam CT based soft-tissue registration for locally advanced lung cancer radiotherapyDIBH radiotherapy for lung cancer patients. Radiother Oncol, 2016;119:432 –7.

[12]   Chin E, Loewen SK, Nichol A, Otto K. 4D VMAT, gated VMAT, and 3D VMAT for stereotactic body radiation therapy in lung. Phys Med Biol, 2013;58:749 –70.

[13]   Keall PJ, Mageras GS, Balter JM, Emery RS, Forster KM, Jiang SB, et al. The management of respiratory motion in radiation oncology report of AAPM Task Group 76. Med Phys, 2006;33:3874 –900.

[14]   Ottosson W, Sibolt P, Larsen C, Lykkegaard Andersen JA, Borissova S, Mellemgaard A, et al. Monte Carlo calculations support organ sparing in Deep-Inspiration Breath-Hold intensity-modulated radiotherapy for locally advanced lung cancer. Radiother Oncol, 2015;117:55 –63.

[15] Schmidt ML, Hoffmann L, Kandi M, Moller DS, Poulsen PR. Dosimetric impact of respiratory motion, interfraction baseline shifts, and anatomical changes in radiotherapy of non-small cell lung cancer. Acta Oncol (Madr), 2013;52:1490–6.

[16] Marks LB, Bentzen SM, Deasy JO, Kong F-M (Spring), Bradley JD, Vogelius IS, et al. Radiation Dose–Volume Effects in the Lung. Int J Radiat Oncol Biol Phys, 2015;76:S20–7.

[17] Nyman J, Hallqvist A, Lund JÅ, Brustugun OT, Bergman B, Bergström P, et al. SPACE – A randomized study of SBRT vs conventional fractionated radiotherapy in medically inoperable stage I NSCLC. Radiother Oncol, 2016;121:1–8.

[18] Chun SG, Hu C, Choy H, Komaki RU, Timmerman RD, Schild SE, et al. Impact of intensity-modulated radiation therapy technique for locally advanced non-small-cell lung cancer: A secondary analysis of the NRG oncology RTOG 0617 randomized clinical trial. J Clin Oncol, 2017;35:56–62.

[19] Grills IS, Yan D, Martinez AA, Vicini FA, Wong JW, Kestin LL. Potential for reduced toxicity and dose escalation in the treatment of inoperable non-small-cell lung cancer: A comparison of intensity-modulated radiation therapy (IMRT), 3D conformal radiation, and elective nodal irradiation. Int J Radiat Oncol Biol Phys, 2003;57:875–90.

[20] Murshed H, Liu HH, Liao Z, Barker JL, Wang X, Tucker SL, et al. Dose and volume reduction for normal lung using intensity-modulated radiotherapy for advanced-stage non-small-cell lung cancer. Int J Radiat Oncol Biol Phys, 2004;58:1258–67.

[21] Wu VWC, Kwong DLW, Sham JST. Target dose conformity in 3-dimensional conformal radiotherapy and intensity modulated radiotherapy. Radiother Oncol, 2004;71:201–6.

[22] Liu HH, Wang X, Dong L, Wu Q, Liao Z, Stevens CW, et al. Feasibility of sparing lung and other thoracic structures with intensity-modulated radiotherapy for non-small-cell lung cancer. Int J Radiat Oncol Biol Phys, 2004;58:1268–79.

[23] Liao ZX, Komaki RR, Thames HD, Liu HH, Tucker SL, Mohan R, et al. Influence of Technologic Advances on Outcomes in Patients With Unresectable, Locally Advanced Non-Small-Cell Lung Cancer Receiving Concomitant Chemoradiotherapy. Int J Radiat Oncol Biol Phys, 2010;76:775–81.

[24] Ong CL. Volumetric modulated arc therapy for stereotactic body radiotherapy : Planning considerations , delivery accuracy and efficiency. 2012.

[25] Ong C, Verbakel WFAR, Cuijpers JP, Slotman BJ, Senan S. Dosimetric impact of interplay effect on RapidArc lung stereotactic treatment delivery. Int J Radiat Oncol Biol Phys, 2011;79:305–11.

[26] Berbeco RI, Pope CJ, Jiang SB. Measurement of the interplay effect in lung IMRT treatment using EDR2 films. J Appl Clin Med Phys, 2006;7:33–42.

[27] Court L, Wagar M, Berbeco R, Reisner A, Winey B, Schofield D, et al. Evaluation of the interplay effect when using RapidArc to treat targets moving in the craniocaudal or right-left direction. Med Phys, 2010;37:4–11.

[28] Møller DS, Khalil AA, Knap MM, Hoffmann L. Adaptive radiotherapy of lung cancer patients with pleural effusion or atelectasis. Radiother Oncol, 2014;110:517–22.

[29] Vedam SS, Keall PJ, Kini VR, Mostafavi H, Shukla HP, Mohan R. Acquiring a four-dimensional computed tomography dataset using an external respiratory signal. Phys Med Biol, 2003;48:45–62.

[30] Ford EC, Mageras GS, Yorke E, Ling CC. Respiration-correlated spiral CT: A method of measuring respiratory-induced anatomic motion for radiation treatment planning. Med Phys,

2003;30:88–97.

[31] Fredberg Persson G, Nygaard DE, Af Rosenschöld PM, Richter Vogelius I, Josipovic M, Specht L, et al. Artifacts in conventional computed tomography (CT) and free breathing four-dimensional CT induce uncertainty in gross tumor volume determination. Int J Radiat Oncol Biol Phys, 2011;80:1573–80.

[32] McClelland JR, Hawkes DJ, Schaeffter T, King AP. Respiratory motion models: A review. Med Image Anal, 2013;17:19–42.

[33] The International Commission on Radiation Units and measurements. ICRU Report 62: Prescribing, Recording and Reporting Photon Beam Therapy (Supplement to ICRU Report 50). 1999.

[34] Underberg RWM, Lagerwaard FJ, Slotman BJ, Cuijpers JP, Senan S. Use of maximum intensity projections (MIP) for target volume generation in 4DCT scans for lung cancer. Int J Radiat Oncol Biol Phys, 2005;63:253–60.

[35] Suh Y, Sawant A, Venkat R, Keall PJ. Four-dimensional IMRT treatment planning using a DMLC motion-tracking algorithm. Phys Med Biol, 2009;54:3821–35.

[36] Keall PJ, Colvill E, O' Brien R, Ng JA, Poulsen PR, Eade T, et al. The first clinical implementation of electromagnetic transponder-guided MLC tracking. Med Phys, 2014;41.

[37] Ravkilde T, Keall PJ, Grau C, Høyer M, Poulsen PR. Time-resolved dose distributions to moving targets during volumetric modulated arc therapy with and without dynamic MLC tracking Time-resolved dose distributions to moving targets during volumetric modulated arc therapy with and without dynamic MLC tracki. Med Phys, 2013;40:111723-1-111723–8.

[38] Suh Y, Murray W, Keall PJ. IMRT Treatment Planning on 4D Geometries for the Era of Dynamic MLC Tracking. Technol Cancer Res Treat, 2014;13:505–15.

[39] Kamerling CP, Fast MF, Ziegenhein P, Menten MJ, Nill S, Oelfke U. Real-time 4D dose reconstruction for tracked dynamic MLC deliveries for lung SBRT. Med Phys, 2016;43:6072–81.

[40] Depuydt T, Poels K, Verellen D, Engels B, Collen C, Buleteanu M, et al. Treating patients with real-time tumor tracking using the Vero gimbaled linac system: Implementation and first review. Radiother Oncol, 2014;112:343–51.

[41] Lang S, Zeimetz J, Ochsner G, Schmid Daners M, Riesterer O, Klöck S. Development and evaluation of a prototype tracking system using the treatment couch. Med Phys, 2014;41.

[42] Haas OCL, Skworcow P, Paluszczyszyn D, Sahih A, Ruta M, Mills JA. Couch-based motion compensation: Modelling, simulation and real-time experiments. Phys Med Biol, 2012;57:5787–807.

[43] Wilbert J, Meyer J, Baier K, Guckenberger M, Herrmann C, Heß R, et al. Tumor tracking and motion compensation with an adaptive tumor tracking system (ATTS): System description and prototype testing. Med Phys, 2008;35:3911–21.

[44] Poulsen PR, Fledelius W, Cho B, Keall P. Image-based dynamic multileaf collimator tracking of moving targets during intensity-modulated arc therapy. Int J Radiat Oncol Biol Phys, 2012;83:e265–71.

[45] Cho B, Poulsen PR, Sloutsky A, Sawant A, Keall PJ. First Demonstration of Combined kV/MV Image-Guided Real-Time Dynamic Multileaf-Collimator Target Tracking. Int J Radiat Oncol Biol Phys, 2009;74:859–67.

[46] Keall PJ, Sawant A, Cho B, Ruan D, Wu J, Poulsen P, et al. Electromagnetic-guided dynamic multileaf collimator tracking enables motion management for intensity-modulated arc therapy. Int J Radiat Oncol Biol Phys, 2011;79:312–20.

[47] Cerviño LI, Du J, Jiang SB. MRI-guided tumor tracking in lung cancer radiotherapy. Phys Med Biol, 2011;56:3773–85.

[48] Crijns SPM, Raaymakers BW, Lagendijk JJW. Proof of concept of MRI-guided tracked radiation delivery: Tracking one-dimensional motion. Phys Med Biol, 2012;57:7863–72.

[49] Menten MJ, Fast MF, Nill S, Kamerling CP, McDonald F, Oelfke U. Lung stereotactic body radiotherapy with an MR-linac – Quantifying the impact of the magnetic field and real-time tumor tracking. Radiother Oncol, 2016;119:461–6.

[50] Dietz B, Yip E, Yun J, Fallone BG, Wachowicz K. Real-time dynamic MR image reconstruction using compressed sensing and principal component analysis (CS-PCA): Demonstration in lung tumor tracking. Med Phys, 2017;44:3978–89.

[51] Poulsen PR, Cho B, Ruan D, Sawant A, Keall PJ. Dynamic Multileaf Collimator Tracking of Respiratory Target Motion Based on a Single Kilovoltage Imager During Arc Radiotherapy. Int J Radiat Oncol Biol Phys, 2010;77:600–7.

[52] Sawant A, Smith RL, Venkat RB, Santanam L, Cho B, Poulsen P, et al. Toward Submillimeter Accuracy in the Management of Intrafraction Motion: The Integration of Real-Time Internal Position Monitoring and Multileaf Collimator Target Tracking. Int J Radiat Oncol Biol Phys, 2009;74:575–82.

[53] Poulsen PR, Cho B, Sawant A, Ruan D, Keall PJ. Detailed analysis of latencies in image-based dynamic MLC tracking. Med Phys, 2010;37:4998–5005.

[54] Yeung AR, Li JG, Shi W, Newlin HE, Chvetsov A, Liu C, et al. Tumor Localization Using Cone-Beam CT Reduces Setup Margins in Conventionally Fractionated Radiotherapy for Lung Tumors. Int J Radiat Oncol Biol Phys, 2009;74:1100–7.

[55] Britton KR, Starkschall G, Liu H, Chang JY, Bilton S, Ezhil M, et al. Consequences of Anatomic Changes and Respiratory Motion on Radiation Dose Distributions in Conformal Radiotherapy for Locally Advanced Non–Small-Cell Lung Cancer. Int J Radiat Oncol Biol Phys, 2009;73:94–102.

[56] Attix FH. Introduction to Radiological Physics and Radiation Dosimetry. . John Wiley & Sons., 1986.

[57] Papanikolaou N, Battista JJ, Boyer AL, Kappas C, Klein E, Mackie TR, et al. Tissue Inhomogeneity Corrections for Megavoltage Photon Beams. Report of the AAPM radiation therapy committee task group 65. 2004.

[58] Knöös T, Wieslander E, Cozzi L, Brink C, Fogliata A, Albers D, et al. Comparison of dose calculation algorithms for treatment planning in external photon beam therapy for clinical situations. Phys Med Biol, 2006;51:5785–807.

[59] Behrens CF. Dose build-up behind air cavities for Co-60, 4, 6 and 8 MV. Measurements and Monte Carlo simulations. Phys Med Biol, 2006;51:5937–50.

[60] Van Esch A, Tillikainen L, Pyykkonen J, Tenhunen M, Helminen H, Siljamäki S, et al. Testing of the analytical anisotropic algorithm for photon dose calculation. Med Phys, 2006;33:4130–48.

[61] Rønde HS, Hoffmann L. Validation of Varian' s AAA algorithm with focus on lung treatments. Acta Oncol (Madr), 2009;48:209–15.

[62]   Aarup LR, Nahum AE, Zacharatou C, Juhler-Nøttrup T, Knöös T, Nyström H, et al. The effect of different lung densities on the accuracy of various radiotherapy dose calculation methods: Implications for tumour coverage. Radiother Oncol, 2009;91:405 –14.

[63]   Robinson D. Inhomogeneity correction and the analytic anisotropic algorithm. J Appl Clin Med Phys, 2008;9:112 –22.

[64]   Tillikainen L, Helminen H, Torsti T, Siljamäki S, Alakuijala J, Pyyry J, et al. A 3D pencil-beam-based superposition algorithm for photon dose calculation in heterogeneous media. Phys Med Biol, 2008;53:3821 –39.

[65]   Ottosson W. Improved radiotherapy for locally advanced Non-Small Cell Lung Carcinoma (NSCLC) patients. DTU Nutech, Tech Univ Denmark (PhD Thesis), 2015:109 –18.

[66]   Bush K, Gagne IM, Zavgorodni S, Ansbacher W, Beckham W. Dosimetric validation of Acurosff XB with Monte Carlo methods for photon dose calculations. Med Phys, 2011;38:2208 –21.

[67]   Lu J, Huang B, Zhang J. SU- E- T- 199: Comparison Between Acuros XB and AAA in Homogeneous Phantoms for Volumetric Modulated Arc Therapy Plans. Med Phys, 2016;42:3377 – 8.

[68]   McCurdy BMC, Greer PB. Dosimetric properties of an amorphous-silicon EPID used in continuous acquisition mode for application to dynamic and arc IMRT. Med Phys, 2009;36:3028 – 39.

[69]   Bakhtiari M, Kumaraswamy L, Bailey DW, De Boer S, Malhotra HK, Podgorsak MB. Using an EPID for patient-specific VMAT quality assurance. Med Phys, 2011;38:1366 –73.

[70]   Liu B, Adamson J, Rodrigues A, Zhou F, Yin F, wu Q. WE- G- 108- 08: A Novel Technique for VMAT QA with EPID in Cine Mode On Varian TrueBeam. Med Phys, 2013;40:502.

[71]   Damkjær SMS. Time-Resolved Luminescence Dosimetry using Fiber-Coupled Al2O3:C and Applications in External Beam Radiotherapy. Niels Bohr Institute, Univ Copenhagen (PhD Thesis), 2011.

[72]   Sadagopan R, Bencomo JA, Martin RL, Nilsson G, Matzen T, Balter PA. Characterization and clinical evaluation of a novel IMRT quality assurance system. J Appl Clin Med Phys, 2009;10:2928.

[73]   Beddar AS, Law S. Water-equivalent plastic scintillation detectors for high-energy beam dosimetry: I. Physical characteristics and theoretical considerations. Phys Med Biol, 1992;37:1883 – 900.

[74]   Beddar AS, Law S. Water-equivalent plastic scintillation detectors for high-energy beam dosimetry: II. Properties and measurements. Phys Med Biol, 1992;37:1901 –13.

[75]   Beierholm AR, Ottosson RO, Lindvold LR, Behrens CF, Andersen CE. Characterizing a pulse-resolved dosimetry system for complex radiotherapy beams using organic scintillators. Phys Med Biol, 2011;56:3033 –45.

[76]   Beierholm AR, Behrens CF, Hoffmann L, Andersen CE. Acquiring beam data for a flattening-filter free linear accelerator using organic scintillators. Radiat Meas, 2013;56:290 –3.

[77]   Beierholm AR, Behrens CF, Andersen CE. Studying the potential of point detectors in time-resolved dose verification of dynamic radiotherapy. Radiat Meas, 2015;82:129 –37.

[78]   Guillot M, Gingras L, Archambault L, Beddar S, Beaulieu L. Spectral method for the correction of the Cerenkov light effect in plastic scintillation detectors: A comparison study of calibration

procedures and validation in Cerenkov light-dominated situations. Med Phys, 2011;38:2140 –50.

[79] Beierholm AR, Behrens CF, Andersen CE. Dosimetric characterization of the Exradin W1 plastic scintillator detector through comparison with an in-house developed scintillator system. Radiat Meas, 2014;69:50 –6.

[80] Ottosson W, Behrens CF, Andersen CE. Dose verification of radiotherapy for lung cancer by using plastic scintillator dosimetry and a heterogeneous phantom. J Phys Conf Ser, 2015;573:7–11.

[81] Andreo P. Monte Carlo Techniques in Medical Radiation Physics. Phys Med Biol, 1991;36:861–920.

[82] Rogers DWO, Faddegon BA, Ding GX, Ma CM, We J. BEAM: A Monte Carlo code to simulate radiotherapy treatment units. Med Phys, 1995;22:503–24.

[83] Chetty IJ, Curran B, Cygler JE, DeMarco JJ, Ezzell G, Faddegon BA, et al. Report of the AAPM Task Group No. 105: Issues associated with clinical implementation of Monte Carlo-based photon and electron external beam treatment planning. Med Phys, 2007;34:4818–53.

[84] Reynaert, N.; Mark, S. vander; Schaart, D.; Zee, W. van der; Tomsej, M.; Vroegindeweij, C. van Vliet; Jansen, J.; Coghe, M.; Wagter, C. De; Heijmen B. Monte Carlo Treatment Planning. vol. 6. 2006.

[85] Kawrakow I, Mainegra-Hing E, Rogers DWO, Tessier F, Walters BRB. The EGSnrc Code System : Monte Carlo Simulation of Electron and Photon Transport. 2018, https://nrc-cnrc.github.io/EGSnrc/doc/pirs701-egsnrc.pdf.

[86] Rogers DWO, Walters B, Kawrakow I. BEAMnrc Users Manual. 2011, http://irs.inms.nrc.ca/software/beamnrc/documentation/pirs0509/pirs0509.pdf.

[87] Lobo J, Popescu IA. Two new DOSXYZnrc sources for 4D Monte Carlo simulations of continuously variable beam configurations, with applications to RapidArc, VMAT, TomoTherapy and CyberKnife. Phys Med Biol, 2010;55:4431–43.

[88] Walters BRB, Kawrakow I, Rogers DWO. History by history statistical estimators in the BEAM code system. Med Phys, 2002;29:2745–52.

[89] Lujan AE, Larsen EW, Balter JM, Haken RK Ten. A method for incorporating organ motion due to breathing into 3D dose calculations. Med Phys, 1999;26:715–20.

[90] McCarter SD, Beckam WA. Evaluation of the validity of a convolution method for incorporating tumor movement and set-up variations into the radiotherapy treatment planning system. Phys Med Biol, 2000;45:923–31.

[91] Chetty IJ, Rosu M, McShan DL, Fraass BA, Balter JM, Ten Haken RK. Accounting for center-of-mass target motion using convolution methods in Monte Carlo-based dose calculations of the lung. Med Phys, 2004;31:925–32.

[92] Chetty IJ, Rosu M, Tyagi N, Marsh LH, McShan DL, Balter JM, et al. A fluence convolution method to account for respiratory motion in three-dimensional dose calculations of the liver: A Monte Carlo study. Med Phys, 2003;30:1776–80.

[93] Heath E, Seco J. Dynamic Beam Delivery and 4D Monte Carlo. In: Monte Carlo Techniques in Radiation Therapy (Edited by Seco, J. & Verhaegen, F.), 2013:95–110.

[94] Brock KK, McShan DL, Ten Haken RK, Hollister SJ, Dawson LA, Balter JM. Inclusion of organ deformation in dose calculations. Med Phys, 2003;30:290–5.

[95] Keall PJ, Siebers J V., Joshi S, Mohan R. Monte Carlo as a four-dimensional radiotherapy treatment-planning tool to account for respiratory motion. Phys Med Biol, 2004;49:3639–48.

[96] Schaly B, Kempe JA, Bauman GS, Battista JJ, Van Dyk J. Tracking the dose distribution in radiation therapy by accounting for variable anatomy. Phys Med Biol, 2004;49:791–805.

[97] Hoon Jung S, Min Yoon S, Ho Park S, Cho B, Won Park J, Jung J, et al. Four-dimensional dose evaluation using deformable image registration in radiotherapy for liver cancer. Med Phys, 2012;40:11706.

[98] Holden M. A review of geometric transformations for nonrigid body registration. IEEE Trans Med Imaging, 2008;27:111–28.

[99] Rosu M, Chetty IJ, Balter JM, Kessler ML, McShan DL, Ten Haken RK. Dose reconstruction in deforming lung anatomy: Dose grid size effects and clinical implications. Med Phys, 2005;32:2487–95.

[100] Heath E, Seuntjens J. A direct voxel tracking method for four-dimensional Monte Carlo dose calculations in deforming anatomy. Med Phys, 2006;33:434–45.

[101] Siebers J V., Zhong H. An energy transfer method for 4D Monte Carlo dose calculation. Med Phys, 2008;35:4096–105.

[102] Zhong H, Siebers J V. Monte Carlo dose mapping on deforming anatomy. Phys Med Biol, 2009;54:5815–30.

[103] Li HS, Zhong H, Kim J, Glide-Hurst C, Gulam M, Nurushev TS, et al. Direct dose mapping versus energy/mass transfer mapping for 4D dose accumulation: Fundamental differences and dosimetric consequences. Phys Med Biol, 2014;59:173–88.

[104] Ziegenhein P, Kamerling CP, Fast MF, Oelfke U. Real-time energy/mass transfer mapping for online 4D dose reconstruction. Sci Rep, 2018;8:1–10.

[105] Belec J, Clark BG. Monte Carlo calculation of VMAT and helical tomotherapy dose distributions for lung stereotactic treatments with intra-fraction motion. Phys Med Biol, 2013;58:2807–21.

[106] Heath E, Tessier F, Kawrakow I. Investigation of voxel warping and energy mapping approaches for fast 4D Monte Carlo dose calculations in deformed geometries using VMC++. Phys Med Biol, 2011;56:5187–202.

[107] Heath E, Badragan I, Popescu I. TU-G-BRA-01: 4D Monte Carlo Simulations of Beam and Patient Motion Using EGSnrc/BEAMnrc. Med Phys, 2012;39:3921.

[108] Gholampourkash S, Vujicic M, Belec J, Cygler JE, Heath E. Experimental veri fi cation of 4D Monte Carlo simulations of dose delivery to a moving anatomy. Med Phys, 2017;44:299–310.

[109] Siebers J V, Keall PJ, Nahum AE, Mohan R. Converting absorbed dose to medium to absorbed dose to water for Monte Carlo based photon beam dose calculations. Phys Med Biol, 2000;45:983–95.

[110] Ma CM, Li J. Dose specification for radiation therapy: Dose to water or dose to medium? Phys Med Biol, 2011;56:3073–89.

[111] Andreo P. Dose to "water-like" media or dose to tissue in MV photons radiotherapy treatment planning: Still a matter of debate. Phys Med Biol, 2015;60:309–37.

[112] Knöös T. 3D dose computation algorithms. J Phys Conf Ser, 2017;847:0–9.

[113] Kawrakow I, Fippel M. Investigation of variance reduction techniques for Monte Carlo photon dose calculation using XVMC. Phys Med Biol, 2000;45:2163–83.

[114] Wulff J, Zink K, Kawrakow I. Efficiency improvements for ion chamber calculations in high energy photon beams. Med Phys, 2008;35:1328–36.

[115] Beierholm AR, Behrens CF, Andersen CE. Comment on "Characterization of the Exradin W1 scintillator for use in radiotherapy" [Med. Phys. 42, 297-304 (2015)]. Med Phys, 2015;42:4414–6.

[116] Engholm G, Ferlay J, Christensen N, Bray F, Gjerstorff ML, Klint Å, et al. NORDCAN - A Nordic tool for cancer information, planning, quality control and research. Acta Oncol (Madr), 2010;49:725–36.

[117] Rosenzweig KE, Hanley J, Mah D, Mageras GS, Hunt M, Toner S, et al. The deep inspiration breath-hold technique in the treatment of inoperable non-small-cell lung cancer. Int J Radiat Oncol Biol Phys, 2000;48:81–7.

[118] Hanley J, Debois MM, Mah D, Mageras GS, Raben A, Rosenzweig K, et al. Deep inspiration breath-hold technique for lung tumors: The potential value of target immobilization and reduced lung density in dose escalation. Int J Radiat Oncol Biol Phys, 1999;45:603–11.

[119] Sjöström D, Bjelkengren U, Ottosson W, Behrens CF. A beam-matching concept for medical linear accelerators. Acta Oncol (Madr), 2009;48:192–200.

[120] Fogliata A, Nicolini G, Vanetti E, Clivio A, Cozzi L. Dosimetric validation of the anisotropic analytical algorithm for photon dose calculation: Fundamental characterization in water. Phys Med Biol, 2006;51:1421–38.

[121] Møller DS, Khalil AA, Knap MM, Muren LP, Hoffmann L. A planning study of radiotherapy dose escalation of PET-active tumour volumes in non-small cell lung cancer patients. Acta Oncol (Madr), 2011;50:883–8.

[122] Aerts HJWL, Bosmans G, van Baardwijk AAW, Dekker ALAJ, Oellers MC, Lambin P, et al. Stability of 18F-Deoxyglucose Uptake Locations Within Tumor During Radiotherapy for NSCLC: A Prospective Study. Int J Radiat Oncol Biol Phys, 2008;71:1402–7.

[123] Vestergaard A, Muren LP, Lindberg H, Jakobsen KL, Petersen JBB, Elstrom U V., et al. Normal tissue sparing in a phase II trial on daily adaptive plan selection in radiotherapy for urinary bladder cancer. Acta Oncol (Madr), 2014;53:997–1004.

[124] Ottosson W, Lykkegaard Andersen JA, Borrisova S, Mellemgaard A, Behrens CF. Deformable image registration for geometrical evaluation of DIBH radiotherapy treatment of lung cancer patients. J Phys Conf Ser, 2014;489:12077.

[125] Ottosson RO, Karlsson A, Behrens CF. Pareto front analysis of 6 and 15 MV dynamic IMRT for lung cancer using pencil beam, AAA and Monte Carlo. Phys Med Biol, 2010;55:4521–33.

[126] Ong CL, Dahele M, Cuijpers JP, Senan S, Slotman BJ, Verbakel WFAR. Dosimetric impact of intrafraction motion during rapidarc stereotactic vertebral radiation therapy using flattened and flattening filter-free beams. Int J Radiat Oncol Biol Phys, 2013;86:420–5.

[127] Bortfeld T, Jokivarsi K, Goitein M, Kung J, Jiang SB. Effects of intra-fraction motion on IMRT dose delivery: Statistical analysis and simulation. Phys Med Biol, 2002;47:2203–20.

[128] Sibolt P, Cronholm RO, Heath E, Andersen CE, Behrens CF. Automated four-dimensional Monte Carlo workflow using log files and real-time motion monitoring. J Phys Conf Ser, 2017;847.

[129] Popescu IA, Atwal P, Lobo J, Lucido J, McCurdy BMC. Patient-specific QA using 4D Monte

Carlo phase space predictions and EPID dosimetry. J Phys Conf Ser, 2015;573.

[130] Ottosson RO, Behrens CF. CTC-ask: A new algorithm for conversion of CT numbers to tissue parameters for Monte Carlo dose calculations applying DICOM RS knowledge. Phys Med Biol, 2011;56.

[131] Guckenberger M, Krieger T, Richter A, Baier K, Wilbert J, Sweeney RA, et al. Potential of image-guidance, gating and real-time tracking to improve accuracy in pulmonary stereotactic body radiotherapy. Radiother Oncol, 2009;91:288–95.

[132] Josipovic M, Persson GF, Dueck J, Bangsgaard JP, Westman G, Specht L, et al. Geometric uncertainties in voluntary deep inspiration breath hold radiotherapy for locally advanced lung cancer. Radiother Oncol, 2016;118:510–4.

[133] Iizuka Y, Matsuo Y, Ishihara Y, Akimoto M, Tanabe H, Takayama K, et al. Dynamic tumor-tracking radiotherapy with real-time monitoring for liver tumors using a gimbal mounted linac. Radiother Oncol, 2015;117:496–500.

[134] Li G, Cohen P, Xie H, Low D, Li D, Rimner A. A novel four-dimensional radiotherapy planning strategy from a tumor-tracking beam's eye view. Phys Med Biol, 2012;57:7579–98.

[135] Sibolt P, Ottosson W, Sjöström D, Larsen C, Behrens CF. Adaptation requirements due to anatomical changes in free-breathing and deep-inspiration breath-hold for standard and dose-escalated radiotherapy of lung cancer patients. Acta Oncol (Madr), 2015;54:1453–60.

[136] Bortfeld T, Jiang SB, Rietzel E. Effects of Motion on the Total Dose Distribution. Semin Radiat Oncol, 2004;14:41–51.

[137] Engelsman M, Damen EMF, De Jaeger K, Van Ingen KM, Mijnheer BJ. The effect of breathing and set-up errors on the cumulative dose to a lung tumor. Radiother Oncol, 2001;60:95–105.

[138] Sibolt P, Andersen CE, Ottosson W, Behrens CF. Time-resolved plastic scintillator dosimetry in a dynamic thorax phantom. Radiat Meas, 2017;106:373–7.

[139] Sibolt P, Cronholm RO, Beierholm AR, Behrens CF. Measurements of the relative backscatter contribution to the monitor chamber for modern medical linear accelerators; A multi-center study. Radiat Meas, 2015;72:75–80.

[140] Kawrakow I, Rogers DWO. The EGSnrc Code System : Monte Carlo Simulation of Electron and Photon Transport. NRCC Rep PIRS-701, 2003:2001–3.

[141] Low D a., Harms WB, Mutic S, Purdy J a. A technique for the quantitative evaluation of dose distributions. Med Phys, 1998;25:656–61.

Appendices

11 Appendix A: Calibration of the TrueBeam Monte Carlo model

In order to compare MC calculated dose distributions with corresponding calculations in a commercial TPS or in order to conduct comparisons with measurements, conversion of the MC calculated dose to absolute dose in Gy is necessary. Converting MC calculated dose to absolute dose thus requires a calibration of the linac MC model. With the primary source being a phase space scored above the first non-static component of the LINAC head, absolute calibration is fairly straight forward as no measurements are required if beam data acquired during commissioning is used. Here the measured relative output factors were necessarily included and applied to render depth dose curves and profiles in absolute absorbed dose, for field sizes ranging from 4x4 cm^2 to 30x30 cm^2. Corresponding fields were MC simulated and doses at 5, 10 and 20 cm depths were extracted. Comparison with measured data then rendered in a set of 15 absolute dose calibration coefficients. Using an average of those rendered in a single absolute dose calibration coefficient of 1.27·10^{12} Gy/MU with a standard deviation of ±1 % (k=1), applicable to the entire range of field sizes and depth to an acceptable level of uncertainty (Figure 31). Dose differences for the field sizes and depth relevant for this thesis were observed to be within 0.5% based on the calibration approach applied here (Figure 32).
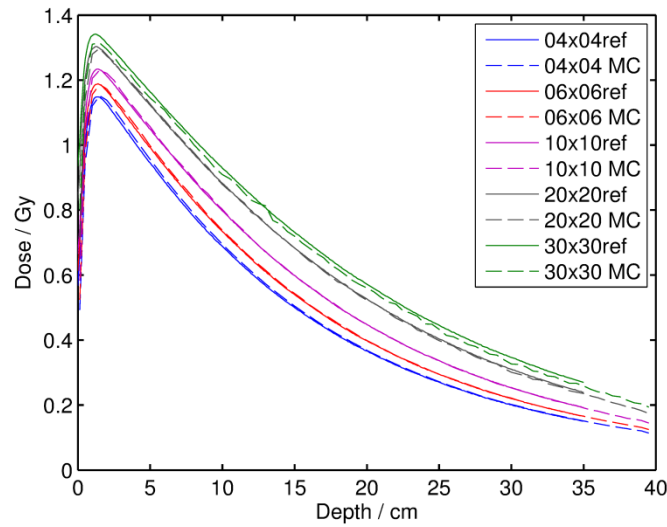

Figure 31. Comparison of a set of MC calculated depth dose curves, absolute calibrated with a general calibration factor, with reference depth dose curves measured during commissioning.
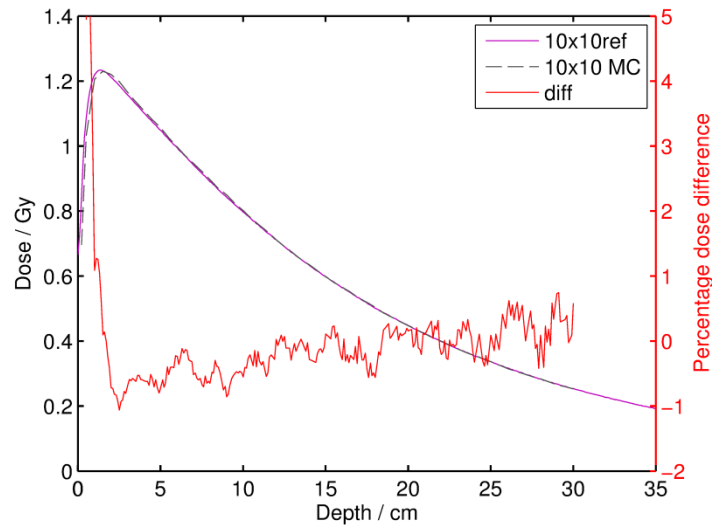

Figure 32. Specific comparison between MC calculated and reference depth dose curves for a 10x10 cm^2 field.